# Experimental Techniques in Gas-Phase Ion Thermochemistry

Kent M. Ervin*

*Department of Chemistry and Chemical Physics Program, University of Nevada, Reno, Nevada 89557*

*Received May 2, 2000*

## Contents



## I. Introduction

Ion thermochemistry is of great practical importance to mass spectrometry. Ion source intensities and fragmentation patterns in mass spectra are intimately related to ion energetics. In chemical ionization mass spectrometry, for example, the absence of appreciably endoergic ion−molecule reactions results in analytical selectivity. Schemes for analyzing and sequencing peptides and other biomolecules by mass spectrometry involve site-specific protonation or metalation.[1] The site specificity is determined by the relative proton affinities or metal-ion affinities of various functional groups. The kinetics of the reactions is important too, but thermodynamics ultimately controls the favored processes.

Measurements on isolated ions yield information about the intrinsic behavior of the species in the absence of solvent effects. Comparison with the behavior of the same ions in the condensed phase shows how solvent influences reactivity. In a famous example, Brauman and Blair[2] showed that the intrinsic acidity of simple alcohols in the gas phase follows the order $CH_3OH < C_2H_5OH < C_3H_7OH < C_4H_9OH$, which is the reverse of the order found in aqueous solution. The solution acidities are actually determined by the solvation energies of the alkoxide

* To whom correspondence should be addressed. Phone: 775-784-6676, Fax: 775-784-6804, E-mail: ervin@chem.unr.edu.

10.1021/cr990081l CCC: $36.00 
Published on Web 01/24/2001

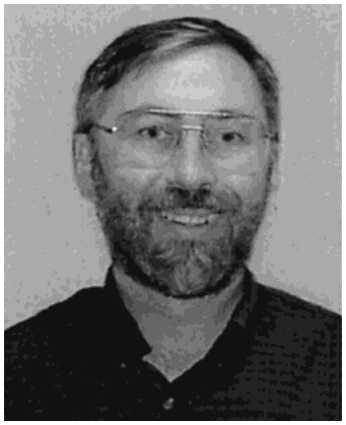

Kent M. Ervin earned his B.A. and B.S. degrees from the University of Kansas in 1981 and his Ph.D. degree in Chemistry from the University of California, Berkeley, in 1986. As a graduate student, he worked with Professor Peter B. Armentrout studying the dynamics of reactions of atomic cations with hydrogen, with emphasis on the reactivity of systems involving multiple electronic potential energy surfaces. Ervin performed postdoctoral research using negative-ion photoelectron spectroscopy at JILA, University of Colorado, with Professor W. Carl Lineberger. At the University of Nevada, Reno, the Ervin group uses ion chemistry techniques to study transition-metal cluster catalysis, gas-phase $S_N2$ reactions, and the thermochemistry of hydrocarbon radicals.

anions, which are larger for the smaller ions. Measurements of stepwise solvation energies of ions in the gas phase can follow the progression from isolated ions to fully solvated species.[3−5]

Thermochemical information about neutral species can also be obtained from measurements on ions. Figure 1 illustrates the relationships between the dissociation energies of anions and cations and their neutral counterparts, eqs 1−3, in terms of ionization energies and electron affinities of the molecules and their fragments.

$$D(\mathrm{X-Y}) = D(\mathrm{X^+-Y}) + \mathrm{IE(XY)} - \mathrm{IE(X)} \quad (1)$$

$$D(\mathrm{X-Y}) = D(\mathrm{X^--Y}) + \mathrm{EA(X)} - \mathrm{EA(XY)} \quad (2)$$

$$D(\mathrm{X-Y}) = D(\mathrm{X^+-Y^-}) - \mathrm{IE(X)} + \mathrm{EA(Y)} \quad (3)$$

Figure 2 shows the more specialized proton affinity cycle (eq 4), negative-ion cycle (eq 5), and appearance energy cycle (eq 6), which relate ion thermochemical quantities to C−H bond dissociation energies in neutral organic compounds.[6,7] Thermochemical quantities are illustrated in Figures 1 and 2 and will be defined explicitly in section II, where temperature effects are also discussed.

$$D(\mathrm{R-H}) = \mathrm{PA(R^\cdot)} + \mathrm{IE(RH)} - \mathrm{IE(H)} \quad (4)$$

$$D(\mathrm{R-H}) = \Delta_{\mathrm{acid}}H(\mathrm{RH}) + \mathrm{EA(R^\cdot)} - \mathrm{IE(H)} \quad (5)$$

$$D(\mathrm{R-H}) = \mathrm{AE(R^+,RH)} - \mathrm{IE(R^\cdot)} \quad (6)$$

Through these relationships, ion thermochemistry measurements can yield accurate bond dissociation energies for neutral hydrocarbon molecules.[6] The bond dissociation energies are directly related to the enthalpies of formation of the radicals, which are important for modeling complex chemical systems including combustion and atmospheric reactions. For

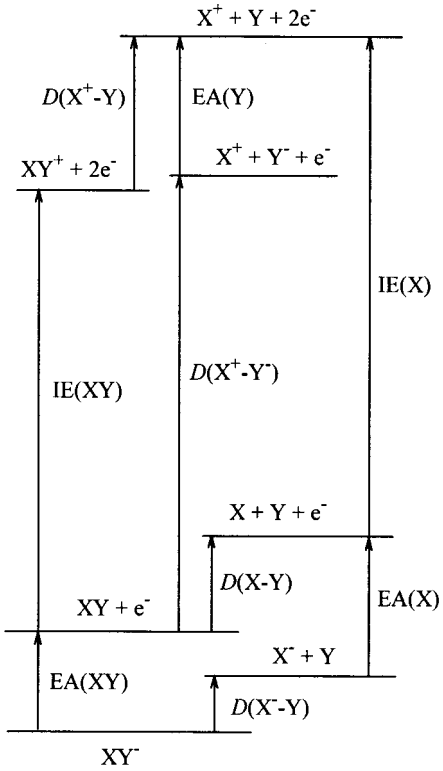


**Figure 1.** Energy level diagram showing the relationships between anionic, neutral, and cationic dissociation energies. Relative energy levels are scaled approximately for XY = $Cl_2$. In general, the relative orderings of XY + $e^-$ versus $X^-$ + Y and $XY^+$ versus $X^+$ + $Y^-$ may change.

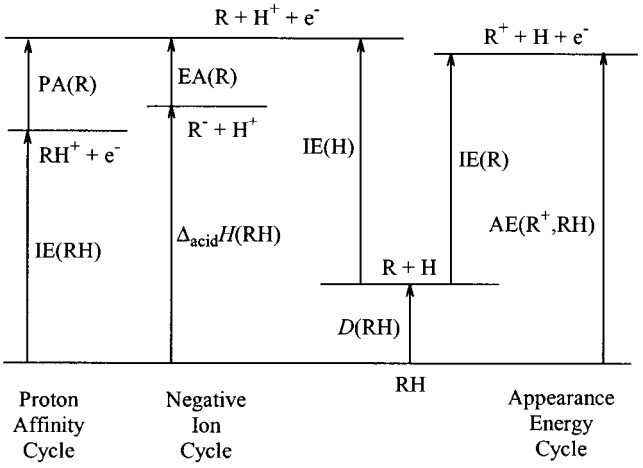


**Figure 2.** Energy level diagram depicting how R−H bond dissociation energies are measured using the proton affinity cycle, negative-ion cycle, and appearance energy cycle, eqs 4−6. Relative energy levels are scaled approximately for HR = HCl.

modeling kinetic systems, "chemical accuracy" of about ±4 kJ/mol is generally required.[8] Enthalpies of formation are well established for many stable compounds, and there is a sufficiently large database for estimation of other compounds by empirical additivity methods.[9−13] The state of the art is considerably less advanced for radicals, primarily because these reactive species cannot be burned in a bomb calorimeter to obtain combustion enthalpies directly, and for compounds with functional groups containing elements other than nitrogen, oxygen, and the halogens, especially organometallics.

**Table 1. Comparison of Bond Dissociation Enthalpies at 298 K (kJ/mol)**

| R−H | McMillen and Golden (1982)[14] | Berkowitz et al. (1994)[6] | Tsang (1996)[15] | other | ref |
|---|---|---|---|---|---|
| $CH_3$−H | 439.7 ± 0.8 | 438.9 ± 0.4 | 440 ± 1 | 439.28 ± 0.13* | 16 |
| HCC−H | 552 ± 20* | 555.6 ± 2.9* | 548 ± 8 | 557.2 ± 0.2[a] | 17 |
| H−CH=$CH_2$ | 460 ± 8 | 465.3 ± 3.3* | 464 ± 5 | 463 ± 5 | 18 |
| | | | | 464 ± 14 | 19 |
| | | | | 460.9 ± 1.7 | 20 |
| $C_6H_5$−H | 464 ± 8 | 465.3 ± 3.3* | 474 ± 8 | 474.9 ± 2.1* | 21 |
| H−$CH_2$CH=$CH_2$ | 361 ± 6 | 369 ± 9* | 368 ± 3 | 363.9 ± 4.3 | 22 |
| | | | | 371.5 ± 1.7* | 23 |
| H−$CH_2C_6H_5$ | 368 ± 4 | 370 ± 6 | 375 ± 4 | 375.7 ± 2.5* | 23 |
| H−CHO | 364 ± 4 | 368.4 ± 0.7 | 376 ± 4 | 370.86 ± 0.28 | 24 |
| H−$COCH_3$ | 360 ± 3 | 374.0 ± 1.3 | 372 ± 2 | | |
| H−$CH_2$OH | 393 ± 8 | 401.9 ± 0.6* | 411 ± 4 | 402.3 ± 1.3 | 25 |
| | | | | 401.1 ± 1.4 | 26 |
| $CH_3$O−H | 437 ± 4 | 436 ± 4 | 437 ± 4 | 440.2 ± 2.1* | 27 |
| | | | | 439 ± 3* | 28,29 |
| $CH_3CH_2$O−H | 436 ± 4 | 437.6 ± 0.8 | | 440 ± 5* | 28,29 |
| H−$CH_2CH_3$ | 411 ± 4 | 423.0 ± 1.7* | 422 ± 2 | 420.5 ± 1.5 | 30 |
| H−$CH_2CH_2CH_3$ | 410 ± 4 | | 422 ± 2 | 423.3 ± 2.1 | 31 |
| H−$CH(CH_3)_2$ | 398 ± 4 | 412.5 ± 1.7 | 412 ± 2 | 409.1 ± 2.0 | 31 |
| H−$CH(CH_3)CH_2CH_3$ | 400 ± 4 | 410.9 ± 2.1 | 413 ± 2 | 411.2 ± 2.1 | 31 |
| $(CH_3)_3$C−H | 390 ± 8 | 403.8 ± 1.7 | 400 ± 3 | 404.3 ± 1.3 | 31 |
| $C_6H_5$O−H | 362 ± 4 | | 368 ± 6 | 371.3 ± 2.3 | 32 |
| | | | | 377 ± 13* | 33,34 |
| | | | | 381 ± 4* | 35 |
| $(CH_3)_2$CHO−H | 432.6 ± 4 | | | 443 ± 4* | 28,29 |
| $(CH_3)_3$CO−H | 439.7 ± 4 | | | 446 ± 3* | 28,29 |
| $NH_3$ | 449 ± 5 | 452.6 ± 1.1*, [a,c] | | 451.9 ± 1.3*,[d] | 36,37,39 |
| | | | | 450.1 ± 0.2[a] | 38 |
| $CH_3$S−H | 379 ± 8 | 365.7 ± 2.1* | | 364.2 ± 1.6*,[e] | 40 |
| H−$CH_2$CN | 389 ± 10 | 397 ± 9* | | | |
| H−$CH_2$CCH | 374 ± 8 | | 372 ± 4 | 378 ± 13* | 41 |
| HF | | 570.7 ± 0.8 | | 570.09 ± 0.01*,[a,b] | |
| HCl | | 431.58 ± 0.13 | | 431.48 ± 0.01*,[a,b] | |
| HCN | 518 ± 8 | 527.6 ± 1.7* | | 528.5 ± 0.9[a] | 44 |
| $H_2O$ | 498 ± 4 | 499.2 ± 0.2 | | | |
| $H_2S$ | 381 ± 4 | 381.6 ± 2.9 | | 381.9 ± 0.5 [a] | 42 |
| | | | | 379.8 ± 4.4* | 43 |
| | | | | 381.6 ± 0.1*,[a,b] | 45 |

*Quantities obtained from gas-phase ion chemistry techniques. [a] Thermal corrections to 298 K from Gurvich et al.[78,79] [b] $\Delta_{acid}H_0$(RH) + $EA_0$(R) − $IE_0$(H) from Table 4. [c] $AE_0(NH_2^+, NH_3)^{202}$ = 15.768 ± 0.004 eV minus $IE_0(NH_2^+)^{466}$ = 11.14 ± 0.01 eV. [d] Using $\Delta_rH_{298}(NH_2^- + H_2 \rightarrow NH_3 + H^-)^{36}$ = −13.4 ± 1.3 kJ/mol, electron affinities[37,39] of H and $NH_2$, and $D_0(H_2)$ and IHC corrections from Gurvich et al.[78,79] [e] Using $\Delta_fH_{298}(CH_3SH)$ = −22.9 ± 0.6 kJ/mol from Pedley,[13] $\Delta_fH_{298}(CH_3)^{16}$ = 146.6 ± 0.4 kJ/mol, and $\Delta_fH_{298}$(H) and IHC corrections for $CH_3$, S, and $CH_3S$ (≈$CH_3Cl$) from Gurvich et al.[78,79]

Accepted values for R−H bond dissociation enthalpies for relatively small hydrocarbons have undergone significant revisions in the past two decades, and some values are still uncertain. Table 1 presents bond dissociation enthalpies of organic compounds from three past reviews for comparison. The frequently quoted review of McMillen and Golden[14] from 1982 is based mostly on halogenation kinetics and gives a historical perspective. The 1994 review by Berkowitz, Ellison, and Gutman[6] evaluates values from the negative-ion cycle (eq 5), the appearance energy cycle (eq 6), and flash photolysis radical kinetics using photoionization mass spectrometry as a detection technique. The 1996 review by Tsang[15] evaluates bond energies obtained by shock tube techniques and other neutral kinetics measurements. All bond dissociation enthalpies that appear in at least two of these reviews have been listed, along with some values that have been remeasured recently.[16−45] A majority of the values have changed by more than chemical accuracy of 4 kJ/mol since 1982, and several still have larger error bars. The upward revision of the R−H bond energies for primary, secondary, and tertiary alkanes began in the late 1970s and continued into the 1990s, and some of the values still generate controversy.[6,30,46−50] The general increase of hydrocarbon bond energies led Tsang to observe that "Bond energies increase with time!!"[50] Nevertheless, convergence seems in sight, and most values in the two reviews[6,15] from the mid-1990s agree with at least overlapping uncertainties. Quantities denoted by asterisks in Table 1 were determined by various methods discussed in this review, demonstrating the role gas-phase ion thermochemistry can play in the endeavor to improve these important quantities.

The thermochemistry of organometallic species is another area where gas-phase ion chemistry methods have played a major part.[51−55] Traditional calorimetric methods are especially difficult to apply to compounds containing metals because of the difficulty of characterizing metal oxide or other products.[56] Ion methods allow determination of metal-ion−ligand binding energies and of M−C and M−H bond dissociation energies in ions, including systems where the metal center is unsaturated. Using eqs 1 and 2,

the ionic dissociation energies can be converted to dissociation energies for the corresponding neutral species.

A variety of mass spectrometry and ion spectroscopy techniques have been developed to measure ion thermochemical quantities. Mass spectrometry allows a gas-phase ion of known mass to be isolated and manipulated, which circumvents issues of sample synthesis and purification in thermochemical measurements on condensed-phase systems. The most precise and accurate measurements of molecular energetics, including ions, come from spectroscopic measurements, where transitions between initial and final quantum states are individually resolved and assigned. Direct absorption measurements on gas-phase molecular ions as a function of wavelength[57−60] are far from routine because of low attainable ion densities (in mass-selected beams) or complex mixtures of neutral and ionic species (in discharge plasmas). Cryogenic matrix isolation techniques can also yield spectra of ions,[61−63] including mass-selected ions.[64] Action spectroscopy, in which a spectroscopic transition is observed indirectly via detection of a particle, is ideally suited for ions using mass spectrometry techniques.[65−67] Mass spectrometry allows a spectroscopic event to be detected and at the same time can provide initial mass selection of the absorber, or mass analysis of the products, or both. Most of the spectroscopy techniques applied to gas-phase ion thermochemistry measurements involve some form of action spectroscopy, with detection of electrons, molecular ions, or fragment ions.

Aside from spectroscopic determinations, ion−molecule reaction equilibrium measurements can provide the most accurate ion thermochemistry values. Ion concentrations are sampled directly from an equilibrium system using mass spectrometry. For nonequilibrium systems or where not all the reactants and products are stable or easily produced, unimolecular and bimolecular kinetics methods have been developed by ion chemists to obtain thermochemical information. This work surveys experimental methods available for ion thermochemistry measurements with case studies presented for many of the techniques. Because both comprehensive compilations and specialized reviews of ion and neutral thermochemical quantities are available,[6,13,15,50,54,68−93] this work does not attempt to review individual measurements except as representative examples of experimental methods. Techniques that use mass spectrometry primarily for detection of neutral molecules are not included. Ion structure is intimately related to ion energetics, and the spectroscopic techniques discussed here often depend on assignment of structures. However, this review concentrates on the thermochemical applications rather than spectroscopic results. Theoretical calculations using ab initio molecular orbital theory or density functional theory have become extremely important for the experimental chemist in general and for ion chemists in particular. Modern theory rivals the accuracy of experimental thermochemistry in some cases and is indispensable for the interpretation of experiments in others. Thermochemical applications of theory have been reviewed recently[94] and are beyond the scope of this work.

The next section defines thermochemical quantities and conventions of interest in ion chemistry. Section III describes the major thermochemical compilations. Sections IV and V summarize basic concepts of statistical rate theory and threshold measurements, which are important in the analysis of many of the experiments reviewed here. The rest of the review is organized into broad categories of experimental methods, grouped according to the chemical or photophysical processes studied rather than by the specific instrumentation used. Various instrumental techniques for mass spectrometry and for studying ion−molecule reactions have been reviewed by Farrar and Saunders[95] and elsewhere in this issue. A historical perspective is given as appropriate for the thermochemical techniques discussed here, but methods currently in wide use and new methods developed in the past decade are emphasized.

## II. General Information

### A. Thermodynamic Quantities

Ion thermochemical values are usually reported as differences of molar enthalpies ($\Delta H$) or molar Gibbs energies ($\Delta G$) between products and reactants of a specified reaction. These fundamental quantities are related by the standard thermodynamic relationships $\Delta H = \Delta U + \Delta(pV)$ and $\Delta G = \Delta H - T\Delta S$ for molar internal energy change $\Delta U$, pressure $p$, molar volume $V$, temperature $T$, and molar entropy change $\Delta S$. Gibbs energies of reaction are commonly reported from equilibrium constant measurements using eq 7.

$$\Delta G_T^\circ = -RT \ln K_T^\circ \tag{7}$$

At 0 K, $\Delta_r H_0 = \Delta_r U_0 = \Delta_r G_0$ for any gas-phase reaction. Corrections for thermal effects at other temperatures are outlined in section II.C.

Quantities that are actually enthalpies are often loosely called energies in the literature, an imprecise but mostly harmless practice. The term “free energy” is discouraged because of possible confusion between the Gibbs energy, $G = H - TS$, and the Helmholtz energy, $A = U - TS$. Other terms in frequent use include “affinity”, which usually implies an energy or enthalpy change, and gas-phase “acidity” and “basicity”, which are often defined as Gibbs energies but more loosely may be enthalpies. These quantities are typically defined as positive values, i.e., for the reaction written in the endothermic ($\Delta H > 0$) or endergonic ($\Delta G > 0$) direction. In this review, I retain these terms in wide use and thus avoid accurate but awkward phrases such as “enthalpy of electron detachment” for electron affinity (to give one example). Regardless of the naming of various quantities, thermodynamic quantities and temperatures should be specified explicitly as $\Delta_r U_T$, $\Delta_r H_T$, or $\Delta_r G_T$ in experimental reports.

### B. Ion Thermochemical Quantities

The *ionization energy* or *enthalpy* (IE) of an atom or molecule refers to the removal of an electron from

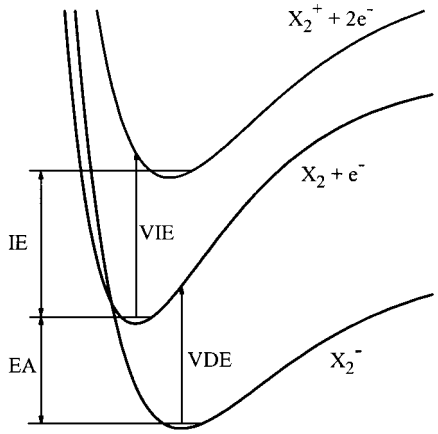


**Figure 3.** Schematic potential energy curves showing the definitions of the adiabatic electron affinity (EA), adiabatic ionization energy (IE), vertical detachment energy (VDE), and vertical ionization energy (VIE).

a neutral species, eq 8.

$$M \rightarrow M^+ + e^- \quad \Delta_I H_T = IE_T(M) \tag{8}$$

The ionization energy is historically termed the ionization potential (IP). The analogous energy required to remove an electron from an anion is the *electron affinity* (EA) of the neutral, eq 9.

$$M^- \rightarrow M^+ + e^- \quad \Delta_{EA} H_T = EA_T(M) \tag{9}$$

With this convention, stable anions are associated with positive values of the electron affinity. Traditionally, process 8 is called *ionization* and process 9 is called *detachment*. As used here, $IE_0$ and $EA_0$ for molecules are adiabatic energies for the transitions between the ground states of the ions and neutrals. *Vertical ionization energies* (VIE) or *vertical detachment energies* (VDE) are defined as the energies between the lower charge state and the potential energy surface of the upper charge state at the equilibrium geometry of the lower state. These relationships are depicted in Figure 3. In spectroscopic processes governed by the Franck−Condon principle, vertical transitions have the highest probability. A glossary of abbreviations is given in Table 2.

The *appearance energy* or *enthalpy* (AE) is the minimum energy required to form a cationic fragment from a neutral molecule via dissociative ionization, eq 10.

$$AB \rightarrow A^+ + B \quad \Delta_{AE} H_T(A^+, AB) = AE_T(A^+, AB) \tag{10}$$

Appearance energies (historically called appearance potentials) have been measured by both electron ionization and photoionization threshold measurements for a large variety of systems. Accurate values are important for applying the appearance energy cycle, eq 6. Appearance energies for negative-ion fragments or ion-pair formation can also be measured.

The *proton affinity* (PA) of neutral molecule B is defined as the enthalpy of eq 11.

$$BH^+ \rightarrow B + H^+ \quad \Delta_{PA} H_T(B) = PA_T(B) \tag{11}$$

The Gibbs energy change for eq 11, $\Delta_{PA} G_T(B)$, is called the *gas-phase basicity* of B. The proton affinity of an anion $A^-$ is known as the *gas-phase acidity* of HA and is expressed either as the Gibbs energy or enthalpy of eq 12.

$$HA \rightarrow A^- + H^+ \quad \Delta_{acid} G_T(HA) \text{ or } \Delta_{acid} H_T(HA) \tag{12}$$

A *bond dissociation enthalpy* (BDE) applies to a fragmentation process where it is known that a specific bond is cleaved, for example, eq 13 for breaking the R−H bond.

$$RH \rightarrow R\cdot + H\cdot \quad \Delta_D H_T(R{-}H) = BDE_T(R{-}H) = DH_T(R{-}H) \tag{13}$$

BDEs usually refer to neutral species RH at 298 K. The corresponding 0 K bond dissociation energy,

**Table 2. Abbreviations**

| | | | |
|---|---|---|---|
| acid | acidity (deprotonation) | PD | photodissociation |
| AE | appearance energy | PES | photoelectron spectroscopy |
| at | atomization | PFI | pulsed field ionization |
| BIRD | blackbody infrared dissociation | PIE | photoionization efficiency |
| BDE | bond dissociation energy or enthalpy | PIMS | photoionization mass spectrometry |
| CID | collision-induced dissociation | PST | phase space theory |
| D | dissociation | PT | proton transfer |
| EA | electron affinity | PTS | photofragment translational spectroscopy |
| eBE | electron binding energy | REMPI | resonantly enhanced multiphoton ionization |
| ECD | electron capture detector | RRKM/QET | Rice−Ramsperger−Kassel−Marcus/quasi-equilibrium theory |
| EI | electron ionization | S | solvation |
| eKE | electron kinetic energy | SIFDT | selected-ion flow-drift tube |
| ET | electron transfer | SIFT | selected-ion flow tube |
| FALP | flowing afterglow Langmuir probe | SORI | sustained off-resonance irradiation (ICR) |
| GIB | guided-ion beam | TPEPICO | threshold photoelectron photoion coincidence |
| HPMS | high-pressure mass spectrometry | TCID | threshold collision-induced dissociation |
| ICR | ion cyclotron resonance | TIPPS | threshold ion-pair production spectroscopy |
| I | ionization | TPES | threshold photoelectron spectroscopy |
| IE | ionization energy | VDE | vertical detachment energy |
| IHC | integrated heat capacity | VIE | vertical ionization energy |
| IRMPD | infrared multiphoton dissociation | ZEKE | zero electron kinetic energy |
| MATI | mass-analyzed threshold ionization | ZTRID | zero-pressure thermal radiation-induced dissociation |
| PA | proton affinity (basicity) | | |

$D_0(\mathrm{R-H}) = \Delta_D H_0$, refers here to the dissociation of a molecule in its ground electronic, vibrational, and rotational state to form the ground states of the products (regardless of whether an adiabatic potential energy surface connects to those products). Above 0 K, RH bond dissociation enthalpies are related to bond dissociation energies by $\Delta_D H_T(\mathrm{R-H}) = \Delta_D U_T(\mathrm{R-H}) + RT$.

The energetics of the association of gas-phase ions with neutral molecules has been studied extensively.[3−5] Enthalpies for the process in eqs 14 and 15 are termed $M^+$ or $X^-$ ion affinities of species L.

$$\mathrm{M^+(L) \rightarrow M^+ + L} \quad \Delta_{\mathrm{M^+}} H_T(\mathrm{L}) \tag{14}$$

$$\mathrm{X^-(L) \rightarrow X^- + L} \quad \Delta_{\mathrm{X^-}} H_T(\mathrm{L}) \tag{15}$$

When the emphasis is on the neutral reagent for various ions, the enthalpy change for the analogous reaction is variously named complexation enthalpy, solvation or hydration enthalpy, ligation enthalpy, or clustering enthalpy depending on the nature of the system. Stepwise solvation enthalpies are given by eqs 16 and 17, for which the solvation or complexation enthalpies are negative quantities.

$$\mathrm{M^+(S)}_{n-1} + \mathrm{S \rightarrow M^+(S)}_n \quad \Delta_{\mathrm{S},n} H_T(\mathrm{M^+}) \tag{16}$$

$$\mathrm{X^-(S)}_{n-1} + \mathrm{S \rightarrow X^-(S)}_n \quad \Delta_{\mathrm{S},n} H_T(\mathrm{X^-}) \tag{17}$$

For comparison with theoretical calculations, it is useful to use *atomization energies* instead of enthalpies of formation,[96,97] since enthalpies of formation are impractical to calculate directly for elements with condensed phases as standard reference states. The atomization energy is defined as the energy to dissociate a molecule into its constituent gas-phase atoms, eq 18.

$$\mathrm{ABC \rightarrow A + B + C} \quad \Delta_{\mathrm{at}} H_T(\mathrm{ABC}) \tag{18}$$

For comparison with experiment, theoretical calculations of $\Delta_{at}H_0$ must include zero-point energies obtained from vibrational frequencies. Further thermal corrections are required to obtain reaction energies or enthalpies at 298 K. In some hybrid empirical and theoretical methods, experimental enthalpies of formation of the gaseous atoms or elements are combined with theoretical energies to estimate the molecular enthalpy of formation,[80,81,97,98] otherwise, isodesmic reactions are employed to relate a calculated energy with an experimental reference bond energy.[49,99] For ions, atomization energies may be defined[78] by the reactions $\mathrm{ABC^+ + e^- \rightarrow A + B + C}$ and $\mathrm{ABC^- \rightarrow A + B + C + e^-}$, but calculated ionization energies and electron affinities are usually compared directly with experimental values.[81,98]

## C. Temperature Effects

Because ionization energies and electron affinities are often measured spectroscopically from an assigned 0←0 ground-state transition, they are typically reported as 0 K energy differences. In contrast, ion−molecule reaction equilibrium and kinetics measurements are often carried out at room temperature or higher. The effects of different (and sometimes poorly known) temperatures for various experiments has caused considerable difficulty for establishing unified proton affinity[84] and gas-phase acidity[75] scales. This section describes how thermochemical quantities are converted from one temperature to another.

Enthalpy changes at different temperatures are related by Kirchhoff's law, eq 19.

$$\Delta_r H_T = \Delta_r H_{0\mathrm{K}} + \int_{0\mathrm{K}}^{T} \Delta_r C_p(T)\, \mathrm{d}T \tag{19}$$

The integrated heat capacities for gas-phase species can often be calculated with sufficient accuracy using standard statistical mechanics formulas in the independent mode, harmonic oscillator, and rigid rotor approximations using either experimental, ab initio, or semiempirical molecular parameters.[100] Calculated vibrational frequencies may be scaled by empirical factors to improve their accuracy.[101] Cases where anharmonicity is significant or there are internal free or hindered rotors may require more refined treatment.[10,102]

Conversion between $\Delta H_T$ and $\Delta G_T = \Delta H_T - T\Delta S_T$ requires knowledge of the entropy change $\Delta S_T$, either experimentally from temperature-dependent equilibrium measurements or theoretically by eq 20 and statistical mechanics for the heat capacity functions.[100]

$$\Delta S_T = \Delta S_{0\mathrm{K}} + \int_{0\mathrm{K}}^{T} (1/T)\, \Delta C_p(T)\, \mathrm{d}T \tag{20}$$

Often the primary contributions to $\Delta S$ are obtained from the translational effects (change in the number of species from reactants to products) and rotational effects (change in the number of rotational degrees of freedom, the rotational symmetry, or the number of internal rotors).[21,100,103]

Conversions from $\Delta U_T$ to $\Delta H_T = \Delta U_T + \Delta(pV)$ use the ideal gas law to calculate $\Delta(pV) = RT\Delta n$, where $\Delta n$ is the change in the number of gas-phase atoms or molecules in the reaction. For compatibility with enthalpies of reaction tabulated for neutrals, the $\Delta pV$ work term in the enthalpy is properly included for ions. Using the hypothetical ideal gas as the standard state simply means that intermolecular interactions are neglected,[83,104] avoiding the obvious difficulties with intermolecular interactions for charged species actually at the standard pressure of $p^\circ = 1$ bar. Interactions between charged particles may need to be considered in dense plasmas.

## D. Thermodynamics of the Electron

Ionization or other processes producing or consuming free electrons require special treatment. For IEs and EAs, the enthalpy change at standard ambient temperature (298 K) is obtained by applying Kirchhoff's law, eq 19, for eqs 8 and 9. The abbreviation $\mathrm{IHC}_T(\mathrm{X})$ will be adopted for the integrated heat capacity of species X[105]

$$\mathrm{IHC}_T(\mathrm{X}) = H_T(\mathrm{X}) - H_0(\mathrm{X}) = \int_0^T C_p(\mathrm{X})\, \mathrm{d}T \tag{21}$$

yielding eqs 22 and 23.

$$\Delta_I H_T = IE_0 + IHC_T(M^+) + IHC_T(e^-) - IHC_T(M) \quad (22)$$

$$\Delta_{EA} H_T = EA_0 + IHC_T(M) + IHC_T(e^-) - IHC_T(M^-) \quad (23)$$

If the geometry and frequencies of the charged molecule are similar to those of the neutral, as is often the case, and neither has low-lying electronically excited states, then the neutral/ion pair have about the same integrated heat capacities and those two terms approximately cancel, i.e., $IHC(M^+) \approx IHC(M)$ and $IHC(M^-) \approx IHC(M)$. Bartmess[105] has shown for a variety of anions that this common approximation usually produces errors of less than 2 kJ/mol. For more precise determinations, calculating the IHC correction is straightforward for most systems using experimental or theoretical molecular parameters.[100]

The remaining term in eqs 22 and 23 is the integrated heat capacity of the electron, $IHC_T(e^-)$, which is problematic because of different conventions for the treatment of the electron.[104] The "electron convention", adopted by the NIST-JANAF tables,[83] Gurvich et al.,[78,79] and other neutral thermochemistry compilations, treats the standard reference state of the electron as for elements, i.e., its enthalpy of formation is defined as zero at all temperatures, $\Delta_f H_T°(e^-) = 0$. The integrated heat capacity of the electron at 298 K is calculated for an ideal gas using classical Boltzmann statistics,[83] yielding $IHC_{298}(e^-) = {}^5/_2 RT = 6.197$ kJ/mol. The "ion convention" has been adopted in *Gas-Phase Ion and Neutral Thermochemistry*,[73] the *NIST Chemistry Webbook*,[106] and other ion thermochemistry compilations. As described by Lias and Bartmess,[107] in the ion convention the enthalpy of formation of the electron is defined as equal to its integrated heat capacity, $\Delta_f H_T^{(+)}(e^-) \equiv IHC_T(e^-)$, at all temperatures. Bartmess[104] recommends that quantum Fermi−Dirac statistics be used for calculating $IHC_T(e^-)$, recognizing that for electrons as fermions the number of populated quantum states is restricted at low temperatures compared with classical noninteracting particles. The thermodynamic values[104] for the electron using Fermi−Dirac statistics at 298 K are $IHC_{298}(e^-) = 3.145$ kJ/mol and $S_{298}(e^-) = 22.73$ J mol$^{-1}$ K$^{-1}$.

The actual value of $IHC_T(e^-)$ need not be known for calculating ion enthalpies of formation using the ion convention. The ion enthalpy of formation is related to that of the neutral by eqs 24 and 25.

$$\Delta_f H_T(M^+) = \Delta_f H_T(M) + \Delta_I H_T(M) - \Delta_f H_T(e^-) \quad (24)$$

$$\Delta_f H_T(M^-) = \Delta_f H_T(M) - \Delta_{EA} H_T(M) + \Delta_f H_T(e^-) \quad (25)$$

Combining these with eqs 22 and 23, one obtains eqs 26 and 27.

$$\Delta_f H_T(M^+) = \Delta_f H_T(M) + IE_0 - [\Delta_f H_T(e^-) - IHC_T(e^-)] + [IHC_T(M^+) - IHC_T(M)] \quad (26)$$

$$\Delta_f H_T(M^-) = \Delta_f H_T(M) - EA_0 + [\Delta_f H_T(e^-) - IHC_T(e^-)] + [IHC_T(M^-) - IHC_T(M)] \quad (27)$$

In each case, the terms inside the first set of square brackets cancel exactly in the ion convention because $\Delta_f H_T^{(+)}(e^-) \equiv IHC_T(e^-)$ by definition. The terms inside the second set of square brackets approximately cancel as discussed above. Thus, one obtains the approximate relations, eqs 28 and 29.

$$\Delta_f H_T^{(+)}(M^+) \approx \Delta_f H_T°(M) + IE_0 \quad (28)$$

$$\Delta_f H_T^{(+)}(M^-) \approx \Delta_f H_T°(M) + EA_0 \quad (29)$$

These approximations have been used to derive most of the ion enthalpies of formation at 298 K in the ion chemistry literature. Considerable confusion and not a little revisionism exists in the literature regarding the ion convention, variously described in earlier work as the "stationary electron" convention, as $IHC_T(e^-) = 0$ (incorrect but moot for eqs 26 and 27) or as $\Delta_f H_T(e^-) = 0$ (incompatible with the current definition).[7,73,103,104,108−111] The ion convention originated historically from the neglect of thermal corrections in early compilations of ion heats of formation obtained from appearance potentials and ionization potentials,[108,109] which was reasonable at the time given the uncertainty of most experiments. Later, the approximate eqs 28 and 29 became the de facto definitions of the "ion convention".

In practical terms, enthalpies of formation of gas-phase cations at 298 K are uniformly 6.197 kJ/mol higher in the electron convention than in the ion convention. For example, the enthalpy of formation of the proton is $\Delta_f H_{298}°(H^+) = 1536.2$ kJ/mol in the electron convention[78] and $\Delta_f H_{298}^{(+)}(H^+) = 1530.0$ kJ/mol in the ion convention. The enthalpies of formation of anions have the reverse relationship, lower by 6.197 kJ/mol in the electron convention than in the ion convention, for example $\Delta_f H_{298}°(H^-) = 139.0$ kJ/mol and $\Delta_f H_{298}^{(+)}(H^-) = 145.2$ kJ/mol. These differences cancel exactly for calculations of reaction enthalpies except when a free electron appears as a reactant or product. For example, the gas-phase acidity of $H_2$ is given by $\Delta_{acid} H_{298}(H_2) = \Delta_f H_{298}(H^+) + \Delta_f H_{298}(H^-) = 1675.2$ kJ/mol in both conventions. In practice, either convention works as long as enthalpies of formation for charged species using different conventions are not mixed.

## E. Units

Proton affinities, gas-phase acidities and basicities, and bond energies have traditionally been reported in kcal/mol units. Use of SI units, kJ/mol instead of kcal/mol (1 cal = 4.184 J), is becoming widespread. Energy unit conversions used in this work are taken from the 1998 CODATA revision of the fundamental constants.[112] For ion chemists, kJ/mol units have the advantage of reducing conversion round-off error for measurements made in electronvolts[55] (1 eV = 96.4853 kJ/mol ≈ 100 kJ/mol). Electron affinities and ionization energies are traditionally reported in electronvolts or wavenumbers ($hc \times 8065.54477(32)$ cm$^{-1}$ =

1 eV). For spectroscopically determined transition energies at 0 K, e.g., for $EA_0$ and $EI_0$, continued use of energies per molecule in (SI-related) electronvolts rather than molar energies in kJ/mol is reasonable. Reporting extremely precise spectroscopic results as frequencies or wavenumbers is necessary because the conversions to eV and kJ/mol have uncertainties ($1\sigma$) of 40 and 8 ppb, respectively.[112]

## F. Uncertainties

A reported physical quantity is of use only when both its value and its reliability are known. This is especially true in thermochemistry, where experimental values from different measurements are often combined to derive new information. Therefore, it is crucial that the uncertainties including those from both random effects and systematic effects on the measurement be estimated and reported for thermochemical values. Unfortunately, papers with incomplete error analyses remain all too common. Statistical methods for estimating uncertainties from random effects based on replicate measurements have been treated extensively.[113−116] Additional sources of uncertainties may be estimated from calibration measurements using the same method, uncertainties of auxiliary data and model parameters used in the analysis, and the scientific judgment of the experimenters. A guide for expressing both types of uncertainties as the "combined standard uncertainty" has been published by NIST.[116] Experimental work should specify the method of estimation and the type of uncertainty reported.[116] For physical measurements, reporting 95%-confidence intervals or roughly ±2 combined standard uncertainties is the norm but not universal. Qualitatively, that uncertainty should mean that if two independent measurements differ by more than the sum of their 95%-confidence-interval uncertainties, then at least one most likely has serious systematic errors.

Ion energy scales such as the proton affinity scale[84] and the gas-phase acidity scale[75,86] rely on many relative measurements to create a ladder of values. These relative values are anchored to independent absolute measurements for a few or many reference molecules. Hence, the relative uncertainties and the absolute uncertainties may be different. For the proton affinity and gas-phase acidity scales, the relative uncertainties of equilibrium measurements for species with similar values are often within ±1 kJ/mol, but of course other measurements are much less precise. The absolute uncertainty of the anchoring of each scale as a whole is around ±8 kJ/mol. When older reports give a relative measurement based on an out-of-date anchoring of the ion energy scale, then it is necessary to revise the absolute quantity based on the updated values for the reference species used in the original work.

# III. Thermochemistry Compilations

Table 3 lists major compilations and specialized reviews of gas-phase ion and neutral thermochemistry.[6,13,15,50,54,68−93,117−128] Older compilations that have been substantially superseded are not included. Compilations of thermochemical values, especially those that include critically evaluated quantities, are useful for accessing a wide range of thermochemical data that otherwise may be difficult to find in the huge primary literature. A recent and extraordinarily useful entrant into this arena is the NIST Chemistry Webbook,[106] which allows online access to multiple databases for physical properties of molecules including several of the other compilations listed in Table 3. On-line access means, for example, that a question about the thermochemistry of a putative fragment ion in a mass spectrum can often be answered immediately at a computer terminal in the mass spectrometry laboratory.

Use of the compilations requires some discrimination. First, one must be aware of different conventions used for ion enthalpies of formation, as discussed in section II.D. Second, while access may be instant, the information in any compilation is necessarily dated by the time it is published. Some of the compilations in Table 3 are now seriously dated, and newer editions are not necessarily fully updated. For standard enthalpies of formation of neutral compounds, the compilations of Gurvich et al.[78,79] and Pedley[13] are most up-to-date and self-consistent. Third, the quality and sources of the original data may vary widely between different compilations and within the same compilation. A compilation can only include partial information about the quality of the experiments through cited uncertainties and indication of the experimental method. For critical information, i.e., for auxiliary values used to derive new thermochemical quantities, the compilations should serve as an initial guide, not as a replacement for a literature review. Finally, the still-evolving NIST Chemistry Webbook[106] as currently structured is not of archival quality—newer revisions may correct or update quantities or recommendations with no record of change. Therefore, it is prudent to cite critical thermochemical values as numerical values from the original literature or at least from an archival version of the compilation.

# IV. Statistical Rate Theory of Unimolecular Dissociation

Many of the kinetic methods described here rely on measurement of the rate of dissociation of a molecular ion to extract a dissociation energy. Other experiments are dissociation threshold energy measurements, but because the mass spectrometric detection of products has a limited time window, a "kinetic shift" may be present.[129,130] A kinetic shift occurs when some ions have internal energy above the threshold for dissociation but do not actually dissociate before mass analysis and detection. In the case of multiple dissociation channels, the higher channel can be subject to a "competitive shift" in which its apparent threshold is shifted to a higher energy because the more favorable channel predominates.[129,130] A basic tenet of statistical rate theory is that only the total energy and angular momentum of an activated ion determines the dissociation rate, not the method of activation. Therefore, the statistical theory can be applied in many of the ion experiments

**Table 3. Thermochemical Compilations and Reviews**

| compilation | quantities[a] | species | convention[b] | ref |
|---|---|---|---|---|
| *NIST-JANAF Thermochemical Tables* (Chase et al.) | enthalpies of formation (*T*) | inorganic compounds and small molecules | electron | 83 |
| *Thermochemical Data of Organic Compounds* (Pedley) | enthalpies of formation (298 K) | neutral organic compounds | n/a | 13 |
| *Gas-Phase Ion and Neutral Thermochemistry* (Lias et al.) | enthalpies of formation (0 and 298 K), electron affinities and ionization energies (0 K), gas-phase acidities (298 K) | positive and negative ions | ion | 73 |
| *Negative Ion Energetics Data* (Bartmess) | electron affinities (0 K), gas-phase acidities (298 K) | negative ions | ion | 86 |
| *Proton Affinity Evaluation* (Hunter and Lias) | proton affinities (298 K) | positive ions | ion | 87 |
| *Ionization Energy Evaluation* (Lias) | ionization energies (0 K) | positive ions | ion | 88 |
| *Ion Energetics Data* (Lias et al.) | enthalpies of formation (298 K) | positive ions | ion | 89 |
| *Binding Energies Between Ions and Molecules, and the Thermochemistry of Cluster Ions* (Mautner) | complexation enthalpies | positive and negative ions | ion | 92 |
| *Electron Affinities of Atoms and Molecules: Theory and Experiment* (Rienstra-Kiracofe et al.) | electron affinities (0 K) | organic and inorganic molecules and radicals | n/a | 93 |
| *Binding Energies in Atomic Negative Ions* (Hotop and Lineberger) | electron affinities (0 K) | atoms | n/a | 70 |
| *Evaluated Gas-Phase Basicities and Proton Affinities of Molecules: An Update* (Hunter and Lias) | proton affinities (298 K) | positive ions | *ion* | 84 |
| *Thermochemical Data on Gas-Phase Ion−Molecule Association and Clustering Reactions* (Keesee and Castleman) | complexation enthalpies | positive and negative ions | n/a | 71 |
| *Thermochemical Properties of Individual Substances* (Gurvich et al.) | enthalpies of formation (*T*) | inorganic and small organic neutrals | electron | 78,79 |
| *Neutral Thermochemical Data* (Afeefy et al.) | enthalpies of formation (298 K) | gas-phase neutrals | n/a | 91 |
| *Organometallic Thermochemistry Data* (Martinho Simões) | enthalpies of formation and entropies (298 K) | organometallic compounds | n/a | 90 |
| *CODATA Key Values for Thermodynamics* (Cox et al.) | enthalpies of formation (*T*) | small gas- and condensed-phase species | n/a | 77 |
| *Organometallic Ion Chemistry: Table of Bond Energies* (Freiser) | dissociation energies (0 K) | transition-metal cation/ligand systems | n/a | 54 |
| *Atomic Energy Levels* (Moore et al.) | ionization energies and excited-state levels (0 K) | neutral and cationic atomic ions | n/a | 68,117−128 |
| *G3/99 Test Set* (Curtiss et al.) | enthalpies of formation (298 K), ionization energies and electron affinities (0 K) | molecules of first- and second-row elements | n/a | 80−82 |
| *Three Methods to Measure RH Bond Energies* (Berkowitz et al.) | EAs and IEs (0 K), gas-phase acidities, bond dissociation enthalpies, enthalpies of formation (0 and 298 K) | small organic molecules and inorganic hydrides | ion | 6 |
| *Constants of Diatomic Molecules* (Huber and Herzberg) | dissociation energies and spectroscopic constants (0 K) | neutral and ionic diatomics | n/a | 69 |
| *Electron Affinities and Electron-Transfer Reactions* (Kebarle and Chowdhury) | electron affinities (Gibbs energies) (353−423 K) | negative ions | ion | 72 |
| *Gas-phase Equilibrium Affinity Scales* (Bartmess) | gas-phase acidities (298 K) | negative ions | ion | 75,76 |
| *Clusters of Transition Metals* (Morse) | dissociation energies and spectroscopic constants (0 K) | transition-metal diatomics | n/a | 74 |
| *ZEKE Spectroscopy* (Schlag) | ionization energies and electron affinities (0 K) | neutral molecules and anions | n/a | 85 |
| *Heats of Formation of Organic Free Radicals by Kinetic Methods* (Tsang) | dissociation enthalpies and radical enthalpies of formation (298 K) | organic molecules | n/a | 15,50 |

[a] Temperatures in parentheses; *T* indicates temperature-dependent data. [b] Treatment of electron heat capacity (section II.D); n/a = not applicable (gas-phase ion enthalpies of formation not reported).

reviewed here, including thermal activation, radiative activation, laser photodissociation, dissociative photoionization, dissociative electron ionization, collision-induced dissociation, and metastable ion dissociation. Because of their importance for evaluating experimental measurements, the basic equations are restated here.

Statistical rate theory defines the microcanonical rate coefficient $k(E)$ or the canonical rate coefficient $k(T)$ for unimolecular dissociation as a function of the

dissociation energy and molecular parameters. The statistical rate theory for unimolecular reactions is known as Rice−Ramsperger−Kassel−Marcus (RRKM) or quasi-equilibrium theory (QET).[131−139] Historically, QET was developed independently and used in the mass spectrometry literature to explain breakdown curves while RRKM was developed for neutral reaction kinetics, but they are identical.[131,132]

The simplest form of microcanonical unimolecular rate theory is the classical Rice−Ramsperger−Kassel (RRK) theory, which models the system as $s$ identical classical harmonic oscillators. The classical RRK rate coefficient is given by eq 30

$$k(E) = \nu\left(\frac{E - E_0^{\ddagger}}{E}\right)^{s-1} \tag{30}$$

where $k(E)$ is the rate coefficient for a microcanonical ensemble of isolated molecules, each with internal energy $E$, $\nu$ is the frequency of the harmonic oscillators, and $E_0^{\ddagger}$ is the minimum energy required to dissociate the molecule. Because the classical RRK model underestimates rates, the number of oscillators is sometimes empirically reduced by a factor of 2−5.[133,134,140] The classical RRK model or its quantum version[132,133] captures the essentials of statistical rate theory and thus is useful for qualitative analysis of energy-dependent rates[140,141] or for crude order-of-magnitude estimates of rates (with the empirical reduction in $s$), but it is inadequate for quantitative modeling of experiments.

Microcanonical RRKM/QET theory is the preferred method for quantitative modeling of experiments on isolated ions whose internal energy is a fixed quantity. Its basic form is given by eq 31

$$k(E,J) = s\,\frac{W^{\ddagger}(E - E_0^{\ddagger},J)}{h\rho(E,J)} \tag{31}$$

where $W^{\ddagger}(E - E_0^{\ddagger},J)$ is the number of rovibrational energy states of the transition-state configuration at total energy $E$, total angular momentum $J$, and with a minimum potential energy barrier $E_0^{\ddagger}$; $\rho(E, J)$ is the density of rovibrational states of the energized molecule; $s$ is the reaction degeneracy; and $h$ is Planck's constant. Variations of RRKM theory relate to the treatment of angular momentum (whether and how angular momentum is conserved when counting quantum states), how the number and densities of states are calculated, how the transition state is defined or optimized in the case of variational transition-state theory, and how multiple potential energy surfaces or multiple wells are handled.[133−139,142,143] Equation 31 may be averaged over the distribution of angular momentum $J$ (or as an approximation calculated for an average value of $J$ or for $J = 0$) to obtain the energy-dependent microcanonical rate $k(E)$.

For the transition-state energy, $E_0^{\ddagger}$, to be equated with a thermochemical reaction energy, the reverse process must have zero activation energy. That is often valid for ionization processes and for dissociation of molecular ions. The strong long-range attractive electrostatic forces for charged products (proportional to $1/r$ for electron−cation products, $1/r^2$ for the ion−dipole potential, or $1/r^4$ for the ion-induced-dipole potential) tend to reduce activation barriers that might exist from valence interactions in neutral systems.[144]

For a reaction occurring under thermal conditions, $k(E)$ is averaged over the Boltzmann distribution of energies $E$ to yield the canonical rate constant for unimolecular dissociation as a function of temperature, $k(T)$. In its thermodynamic formulation, the canonical rate coefficient is given by eq 32[133]

$$k(T) = \frac{k_B T}{h}\frac{Q^{\ddagger}(T)}{Q_0(T)}e^{-\Delta^{\ddagger}E_0/RT} = \frac{k_B T}{h}e^{-\Delta^{\ddagger}G_T/RT} = \frac{k_B T}{h}e^{\Delta^{\ddagger}S_T/R}e^{-\Delta^{\ddagger}H_T/RT} \tag{32}$$

where $Q^{\ddagger}(T)$ is the partition function for the transition-state configuration, $Q_0(T)$ is the partition function of the energized molecule, and $\Delta^{\ddagger}E_0$, $\Delta^{\ddagger}G_T$, $\Delta^{\ddagger}S_T$, and $\Delta^{\ddagger}H_T$ refer to the transition-state configuration relative to the parent molecule. Equation 32 shows the connection between rates and thermodynamic quantities clearly, but it applies only to reactions under conditions of thermal equilibrium.

In the statistical approximation, the rate coefficients for multiple product channels are independent—$k_j(E)$ or $k_j(T)$ for product channel $j$ is obtained by substituting the appropriate transition-state parameters in eq 31 or eq 32, respectively. For isolated ions undergoing first-order decomposition, the probability $P_j(E)$ of dissociation to channel $j$ depends on the total microcanonical rate coefficient, $k_{tot}(E) = \sum k_j(E)$, and the time window of the experiment, as given in eq 33.

$$P_j(E) = \frac{k_j(E)}{k_{tot}(E)}\left(\exp[-k_{tot}(E)\cdot\tau_1] - \exp[-k_{tot}(E)\cdot\tau_2]\right) \tag{33}$$

The dependence on the angular momentum $J$ is suppressed here for notational convenience. For collision-induced or photon-induced processes, $\tau_1 = 0$ and $\tau_2$ is the time between activation and detection. For metastable ion dissociation, $\tau_1$ is the time-of-flight between the ion source and the field-free region of the mass spectrometer where dissociation occurs and $\tau_2$ is the time at the end of the field-free region. Equation 33 describes the kinetic selection of those ions that have energies corresponding to rates that allow dissociation within the instrumental time window.[141]

The nature of the transition state has a great influence on the calculated statistical rates, $k$(E) or $k(T)$, and thus needs to be considered carefully for modeling experiments. A "tight" transition state is typically but not always located at a potential energy barrier along the reaction path and has the same number of vibrational modes as the energized molecule less one treated as the reaction coordinate. A "loose" transition state is similar to the product fragments, and the transitional vibrational modes are treated as free or hindered internal rotations. A loose transition state is often appropriate for the barrier-

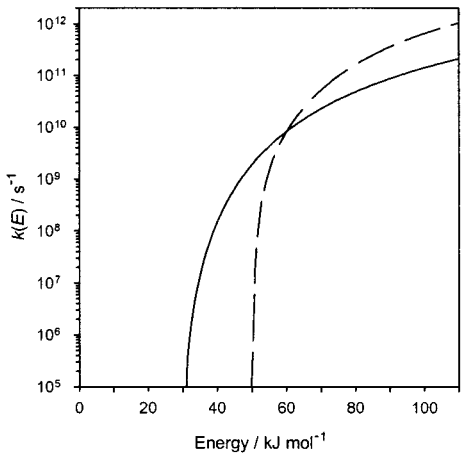


**Figure 4.** Schematic rate−energy curves showing the dependence of the RRKM unimolecular dissociation rate coefficient, $k(E)$, on total available energy for two product channels, one with a "tight" transition state with $\Delta^{\ddagger}S_{1000} = -0.4$ J mol$^{-1}$ K$^{-1}$ and $E_0 = 30$ kJ/mol (—) and one with a "loose" transition state with $\Delta^{\ddagger}S_{1000} = +18$ J mol$^{-1}$ K$^{-1}$ and $E_0 = 50$ kJ/mol (---).

less dissociation of ions, especially for dissociation of electrostatically bound ion−molecule complexes. In the "orbiting transition state"[142] or "phase space limit",[145] the transition state is located variationally at the centrifugal barrier of the ion-induced-dipole potential. There is actually a continuum between tight and loose TS models.[136]

The entropy of activation, $\Delta^{\ddagger}S_T$, is a measure of the "looseness" or "tightness" of the transition state. The temperature of the reacting system in the transition-state configuration is not well defined, so values at 1000 K are often used for comparisons.[132,146] Values of $\Delta^{\ddagger}S_T \lesssim 0$ are indicative of a tight transition state, while positive values indicate a loose transition state. Figure 4 is a plot of $k(E)$ curves for model "tight" and "loose" transition states. If a competitive dissociation occurs between a tight TS with lower threshold energy and a loose TS with a higher threshold, the two curves can cross, as in Figure 4. Thus, the energetically disfavored product channel can predominate when the experimental time window selects reactants with high internal energies rather than near-threshold energies. This possibility should provoke caution in the use of unimolecular dissociation rates for thermochemical determinations, especially for methods using a single experimental energy or temperature. Measuring the energy or temperature dependence of the rates over a wide range can expose this kind of behavior. Electronic structure calculations can often also help elucidate the characteristics of transition states.[147]

Processes other than molecular dissociation may compete in the relaxation process, including electron emission or radiative emission.[148−154] The rate theory for these processes is less well established than for unimolecular dissociation, but rapid progress is being made in this area as experiments begin to probe these processes more directly.[155−159] Under conditions where radiative emission or thermionic emission may compete with unimolecular dissociation, these processes must be considered when modeling experiments to extract dissociation energies.

## V. Threshold Behavior

Threshold energy measurements are an important means of obtaining thermochemical information from photoionization, photodetachment, electron ionization, photodissociation, bimolecular reaction, and collision-induced dissociation experiments. Measurement of a threshold energy is intrinsically difficult—the experiment must have the sensitivity and resolution to distinguish between zero signal below threshold and the finite but often small signal above threshold. Energy distributions present in all experiments to some degree tend to obscure the threshold onset. Therefore, a model for the threshold behavior is essential for extrapolating the cross section to the zero onset. The simple threshold power law given by eq 34 applies, at least approximately, for a variety of threshold processes.

$$\sigma(E) = \sigma_0 \frac{(E - E_0)^n}{E^m} \quad \text{if } E > E_0 \qquad (34)$$
$$= 0 \quad \text{if } E \le E_0$$

In eq 34, $\sigma(E)$ is the cross section (proportional to ionization, dissociation, or reaction probability) as a function of energy, $\sigma_0$ is a scaling factor that depends on the intrinsic transition strength or reaction probability, $E_0$ is the state-to-state threshold energy, and $n$ and $m$ are parameters that depend on the specific process under study.

For photoionization of atoms, the Wigner threshold law[160] states that the threshold behavior depends only on the excess kinetic energy of the electron ($E - E_0$) and the charge $Z$ of the product ion, with $m = 0$ and $n = Z - 1$ in eq 34. For photoionization of neutral atoms, $M + h\nu \rightarrow M^+ + e^-$, the Wigner threshold law yields a step function, eq 34 with $n = 0$ and $m = 0$. Experimentally, a step function is the best possible case for sensitivity at threshold. At energies above the initial step, the cross section may rise, fall, or stay level.[161,162] For higher ionization processes,[163] the Wigner threshold law is linear above the onset for $M^+ + h\nu \rightarrow M^{2+} + e^-$, quadratic for $M^{2+} + h\nu \rightarrow M^{3+} + e^-$, etc.

For photodetachment from atomic anions, $M^- + h\nu \rightarrow M + e^-$, the Wigner threshold behavior depends on the angular momentum state of the outgoing electron;[160,164,165] in eq 34, $m = 0$ and $n = l + {}^1/_2$, where $l = 0$ for an outgoing $s$-wave electron, $l = 1$ for a $p$-wave electron, etc. The selection rule is $\Delta l = \pm 1$, so detachment of $s$ electrons gives a $p$ wave ($n = 1.5$) and detachment of $p$ electrons gives a mixture of $s$ and $d$ waves which interfere but $l = 0$ ($n = 0.5$) predominates at the lowest energies. As a result, $p$-detachment, for example from $O^-$, yields a sharply rising cross section from the threshold while $s$-detachment, for example from $H^-$, has a slower-rising behavior, which makes it more difficult to determine the threshold energy.

For electron ionization, $M + e^- \rightarrow M^+ + 2e^-$, the three-body problem for the products cannot be solved analytically. Wannier[166] used statistical arguments to derive a slightly curved threshold law for electron ionization of atoms, $n \approx 1.13$ and $m = 0$ in eq 34 with

electron beam energy $E$. However, experiments tend to show to a linear threshold law, $n = 1$, rather than the Wannier equation.[7,167] For initial excitation to an excited neutral state, e.g., in autoionization, a step function may apply.[168]

The energy range for which the Wigner or Wannier threshold laws are applicable is not known in general. The range may be as little as tens of $cm^{-1}$ for photodetachment in some cases.[169] Furthermore, autoionization resonances, couplings between initially excited electronic states of the parent species and the product states, may arise and complicate the simple threshold behavior. Molecular ionization or detachment presents additional issues. First, a series of thresholds will be present for transitions to higher rotational or vibrational states of the upper charge state. Second, excited states of the parent species may be thermally populated in the sample, leading to hot bands with onsets below the 0 K threshold energy. Third, the threshold law may differ for more complicated systems, for example $n \approx 0.2$ for detachment from $OH^-$ because of the interaction of the departing electron with the dipolar neutral.[170] Finally, for appearance energies in dissociative processes, the theoretical threshold laws for direct ionization do not apply.[171]

For energy-resolved threshold collision-induced dissociation (TCID) processes and collisionally activated bimolecular reactions, the general threshold power law of eq 34 also applies, at least to a first approximation.[172−174] The simple hard-sphere line-of-centers collision model[175] predicts the threshold behavior given by eq 34 with $n = 1$ and $m = 1$, where $E$ is the relative collision energy in the center-of-mass frame and $E_0$ is the dissociation energy. Other models predict[172,175−182] $m = 1$ and various values of $n$ ranging from about 0.5 to 2.5. Because there is variation in the behavior of reactive systems, in practice $n$ is treated as an adjustable parameter.[172]

For dissociative processes, three additional factors must be considered. First, for statistical processes, the initial internal energy contributes to the dissociation and the distribution of internal energies must be considered. As shown for TCID studies,[183] simply correcting the apparent threshold energy by the average internal energy does not necessarily give correct results. For small systems, the thermal populations of individual states may be summed directly. For larger molecules or ions initially at thermal equilibrium, the initial internal energy distribution is given by eq 35,

$$P_0(E_i)\,\mathrm{d}E_i = \frac{\rho(E_i)\exp(-E_i/k_\mathrm{B}T)\,\mathrm{d}E_i}{\int_0^\infty \rho(E_i)\exp(-E_i/k_\mathrm{B}T)\,\mathrm{d}E_i} = \frac{\rho(E_i)\exp(-E_i/k_\mathrm{B}T)\,\mathrm{d}E_i}{Q_0(T)} \quad (35)$$

where $\rho(E_i)$ is the density of states of the reactant species, $E_i$ is the internal energy, and the denominator is the partition function $Q_0(T)$. The Boltzmann energy distribution does not apply to ions formed under nonequilibrium conditions. The second factor is that the statistical dissociation takes time, leading to the RRKM/QET dissociation probability in eq 33. The third factor is that every experiment has some spread in the excitation energy, either the light source bandwidth, the electron beam energy spread, or for collisions the ion energy spread and the thermal motion of the target gas.[184,185] Simplifying, the energy spread is represented as a single distribution $P_E(\epsilon)$, the probability of the actual excitation energy $\epsilon$ for the nominal energy $E$. Putting these factors together with the threshold law, the overall apparent cross section as a function of excitation energy is given by eq 36,

$$\sigma_j(E) = \int_0^\infty P_\mathrm{E}(\epsilon)\int_0^\infty P_0(E_i)P_j(\epsilon + E_i) \times \sigma_0(i,j)\,\frac{[\epsilon + E_i - E_0(j)]^n}{\epsilon^m}\,\mathrm{d}E_i\,\mathrm{d}\epsilon \quad (36)$$

where $P_j(\epsilon + E_i)$ is the RRKM/QET dissociation probability, which is zero for total energies ($\epsilon + \mathrm{E}_i$) less than $E_0(j)$, the 0 K threshold energy for channel $j$. Equation 36 is a generalized expression—it incorporates the major issues of threshold behavior, energy resolution, and kinetic shifts required to analyze dissociation experiments, but some modifications may be required for individual situations. Any dependence of the cross section on state-to-state transition probabilities would be included in $\sigma_0(i,j)$, e.g., Franck−Condon factors in photoionization or

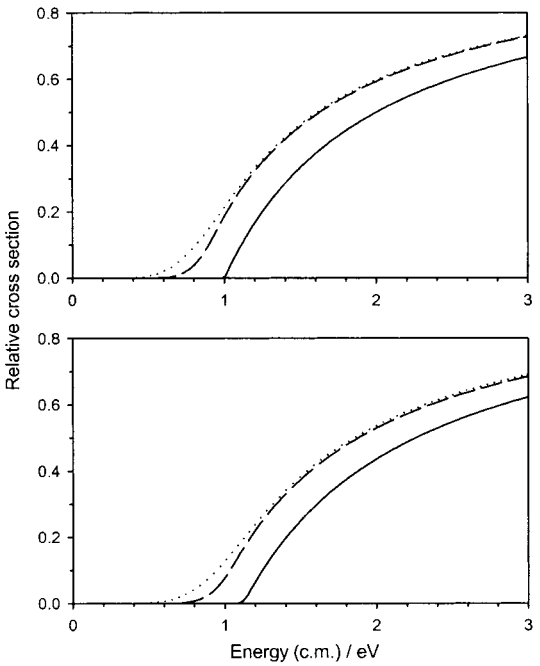


**Figure 5.** Schematic effects of translational energy broadening, internal energy, and kinetic shifts on the measurement of a reaction energy threshold. The threshold law, eq 34, with $n = m = 1$, $\sigma_0 = 1.0$, and $E_0 = 1.0$ eV, is used with molecular parameters appropriate for TCID by xenon of a model 16-atom proton-bound dimer ion with a moderately tight transition state, $\Delta^\ddagger S_{1000} = +0.5$ J mol$^{-1}$ K$^{-1}$, and an average internal energy at 300 K of 0.18 eV. Top: unconvoluted threshold law (—), convoluted with internal energy distribution (---), and convoluted with both internal energy and translational energy (···). Bottom: same but with kinetic shift correction calculated by RRKM theory with a detection time window of $\tau_2 = 0.1$ ms.

electron ionization, in which case an explicit sum over those transitions is required. For collision-induced dissociation with $m = 1$, the denominator in eq 36 is either the collision energy $\epsilon$ as supported by some reaction models[175,181,186] or is replaced by $(\epsilon + E_i)$, the total available energy.[187] In dissociative photoionization or electron ionization, to generate a breakdown curve the relative parent molecule detection probability is obtained by substituting $[1 - \sum P_j(E)]$ for $P_j(E)$ in eq 36. For collision-induced dissociation or electron ionization, a distribution of excitation energies will actually be produced upon a collision at energy $\epsilon$ because of the random distribution of impact parameters. This requires that a model for the energy transfer probability distribution be used and additional integration in eq 36 over that distribution, as described for the case of TCID.[145,187−189] Figure 5 illustrates internal and translational energy broadening and kinetic shifts for a model TCID process with a line-of-centers threshold law ($n = m = 1$). Each of these effects must be considered to obtain accurate thermochemistry from threshold energy measurements.

## VI. Optical Spectroscopy

The ionization energies for most neutral atomic elements, as well as second and higher ionization energies for formation of multicharged atomic cations, have been measured precisely by optical emission spectra of the atoms and ions in discharges,[68] eq 37.

$$A^*(n^*) \rightarrow A(n) + h\nu \qquad (37)$$

The atomic ionization energies are extrapolated from series of transitions originating from highly excited Rydberg energy levels $n^*$ using eq 38

$$E(n^*) = IE_0 - \frac{R}{(n^* - \delta)^2} \qquad (38)$$

where $R$ is the mass-corrected Rydberg constant and $\delta$ is the quantum defect, which empirically describes the deviation from hydrogen-like behavior.[190] The Coulomb potential and Rydberg level structure are depicted in Figure 6, which also applies to ion-pair states discussed below. Empirical extrapolations with higher-order terms may also be used.[191−193] Atomic ionization energies and excited-state energy levels are evaluated in the "Moore Tables"[68] and successor compilations.[117−128] Evaluated first ionization energies for atoms are included in ion thermochemistry compilations.[73,107]

Rydberg spectroscopy may also be applied to diatomic polyatomic molecules, but obtaining ionization energies by extrapolation of Rydberg series in emission is often difficult because of spectral complexity.[85,194] A renaissance in the spectroscopy of Rydberg states has occurred recently with the development of resonantly enhanced multiphoton ionization (REMPI) spectroscopy and zero electron kinetic energy (ZEKE) photoelectron spectroscopy,[85,194−196] discussed in detail in section VII.E. A recent application of Rydberg spectroscopy for the determination

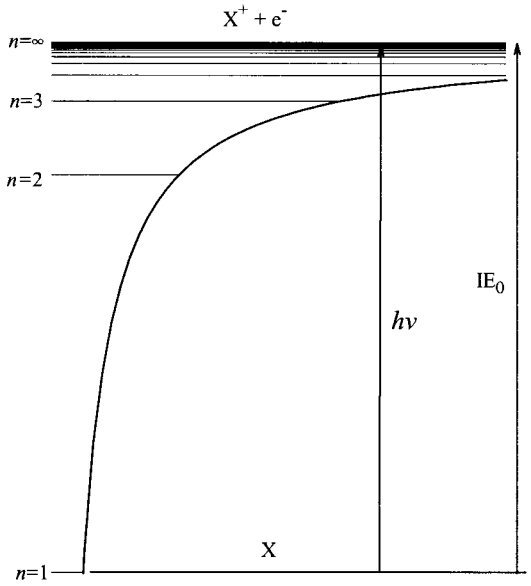


**Figure 6.** Coulomb potential energy curve, $V(r) \propto 1/r$, and energy levels. There are an infinite number of Rydberg states below the ionization energy (IE) limit. The arrow labeled $h\nu$ shows the photon-induced transition to neutral Rydberg states just below the ionization limit (ZEKE states), which can be ionized by a small electric field.

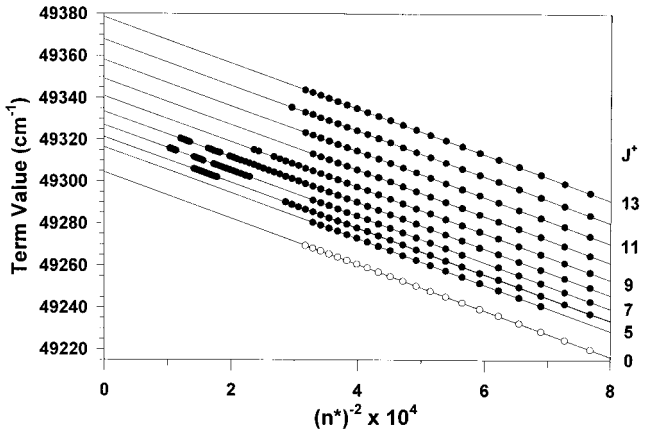


**Figure 7.** Rydberg extrapolations for yttrium monoxide, YO, for individual rotational states of the ion core, $YO^+(J)$. (Reprinted with permission from ref 197. Copyright 1999 American Institute of Physics.)

of the ionization energy of a diatomic is shown in Figure 7. Linton et al.[197] used two-color Rydberg spectroscopy on yttrium monoxide (YO), in which individual rotational states of the $YO^+(J)$ ion core each exhibit a Rydberg series to individual rotational ionization limits. A fit of the Rydberg rotational levels yields the rotationless ionization energy, $IE_0(YO, X\ ^2\Sigma^+) = 589.8106 \pm 0.0004$ kJ/mol.

## VII. Photoionization and Photodetachment Methods

### A. Threshold Ionization and Detachment

Ionization energies of neutral molecules and electron affinities of molecular anions may be obtained from the threshold for removal of an electron as the photon energy is increased, eqs 39 and 40.

$$M + h\nu \rightarrow M^+ + e^- \quad IE_0 = h\nu_0 \qquad (39)$$

$$M^- + h\nu \rightarrow M + e^- \quad EA_0 = h\nu_0 \qquad (40)$$

In photoionization efficiency (PIE)[161,198,199] or photodetachment efficiency[164,165] measurements, the threshold energy $h\nu_0$ for detection of photoions or photoelectrons corresponds, in favorable cases, with the adiabatic ionization energy or electron affinity.

### 1. Photoionization of Neutrals

The step-function Wigner threshold law for photoionization of neutrals (section V) allows sensitive and high-resolution ionization threshold energy measurements for atoms and molecules. The transition intensities (heights of the steps) for polyatomic molecules are governed by the Franck−Condon overlap between the vibrational states of the neutral and the cation,[200] as shown schematically in Figure 8. However, this simple picture is often complicated by non-Franck−Condon behavior, including autoionization resonances resulting from initial photoabsorption to excited neutral states embedded in the ionization continuum, eq 41.[161,195,198,201]

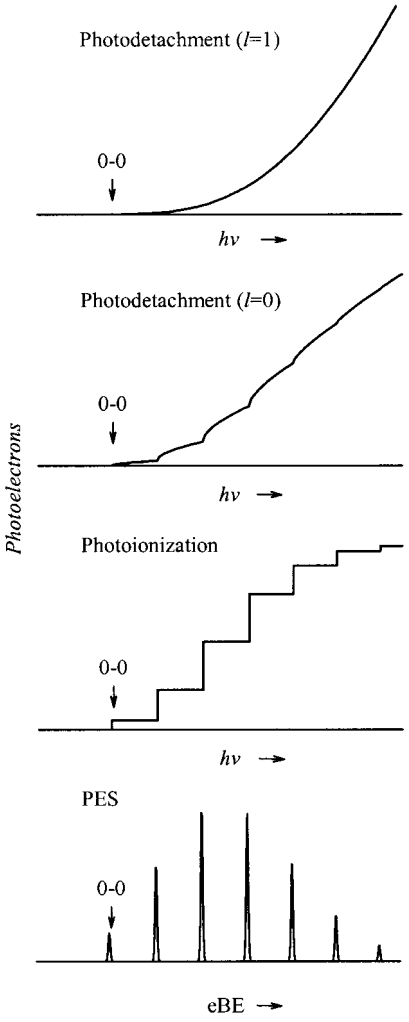


**Figure 8.** Schematic diagram comparing the photoelectron spectrum for a neutral or anionic diatomic molecule (bottom) with the photoionization efficiency curve for a neutral and the photodetachment efficiency curves for pure *s*-wave detachment ($l = 0$) or *p*-wave detachment ($l = 1$). The same energy scale relative to the 0−0 origin is used for each spectrum. The Wigner threshold laws (section V) and Franck−Condon intensities are assumed to apply, and no energy broadening is included for the photoionization and photodetachment efficiency curves.

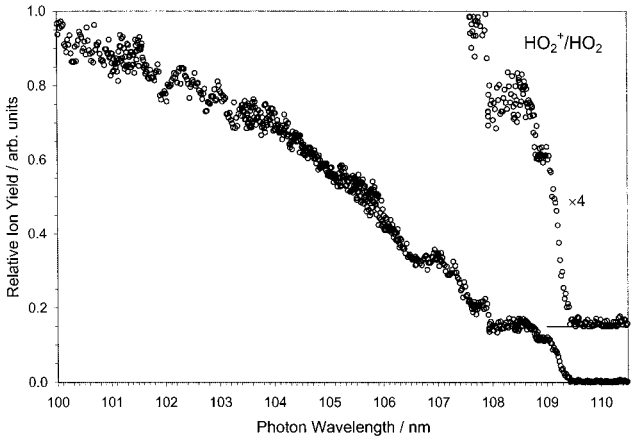


**Figure 9.** Photoionization threshold spectrum of hydroperoxy radical, $HO_2$. (Reprinted with permission from ref 207. Copyright 1998 Elsevier Science.)

$$M + h\nu \rightarrow M^* \rightarrow M^+ + e^- \qquad (41)$$

In addition, the threshold may be shifted by hot bands.[202] In principle, species with large changes of geometry between the neutral and the cation, i.e., with poor Franck−Condon overlap for the origin transition, would exhibit an elevated apparent photoionization threshold energy. However, because of the availability of autoionization transitions to excited states of the neutral including Rydberg states, ionization may be observed in Franck−Condon gaps.[194,201]

Precise ionization energies of numerous stable molecules and transient species have been measured via photoionization thresholds.[161,198,200,203−206] For application of the appearance energy cycle, eq 6, ionization energies of radical species are required. A recent example, the photoionization spectrum of hydroperoxy radical, $HO_2$, is presented in Figure 9.[207] In this photoionization mass spectrometry (PIMS)[198] experiment, the mass-analyzed photoions are detected as a function of photon energy. A 3-m vacuum-ultraviolet monochromator selects the photon wavelength from a continuum source. Various pyrolytic and discharge sources can be used to produce the neutral radicals, which are identified by mass spectrometry of the photoions. A clear steplike threshold behavior is observed (Figure 9). The lowest step corresponds with the vibrationless origin transition, giving $\lambda_0 = 109.22 \pm 0.03$ nm or $IE_0(HO_2) = 11.352 \pm 0.007$ eV. The higher steps are related to the 1560 $cm^{-1}$ O−O stretching frequency of the ground-state cation, while the smaller features on the plateaus result from superimposed autoionization processes.[207]

### 2. Photodetachment Thresholds of Anions

The most precise electron affinities available are obtained from photodetachment threshold measurements.[208] High-resolution determinations of electron affinities of atoms by threshold photodetachment

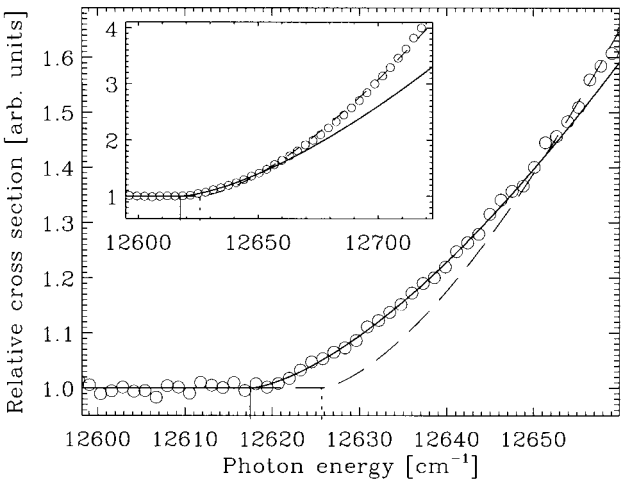


**Figure 10.** Photodetachment threshold spectrum of iridium anions, $Ir^-$. Solid line is the Wigner threshold law determined by the best fit to the data below 12650 cm$^{-1}$. Dashed curve is a Wigner law fit to entire energy range shown in the inset. (Reprinted with permission from ref 169. Copyright 1999 American Physical Society.)

continues to be an active area of atomic physics.[169,208,209] Until the most recent CODATA refinement of the Planck constant,[112] the uncertainty of the conversion from frequency to energy units comprised a large part of the uncertainty for the electron affinities of O, F, and other atoms.[208] Prior mass selection of the negative-ion beam provides certainty of the signal carrier. Figure 10 shows the threshold photodetachment spectrum[169] of $Ir^-$, which shows deviations from the $n = 1.5$ Wigner threshold law about 30 cm$^{-1}$ above the onset. High sensitivity is required for a precise determination of the threshold in such cases.

For molecular anions, individual steps may be observed for transitions to rovibrational levels of the neutral. As shown in Figure 8, however, the steps may be difficult to discern, especially for a *p*-wave photoelectron because of the slow-rising threshold behavior. The Wigner threshold law is further complicated by the mixing of atomic orbitals into molecular orbitals (which may mix *s*, *p*, or higher electronic angular momenta) and the charge distribution of the neutral. For the case of $OH^-$, detachment from a $\pi$ orbital to form a dipolar neutral, a value of $n \approx 0.2$ is found,[170] as shown in Figure 11. In this case, individual rotational and spin−orbit transitions are observed as rounded steps in the threshold cross section. As with neutral photoionization, autoionization resonances may be observed superimposed on the continuum threshold detachment background.[165,210]

The Brauman group has employed threshold detachment of anions trapped in an ion cyclotron resonance (ICR) cell using an arc lamp and monochromator or a dye laser for photodetachment.[211] Photodetachment is detected by depletion of ion signal. Although this method has somewhat lower resolution than beam experiments, the ability to synthesize ions via ion−molecule reactions in the ICR trap allows measurements on complex organic anions. A recent example is the measurement of electron affinities of cyclopentadienyl, indenyl, and

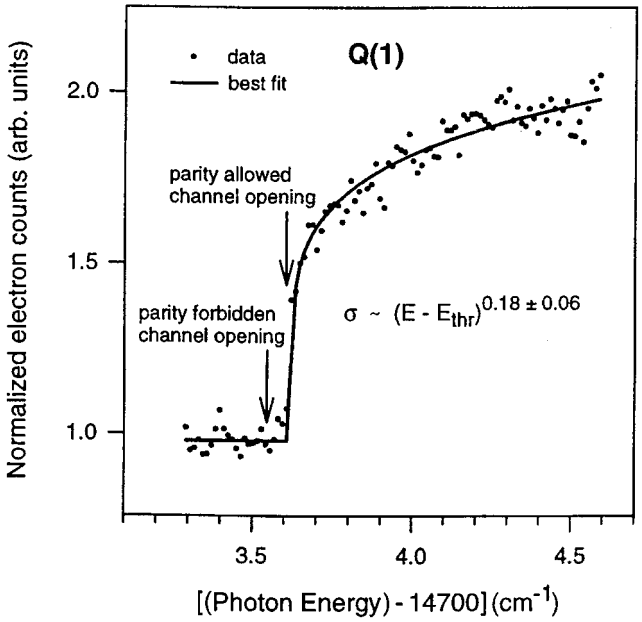


**Figure 11.** Photodetachment threshold spectrum of $OH^-$. (Reprinted with permission from ref 170. Copyright 1997 American Physical Society.)

fluorenyl radicals.[212] The simulated photodetachment efficiency curves in Figure 8 suggest that locating the true threshold may be difficult for polyatomic molecules with significant geometry changes between the anion and neutral and for cases where the detachment is predominated by *p*-wave electrons or higher angular momentum states.

## B. Dissociative Photoionization Thresholds

In dissociative photoionization threshold experiments, the appearance energies for photofragment ions are measured,[146,154,161,204,213] eq 42.

$$AB + h\nu \rightarrow A^+ + B + e^- \quad h\nu_0 = AE_0(A^+,B) \quad (42)$$

The dissociative process may proceed either directly, via initial molecular ionization to form an $AB^+$ intermediate, or via intermediate autoionizing or dissociative neutral excited states.

Figure 12 presents the ion yield curve for $CH_3^+$ from $CH_4$ obtained in photoionization mass spectrometry (PIMS) experiments by Litorja and Ruscic.[16] A convolution of a threshold law over the thermal populations of the internal states of the parent molecule gives a fit to the data and allows correction to 0 K. Ruscic and Berkowitz[171] use a threshold law "kernel" of the form $\sigma(E) \propto (1 - e^{-b(E-E_0)})$ with adjustable parameter *b*, which is qualitatively similar to the power law function of eq 34 with $m = 0$. Combining measurements[16,214,215] of the photoionization appearance energies $AE(CH_3^+,CH_4)$, $AE(CH_2^+,CH_3)$, $AE(CH_2^+,CH_2CO)$ and the ionization energies of $CH_2$ and $CH_3$ leads to the most precise available values for the first and second bond dissociation energies of methane: $D_0(H-CH_3) = 432.71 \pm 0.13$ kJ/mol and $D_0(H-CH_2) = 455.9 \pm 0.8$ kJ/mol. The offset between the 0 K model threshold and the apparent threshold in Figure 12 makes clear the

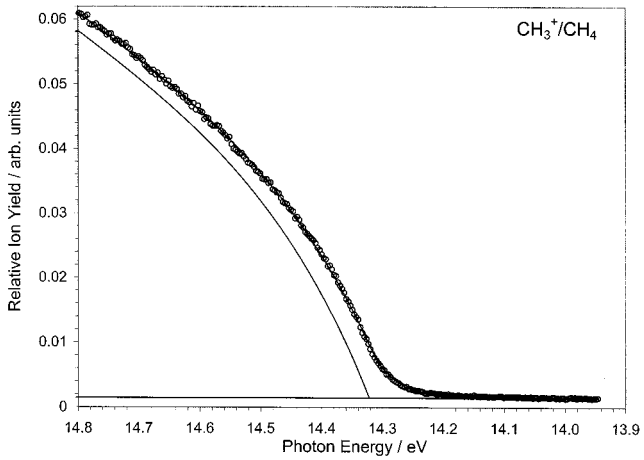


**Figure 12.** Dissociative photoionization threshold spectrum of $CH_3^+$ from $CH_4$. (Reprinted with permission from ref 16. Copyright 1997 American Institute of Physics.)

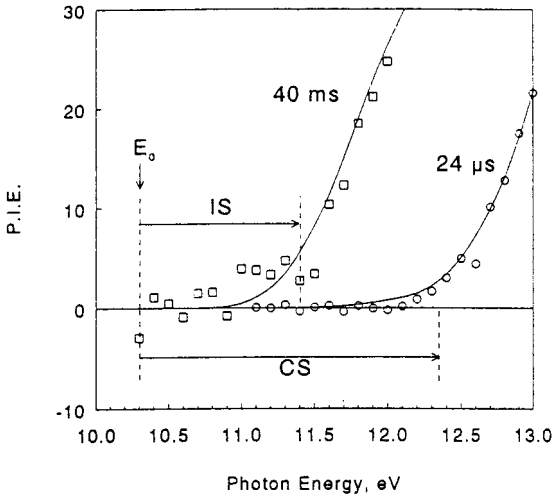


**Figure 13.** Time-resolved dissociative photoionization thresholds for $C_{11}H_9^+$ from 1-methylnaphthalene ($C_{11}H_{10}$). Thresholds are shown at two ion storage times, 24 $\mu$s and 40 ms. The thermodynamic threshold is labeled $E_0$. "IS" is the intrinsic kinetic shift due to radiative relaxation, and "CS" is the conventional kinetic shift. (Reprinted with permission from ref 218. Copyright 1993 John Wiley & Sons.)

importance of accounting for the internal energy of the parent molecule and of a reliable threshold model. In measurement of AE($CF_3^+$,$CF_3X$), X = F, Cl, Br, or I, Asher and Ruscic[216] found deviations from earlier photoionization results well in excess of stated uncertainties, attributed to errors in the earlier work from not accounting for thermal internal energy of the precursors and from the use of a simple linear threshold extrapolation. Irikura[217] has discussed entropy issues related to the determination of IE($CF_3$).

For dissociative photoionization of large molecules, kinetics shifts must also be taken into account. Lifshitz and co-workers[146,154] used time-resolved PIMS studies and RRKM/QET modeling to examine the kinetics of dissociative ionization processes and to extract binding energies. Photoionization by pulsed vacuum ultraviolet light occurs in a radio frequency ion trap, where the photoions are stored for a variable residence time period (20 $\mu$s to 0.5 s) before extraction and mass analysis with a quadrupole mass spectrometer.[146,154] Figure 13 shows the time-resolved photoionization efficiency curves for 1-methylnaphthalene.[218] The apparent threshold energy for $C_{11}H_9^+$ ion formation (H-loss from the molecular ion) shifts lower for longer residence times; beyond 40 ms an "intrinsic" kinetic shift remains due to radiative relaxation. The analysis of these data involve calculation of the breakdown curves for different trapping times using RRKM/QET theory for the dissociation rate $k(E)$ and an energy-independent rate constant for infrared radiative decay. Instead of a model threshold law, experimental photoionization efficiency curves for the parent ion are used as the energy deposition function. Convolutions of the resulting dissociation probability over the thermal energy distributions of the parent molecules and monochromator slit function yield the photofragment ion yield curve for comparison with the data, as shown in Figure 13.[218] The RRKM model and time-resolved photoionization curves are sensitive to the nature of the transition state. For H loss from $C_{11}H_{10}^+$ (Figure 13), a tight transition state characterized by $\Delta^{\ddagger}S_{1000} = -56$ J mol$^{-1}$ K$^{-1}$ is found,[218] which suggests a rearrangement to the benzotropylium structure. In contrast, for Br loss from 1-bromonaphthalene,[154] a loose transition state with $\Delta^{\ddagger}S_{1000} = +9.4$ J mol$^{-1}$ K$^{-1}$ is consistent with simple C−Br bond cleavage.

## C. Photoelectron Spectroscopy

In photoelectron spectroscopy (PES), the photon energy is fixed at a value higher than the IE or EA and the kinetic energies of the ejected photoelectrons (eKE) are measured upon photoionization or photodetachment, eq 43 or 44.[165,219]

$$M + h\nu \rightarrow M^+ + e^- \text{ (eKE)} \qquad (43)$$

$$M^- + h\nu \rightarrow M^+ + e^- \text{ (eKE)} \qquad (44)$$

The electron binding energy (eBE) is the difference between the photon energy and the electron kinetic energy, eq 45.

$$\text{eBE} = h\nu - \text{eKE} \qquad (45)$$

The spectrum of photoelectron energies yields information about the structure of the upper charge state. For thermochemical use, the IEs and EAs should represent adiabatic values, i.e., the energy difference between the ground states of the neutral and ion, $IE_0$ = eBE(0−0) or $EA_0$ = eBE(0−0).

### 1. Negative-Ion Photoelectron Spectroscopy

Figure 14 illustrates simplified negative-ion photoelectron spectra for $O_2^-$ and $F_2^-$. When the 0−0 origin transition is vibrationally resolved and assigned, as in the $O_2^-$ spectrum in Figure 14, photoelectron spectroscopy provides accurate adiabatic transition energies. However, if the geometry change between the two charge states is large, the origin transition may be too weak to observe because of small Franck−Condon factors, as shown for the $F_2^-$ spectrum in Figure 14. The electron affinity of $F_2$ has not been measured by PES but rather only by kinetic

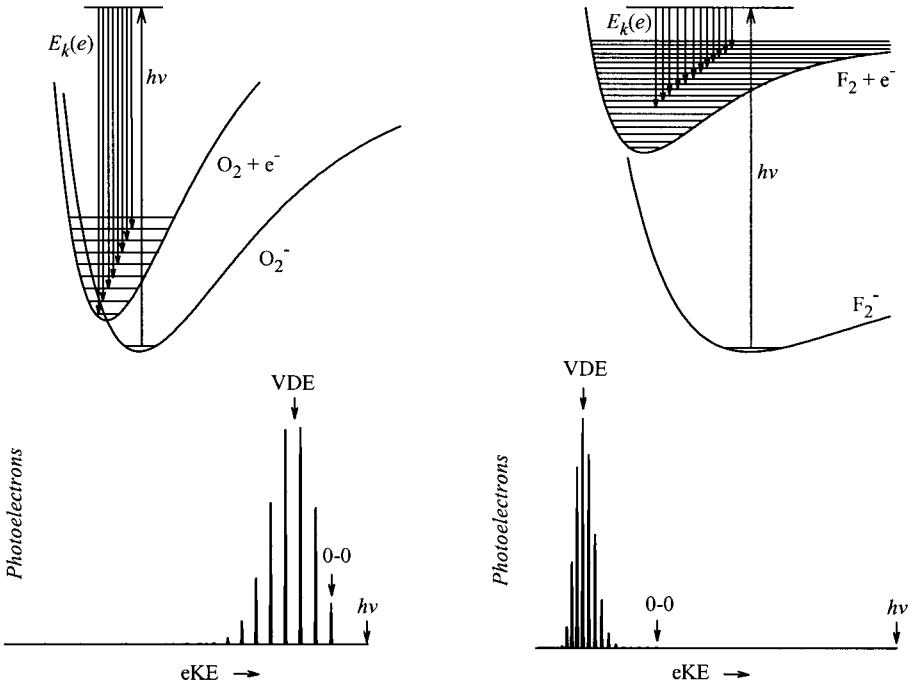


**Figure 14.** Schematic energy diagrams and simulated negative-ion photoelectron spectra of $O_2^-$ and $F_2^-$ (simplified using ground-state Morse oscillator potentials and ignoring spin-orbit states and hot bands). The 0−0 origin transitions and vertical detachment energies (VDE) are shown by arrows.

and appearance energy techniques.[86,220] Vertical detachment energies (VDE) or vertical ionization energies (VIE) are represented by the energy at the peak of the Franck−Condon intensity distribution (Figures 3 and 14). For transitions starting from the ground state of the initial neutral or anion, the vertical transition energy is an upper limit for the adiabatic IE or EA. In cases where the adiabatic origin is not resolved in the photoelectron spectrum, approximate "threshold" photodetachment energies are sometimes reported, taken as the lowest electron kinetic energy where the photoelectron intensity exceeds some arbitrary cutoff or a linear extrapolation of the high binding energy edge of the band.[221−224] These values are valid approximations for the adiabatic IE or EA *only* if the Franck−Condon factors for the origin transition are reasonably high, i.e., if the geometry change between the two charge states is not too large. Hot bands, transitions arising from vibrationally or electronically excited states of the initial state, appear at higher electron kinetic energies than the origin and can be mistaken for the adiabatic transition in low-resolution spectra.

Negative-ion photoelectron spectroscopy has been used extensively to measure electron affinities as well as to examine the structure of the ground and excited states of the corresponding neutral molecule or radical.[93,165,219,225−237] Initial mass analysis of the negative-ion beam removes uncertainty of the assignment. Photoelectron spectrometers with a continuous ion beam, a cw visible or ultraviolet laser, and a hemispherical electrostatic electron energy analyzer can achieve energy resolutions of 3−10 meV over their entire energy range.[219,238] Time-of-flight (TOF) photoelectron spectrometers using pulsed ion sources and pulsed lasers have similar resolutions at low electron kinetic energies, although the resolution degrades as $E^{3/2}$ at higher energies.[165] Magnetic-bottle time-of-flight photoelectron energy analyzers have higher collection efficiency than conventional TOF instruments but at the cost of decreased resolution.[234,237] Pulsed laser systems have the advantage of higher routinely available photon energies, allowing access to species with high EAs and to higher excited states of the neutrals. Cooling the ions via a supersonic expansion source[239] or a liquid-nitrogen-cooled flow tube source[240,241] can eliminate or help identify hot band transitions. A new review compiles electron affinities obtained by negative-ion PES and photodetachment threshold techniques.[93]

Electron affinities obtained with high accuracy by negative-ion photoelectron spectroscopy can be combined with gas-phase acidities obtained by other gas-phase ion chemistry techniques to determine neutral bond dissociation energies by the negative-ion cycle,[6,225] eq 5. Using this method, the bond dissociation energies have been determined for all the bonds in ethene and ethyne[242] and of one or more CH bonds in some unsaturated $C_3$ hydrocarbons,[23,41] aromatics,[23,34] alcohols,[29] and peroxides.[243] Various ion source and ion synthesis techniques have allowed measurement of photoelectron spectra of anions and electron affinities corresponding to novel transient neutral species.[225] For example, photoelectron spectra of the *o*-, *m*-, and *p*-benzynes are presented in Figure 15.[244] The singlet and triplet states are observed for each isomer. In addition, many main-group and transition-metal clusters have been studied by PES.[219,232−237] Novel species studied by negative-ion PES include dipole-bound anions,[245,246] doubly charged anions,[247] and electrons "solvated" in ammonia and water clusters.[248] Bowen and co-workers[249] recently showed that the unbound naphthalene anion,[250,251] $EA(C_{10}H_8) < 0$, can be stabilized by microsolvation with one or

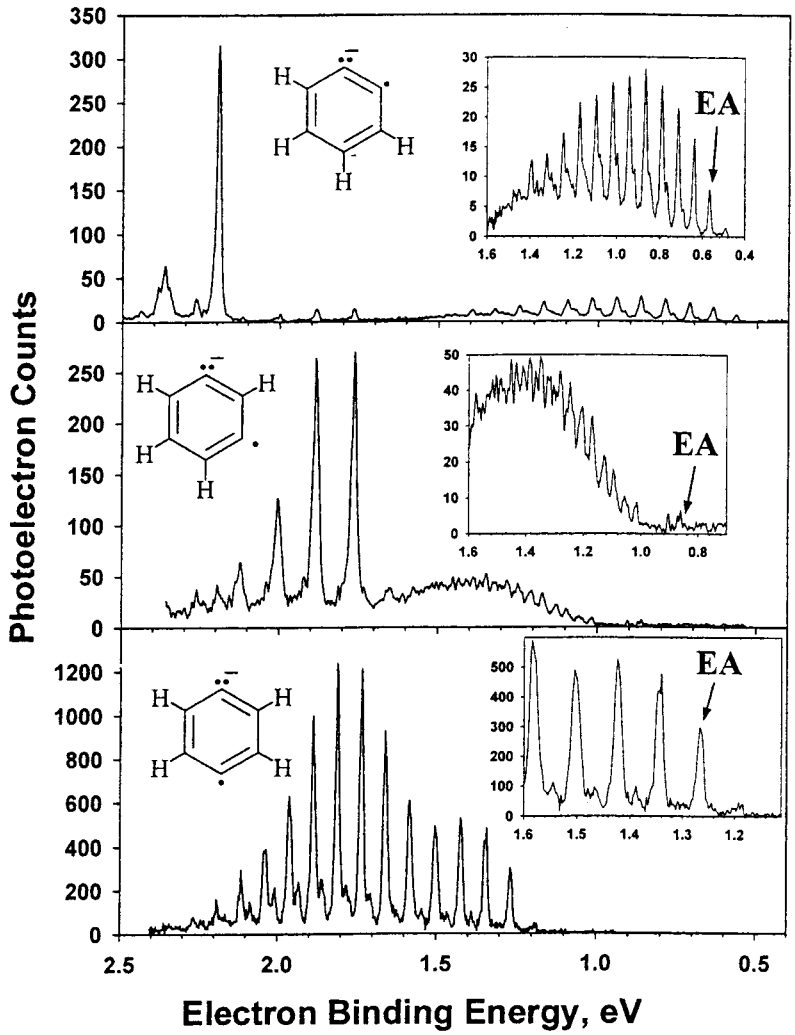


**Figure 15.** Negative-ion photoelectron spectrum at 351 nm of the *o*-, *m*-, and *p*-benzyne anions at room temperature. Electron affinities of the benzynes are indicated on the expanded views of the singlet regions, shown in the insets. (Reprinted with permission from ref 244. Copyright 1998 American Chemical Society.)

more water molecules, consistent with the existence of naphthalene anions in solution. An extrapolation[249] of the measured electron affinities of $C_{10}H_8(H_2O)_n^-$ to $n = 0$ gives $EA(C_{10}H_8) \approx -0.20$ eV, in quantitative agreement with temporary anion resonances in electron transmission spectroscopy.[250]

Despite their importance, electron affinities for most diatomic halogens have not been measured spectroscopically. Both their high electron affinities and the large geometry change, as illustrated for $F_2$ in Figure 14, have prevented photoelectron spectroscopy measurements. Neumark and co-workers[252] circumvented this problem recently for $I_2$ by using a detachment laser at 299 nm (4.141 eV), which can access the $^3\Pi_u$ excited states of neutral $I_2$. Because the term energies of these excited states relative to the ground $^1\Sigma_g^+$ state of $I_2$ are precisely known from neutral spectroscopy, the adiabatic electron affinity can be derived, $EA_0(I_2) = 2.524 \pm 0.005$ eV, even though the ground electronic state origin transition is not observed.

### 2. Neutral Photoelectron Spectroscopy

Ultraviolet photoelectron spectroscopy (UPS) of neutrals, in which the kinetic energies of the ejected electrons are measured at a fixed photoionization energy, began in the early 1960s typically using He I (21.2 eV) excitation or synchrotron radiation.[194,253] Figure 8 compares the photoelectron spectra with the photoionization efficiency curves. The resolved peaks in the kinetic energy spectrum correspond with the steps in the photoionization threshold curve. If the vibrationless 0−0 origin peak is resolved and identified, its energy yields the adiabatic ionization energy. Issues of Franck−Condon overlap and hot bands are the same as for negative-ion photoelectron spectroscopy. Non-Franck−Condon effects are more likely in photoionization than in photodetachment because of the larger number of excited states for neutral molecules than for anions.

In PES of neutral species, spectroscopic information is obtained regarding the cationic states. In mainstream molecular ultraviolet photoelectron spectroscopy of organic and inorganic molecules, the focus is often on electronic characterization of synthetic products and on measuring valence electron orbital energies via Koopmans' theorem.[254] In those applications, the adiabatic origin transitions are not necessarily resolved to obtain a precise ionization energy.

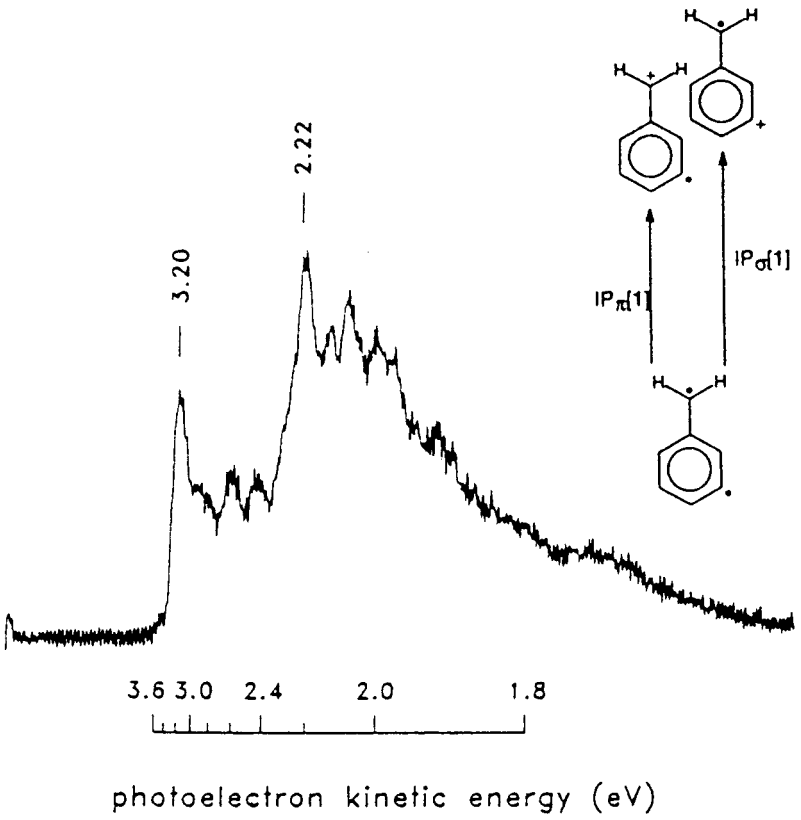


**Figure 16.** Photoelectron spectrum at 10.49-eV photon energy of the α,3-dehydrotoluene biradical from the flash photolysis of *m*-nitrophenyl nitrite. The bands at eKE = 3.20 and 2.22 eV are assigned to the detachment from the $\pi$ system and from the in-plane $sp^2$ orbital, respectively. (Reprinted with permission from ref 257. Copyright 1994 American Chemical Society.)

Photoelectron spectroscopy has been applied to many neutral reactive intermediates and radicals[255−259] to obtain ionization energies, IE(R•), and structural information. Mass analysis of the cationic product provides identification of the neutral radical. As an example, Figure 16 shows the time-of-flight photoelectron spectrum of the singlet α,3-dehydrotoluene biradical.[257] Two electron states are observed with resolved origin transitions of two bands assigned to the removal of the electron either from the benzylic $\pi$ system ($IE_0 = 7.29 \pm 0.04$ eV) or from the in-plane $sp^2$ orbital ($IE_0 = 8.27 \pm 0.04$ eV).[257]

## D. Threshold Photoelectron Spectroscopy

The late 1960s saw the development of threshold photoelectron spectroscopy (TPES), where near-threshold photoionization processes are selectively observed via detection of low-energy photoelectrons.[194,195] Coincidence techniques for simultaneous detection of the photoions to provide information on fragment ions were developed beginning in the 1970s.[195] These techniques essentially yield the derivative of the photoionization efficiency curve at resolutions fixed by the energy selection of slow photoelectrons. The threshold PES may show transitions in Franck−Condon gaps due to autoionization resonances involving Rydberg states of the neutral, as exhibited in Figure 17 for TPES of HBr.[260] Transitions to the $v = 2-20$ vibrational levels of both $^2\Pi_J$ states of $HBr^+$ and $DBr^+$ are more intense than can be explained by Franck−Condon overlap with HBr and DBr and are attributed to neutral Rydberg states near 13, 14, and 15 eV.

In threshold photoelectron photoion coincidence (TPEPICO) spectroscopy, the threshold photoelectron and the photoion are detected simultaneously by time-of-flight.[195,200,204,261,262] By energy balance, the internal energy of the initial photoion in excess of the ionization energy is known from the excitation wavelength. If the detected ion is a fragment, then unimolecular dissociation rate coefficients can be determined as a function of energy, $k(E)$. The rate−energy curve is modeled by RRKM/QET statistical theory. Figure 18 presents a breakdown diagram for the $ICH_2CN^+$ ion obtained in TPEPICO experiments of Lafleur et al.[262] The first fragment ion is $^+CH_2CN$ with a threshold of 12.19 eV followed at higher energy by $I^+$ at 12.35 eV. RRKM theory is used to model both the breakdown curve and the ion time-of-flight distributions, which show asymmetry due to slow dissociation in the threshold region, to obtain the 0 K appearance energies. Complete kinetic energy release distributions have been obtained by Güthe et al.[261] in TPEPICO experiments on fluoroethene ions using high-resolution time-of-flight spectroscopy of the ions.

## E. ZEKE/PFI Photoelectron Spectroscopy

### *1. ZEKE Photoionization of Neutrals*

The resolution of traditional PES and threshold photoelectron techniques is limited by the photoelec-

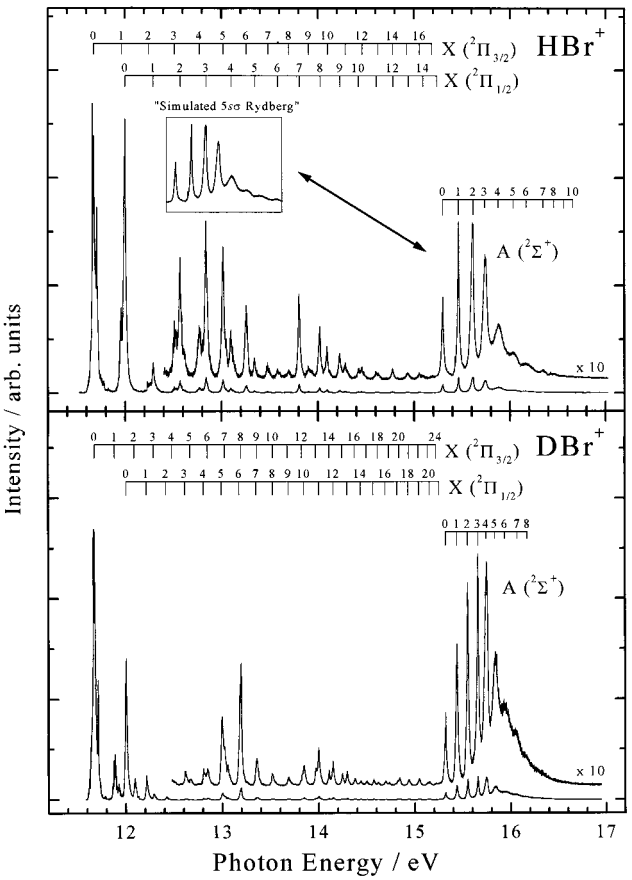


**Figure 17.** Threshold photoelectron spectrum of HBr and DBr with assignment of observed vibrational progressions of the ground and excited states of $HBr^+$ and $DBr^+$. The inset in the upper panel is a simulated Rydberg state originating from the A $^2\Sigma^+$ cation that gives rise to non-Franck−Condon intensities for $v = 3-6$ of the X $^2\Pi$ ground-state cation. (Reprinted with permission from ref 260. Copyright 1998 Elsevier Science.)

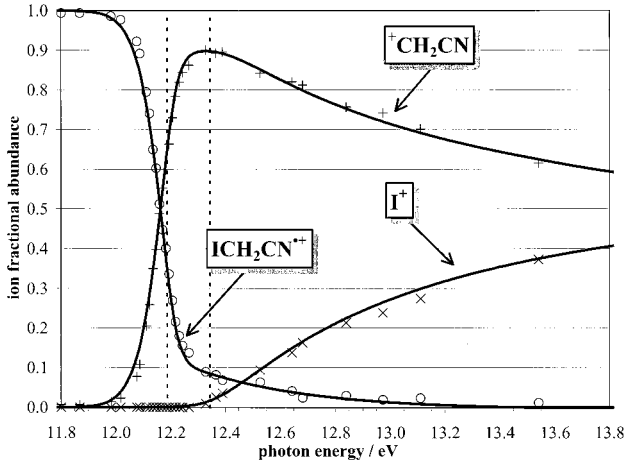


**Figure 18.** Breakdown diagram of $ICH_2CN^+$ ions from TPEPICO experiments. The dashed lines indicate the 0 K dissociation limits determined by modeling the dissociation dynamics by RRKM theory, convoluted by the internal energy distribution of $ICH_2CN$ and the threshold photoelectron analyzer function. (Reprinted with permission from ref 262. Copyright 2000 American Chemical Society.)

tron energy analysis to about 0.005−0.01 eV (0.5−1 kJ/mol or 40−80 $cm^{-1}$). The development of ZEKE/PFI photoelectron spectroscopy provides ionization spectra with resolution limited by the light source rather than by an electron energy analyzer.[85,196] In zero electron kinetic energy (ZEKE) or pulsed-field ionization (PFI) photoelectron spectroscopy, photoabsorption near the threshold for forming the photoion in a particular energy state occurs in a near-zero electric field, then a delay of several microseconds allows any electrons with kinetic energy to leave the ionization region. Stray electric fields are generally sufficient to disperse direct photoelectrons. What remain are long-lived neutral Rydberg states just below the ionization limit for a particular ion-core energy level, also called "ZEKE" states.[85] Then a pulsed field ionizes the Rydberg states and the resulting electrons are detected. The overall scheme is given by eq 46,

$$M + h\nu \rightarrow M^*(n^*) \qquad (46)$$

$$M^*(n^*) + \vec{E} \rightarrow M^+ + e^-$$

where $\vec{E}$ refers to the applied electric field. By using a weak pulsed ionization field, only those states very near the ionization limit are detected and the background of direct photoionization to lower energy states of the ion is eliminated. Various geometric and time discrimination techniques can yield resolution limited only by the light source bandwidth.[85,196] In mass-analyzed threshold ionization (MATI), the photoions from the pulsed-field ionization are detected.[85,194,263]

ZEKE/PFI photoelectron spectroscopy provides high-resolution spectra of cation states with vibrational and rotational resolution. Ionization energies can be measured with high precision, within 10 $cm^{-1}$ or better. Schlag[85] compiled molecular ionization energies determined by ZEKE techniques. As an example of the possible resolution, the ionization energy of benzene[264] is determined by ZEKE as $IE_0(C_6H_6) = 74\,556.575 \pm 0.050$ $cm^{-1}$. Figure 19 compares the ZEKE spectrum of benzene with its photoelectron spectrum and the photoionization threshold spectrum.[265] The vastly improved resolution of the ZEKE spectrum is obvious. Another difference from fixed-wavelength photoelectron spectra is that the intensities do not necessarily follow the Franck−Condon approximation because of autoionization resonances.[85] The ZEKE/PFI method has also been applied to radical species to obtain ionization energies and structural information.[85,256] The rotationally resolved ZEKE/PFI spectrum of methyl radical from Blush et al.[266] is shown in Figure 20. Direct photoelectrons are removed by a 0.1 V/cm field during a 600 ns delay, after which a −0.8 V/cm pulse ionizes long-lived Rydberg states. The spectrum yields an adiabatic ionization energy of $IE_0(CH_3) = 79349 \pm 3$ $cm^{-1}$.

Pulsed field ionization can also be combined with photoelectron photoion coincidence spectroscopy for a higher-resolution form of TPEPICO, described in section VII.D. Baer et al.[267] used PFI/PEPICO with synchrotron radiation to measure the breakdown curves of energy-selected 2-$C_3H_7X^+$ (X = Cl, Br, I) ions. These experiments yield precise values for the enthalpy of formation of $C_3H_7^+$ and the proton affinity of propene.[267]

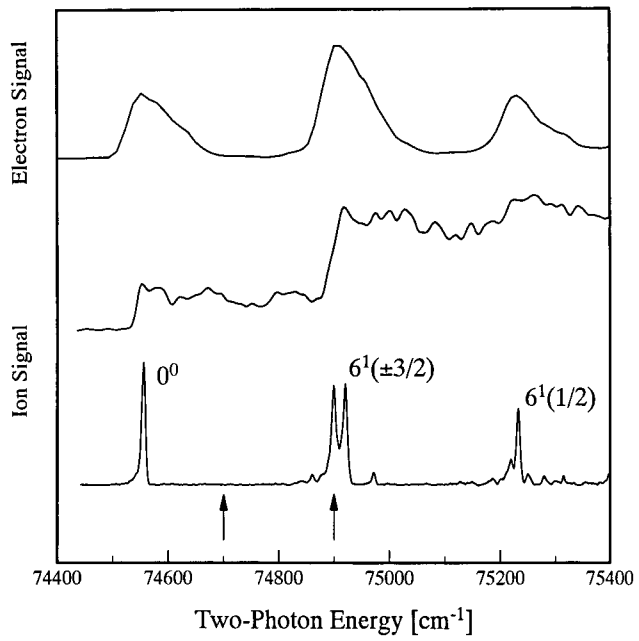


**Figure 19.** Spectra of the benzene cation $C_6H_6^+$ using time-of-flight photoelectron spectroscopy (top), photoionization efficiency spectrum (middle), and zero electron kinetic energy photoelectron spectroscopy (bottom). Labels mark the origin 0−0 transition and two vibrational states of the ion. (Reprinted with permission from ref 265. Copyright 1994 Elsevier Science.)

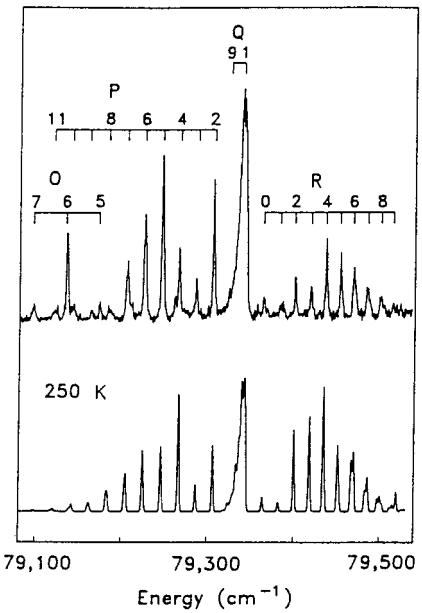


**Figure 20.** Rotationally resolved ZEKE photoelectron spectrum of $CH_3^+$ from $CH_3$ (upper curve) and calculated simulation (lower). (Reprinted with permission from ref 266. Copyright 1993 American Institute of Physics.)

### *2. Negative-Ion ZEKE Photoelectron Spectroscopy*

The ZEKE technique has also been applied to negative ions.[164,268−271] Time-of-flight mass spectrometry of the anions selects the species of interest, which means that after photodetachment the neutral is moving at the original ion beam velocity. Low-energy electrons are collected after a time delay of several hundred nanoseconds following the laser pulse, which allows electrons with higher kinetic energies to leave the detection volume. A weak pulsed electric field then extracts the near-zero electron kinetic energy electrons. Negative ions do not support Rydberg states, so directly detached low-energy electrons are observed. Figure 21 shows the ZEKE spectrum of $FeO^-$, with the photoelectron spectrum for comparison.[271] The dramatic increase in resolution from the ZEKE technique provides not only a precise value for the electron affinity, $EA_0(FeO) = 12054 \pm 5$ cm$^{-1}$, but also clearly resolves a neutral electronically excited-state band that had been misassigned as a vibration in the photoelectron spectrum.[271]

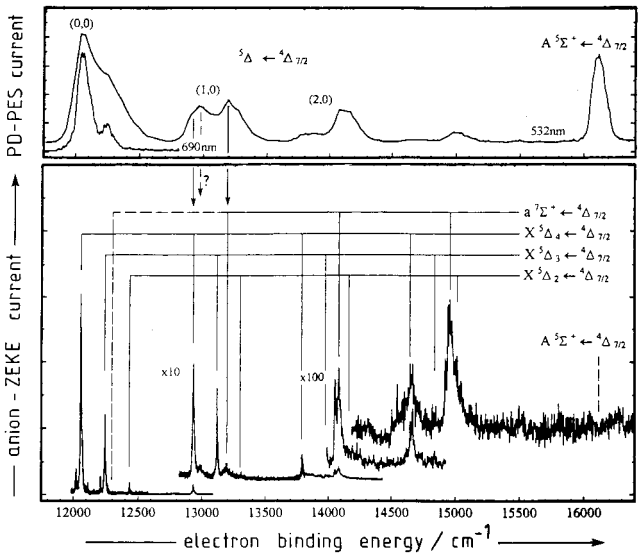


**Figure 21.** Anion ZEKE photoelectron spectrum of $FeO^-$ (lower plot) compared with the conventional photoelectron spectrum (upper plot). Transitions to vibrational states of various electronic states of neutral FeO are labeled. The 0−0 origin transition is at 12054 cm$^{-1}$. (Reprinted with permission from ref 271. Copyright 1997 American Institute of Physics.)

## F. Photoion-Pair Formation

A variant of the dissociative photoionization process is ion-pair formation, eq 47.

$$XY + h\nu \rightarrow X^+ + Y^- \qquad (47)$$

Berkowitz[203] reviewed photoion-pair formation threshold measurements. About 50 examples of ion-pair formation are known.[203] If the electron affinity of Y is greater than the bond dissociation energy of the cation, $D(X^+-Y)$, then the threshold for ion-pair formation is less than the threshold for ionization (Figure 1). Ion pairs are sometimes observed even when the ion−pair threshold is above the ionization energy.[203] Ion-pair formation appears to be more likely for diatomics than for polyatomic molecules, often by several orders of magnitude.[203] The formation of the ion-pair state is often mediated by an initial Franck−Condon transition to an excited Rydberg neutral surface, followed by conversion to the ion-pair surface.[203] When the ion-pair formation is observed at the thermochemical threshold energy, which is often but not always the case, it yields a direct value for the ion-pair formation energy, $D_0(X^+-Y^-)$, which is related to the neutral bond dissociation energy by eq 3.

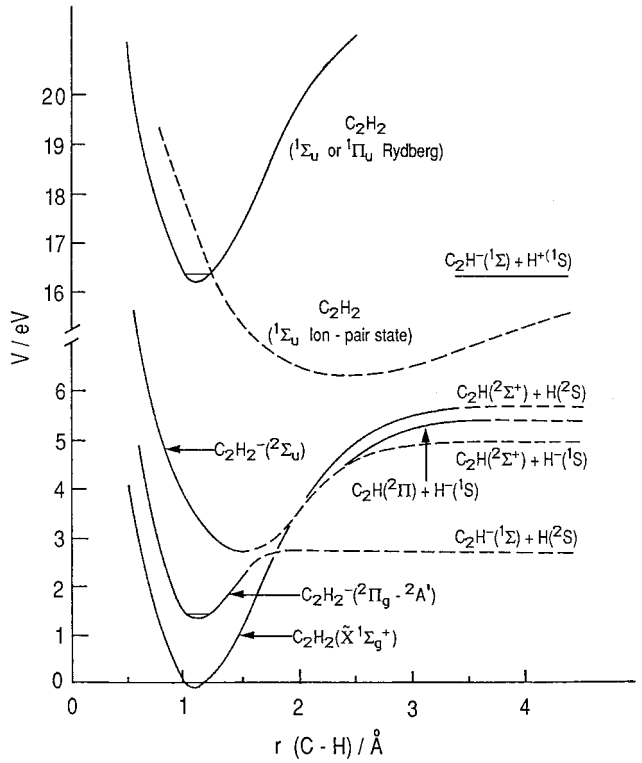


**Figure 22.** Schematic energy level diagrams showing the ion-pair state of acetylene and other neutral and anionic electronic states. Threshold formation of $C_2H^- + H^+$ occurs via a transition to a neutral molecular Rydberg state. (Reprinted with permission from ref 272. Copyright 1990 American Institute of Physics.)

Photoion-pair threshold energies have been measured for $H_2$, $O_2$, NO, CO, halogen-containing diatomics, small hydrohalocarbons, and other small molecules.[203] As an example, schematic potential energy curves[272] for HCCH showing the $C_2H^- + H^+$ ion-pair state are shown in Figure 22. The initial transition occurs via a neutral molecular Rydberg state of HCCH. The photoion-pair formation threshold, $D_0(HCC^- - H^+) = 16.33_5 \pm 0.02$ eV, was observed by photoionization mass spectrometry[198,272] and represents a direct, absolute measure of the gas-phase acidity of acetylene. This can be combined with the electron affinity[273] of $C_2H$ using eq 5 to obtain the C−H bond energy of acetylene, which was controversial at the time.[17,219]

Threshold ion-pair production spectroscopy (TIPPS) is a promising new technique developed by Martin and Hepburn.[45,274−276] The method is similar to ZEKE/PFI photoelectron spectroscopy. A highly vibrationally excited ion-pair state is formed initially by tunable single-photon excitation, eq 48,

$$XY + h\nu \rightarrow [X^+\cdots Y^-]^* \qquad (48)$$

$$[X^+\cdots Y^-]^* + \vec{E} \rightarrow X^+ + Y^-$$

followed by ion-pair formation induced by the electric field $\vec{E}$ and time-of-flight detection of the cationic fragment. The excited ion-pair state can be thought of as a "heavy electron" Rydberg-like state near the dissociation limit with a long average bond length, in analogy with electronically excited Rydberg states

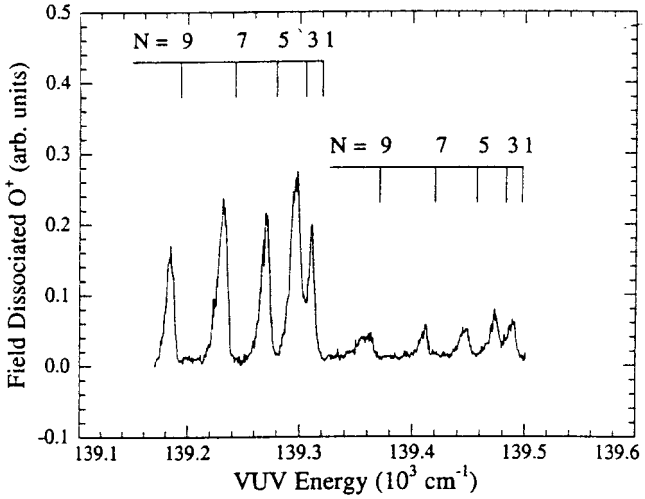


**Figure 23.** Threshold ion-pair production spectrum (TIPPS) of $O_2$. The $O^+$ signal arising from electric-field induced dissociation of near-threshold ion-pair states is plotted versus photoexcitation energy. The rotational states ($N$) of $O_2$ are labeled for the two spin−orbit states of $O^-(^2P_J)$. (Reprinted with permission from ref 274. Copyright 1997 American Physical Society.)

of atoms and molecules near the ionization limit (Figure 6). Gentle electric-field-induced detection preferentially selects those ion-pair states very close to the dissociation threshold, and extrapolation to zero field gives the field-free threshold energy. Figure 23 shows the ion-pair formation spectrum[274] of $O_2$. Separate ion-pair formation thresholds are resolved for thermally populated levels of the molecule, as shown for the rotational levels ($N$) of $O_2$ in Figure 23, and for low-lying states of the fragment ions, as with the $^2P_{3/2}$ and $^2P_{1/2}$ spin−orbit states of $O^-$. TIPPS experiments[45,274−276] have provided the ion-pair formation energies of $O_2$, HF, HCl, and $H_2S$ to within $\pm(1-3)$ cm$^{-1}$. For HF, HCl, and $H_2S$ these are direct absolute measurements of the 0 K gas-phase acidities with extraordinary precision compared with conventional acidity measurements. For molecules larger than triatomics, the utility of threshold ion-pair production spectroscopy is yet to be proven. The low ion-pair formation probabilities for polyatomics[203] may be circumvented with high-intensity synchrotron light sources. When either ionic fragment is polyatomic, a series of ion-pair thresholds will be observed corresponding to excited states of the ion.[274] If these spectral transitions can be resolved and assigned, ion-pair formation energies can be determined with high accuracy. Spectral complexity will likely be an issue as the systems become larger, however.

The accuracy of the ion-pair formation measurements can be examined using the thermochemical cycle in eq 49,

$$\delta = D_0(XY) + IE_0(X) - D_0(X^+ - Y^-) - EA_0(Y) \qquad (49)$$

where $\delta = 0$ for the exact relationship of eq 3, with independently determined bond dissociation energies, electron affinities, and ionization energies. Table 4 shows the data and errors from TIPPS measure-

**Table 4. Thermochemical Comparison of Neutral Bond Dissociation Energies, Ion-Pair Formation Energies, and Electron Affinities (kJ/mol) at 0 K**

| XY | $D_0$(XY) | ref | $IE_0$(X) | ref | $D_0(X^+\text{-}Y^-)$ | ref | $EA_0$(Y) | ref | $\delta$[a] |
|---|---|---|---|---|---|---|---|---|---|
| | | | | | Threshold Ion-Pair Production Spectroscopy | | | | |
| $O_2$ | 493.59 ± 0.20 | 77 | 1313.9426 ± 0.0007 | 83, 112 | 1666.627 ± 0.008 | 275 | 140.9759 ± 0.0002 | 209,284 | 0.07 ± 0.20 |
| HCl | 427.78 ± 0.10 | 77 | 1312.0494 ± 0.0001 | 83, 112 | 1391.122 ± 0.007 | 275 | 348.5750 ± 0.0026 | 285 | 0.13 ± 0.10 |
| HF | 565.97 ± 0.06 | 283 | 1312.0494 ± 0.0001 | 83, 112 | 1549.860 ± 0.004 | 276 | 328.1649 ± 0.0003 | 208 | 0.01 ± 0.06 |
| $H_2S$ | 376.11 ± 0.24 | 42 | 1312.0494 ± 0.0001 | 83, 112 | 1464.92 ± 0.04 | 45 | 223.300 ± 0.024 [b] | 287 | −0.06 ± 0.24 |
| | | | | | | | 223.6 ± 0.2 | 288 | −0.4 ± 0.3 |
| | | | | | Photoion-Pair Threshold Energies | | | | |
| $H_2$ | 432.070 ± 0.012 | 77 | 1312.0494 ± 0.0001 | 83, 112 | 1671.33 ± 0.05 | 279 | 72.7687 ± 0.0018 | 39 | 0.02 ± 0.05 |
| $F_2$ | 154.55 ± 0.60 | 77 | 1681.046 ± 0.005 | 83, 112 | ~1503 | 213 | 328.1649 ± 0.0003 | 208 | ~3 |
| $Cl_2$ | 239.239 ± 0.016 | 77 | 1251.186 ± 0.004 | 83, 112 | ~1123 | 203,278 | 348.5750 ± 0.0026 | 285 | ~19 |
| $Br_2$ | 190.16 ± 0.26 | 77 | 1139.86 ± 0.01 | 83 | 1007.6 | 280 | 324.53696 ± 0.00018 | 208 | −2.2 |
| $I_2$ | 148.82 ± 0.11 | 77 | 1008.39 ± 0.01 | 83 | 863.1 | 213,281 | 295.15218 ± 0.00096 | 208 | −1.0 |
| NO | 626.84 ± 0.12 | 78 | 1402.331 ± 0.004 | 83 | 1887 ± 3 | 282 | 140.9759 ± 0.0042 | 70 | 1 ± 3 |
| CO | 1071.80 ± 0.23 | 78,79 | 1086.454 ± 0.001 | 83 | 2020 ± 2 | 282 | 140.9759 ± 0.0042 | 70 | −3 ± 2 |
| $H_2O$ | 494.07 ± 0.17 | 78 | 1312.0494 ± 0.0001 | 83, 112 | ~1630 | 203 | 176.34177 ± 0.00036 | 170 | −1 |
| HCCH | 551.2 ± 0.1 | 17 | 1312.0494 ± 0.0001 | 83, 112 | 1576 ± 2 | 272 | 286.5 ± 0.6 | 273 | 1 ± 2 |
| HCN | 522.9 ± 0.8 | 44 | 1312.0494 ± 0.0001 | 83, 112 | 1465 ± 2 | 277 | 369.1 ± 0.5 | 286 | 0.8 ± 2 |

[a] Error in the thermodynamic cycle defined by eq 49. [b] "Preliminary" value.

ments[45,274−276] of $O_2$, HF, HCl, and $H_2S$ and from photoion-pair threshold measurements for all the diatomics plus the polyatomic systems with $X^+ = H^+$ for which all four quantities in eq 49 are independently known.[39,45,70,170,203,208,209,213,272−288] The generally small values of $\delta$ demonstrate that the interrelated values are extremely well-defined for these systems. The only major apparent error is $\delta \approx 19$ kJ/mol for $Cl_2$, for which the (uncorrected) ion-pair threshold was observed to be contaminated by hot bands with intensities enhanced by rotational effects.[278] Discounting $Cl_2$, the mean absolute deviation is 1 kJ/mol and only two of nine deviate outside stated uncertainty limits.

## *VIII. Electron Ionization Threshold Methods*

In electron impact ionization threshold measurements, ionization is achieved by the interaction of a neutral species with an energetic electron, eq 50.

$$AB + e^-(E_e) \rightarrow AB^+ + 2e^- \qquad (50)$$

Dissociative ionization may also occur, eq 51.

$$AB + e^-(E_e) \rightarrow A^+ + B + 2e^- \qquad (51)$$

Near-linear threshold behavior of the cross section vs electron energy, $E_e$, is found in high-resolution experiments on atoms and small molecules.[167] For polyatomics, the transition intensities are governed by the Franck−Condon principle.[167,289] Because the threshold onset is near-linear, compared with a step function for photoionization, identifying individual state-to-state thresholds is difficult.[192]

Early appearance energy and ionization energy measurements by electron ionization (EI) threshold measurements using nonmonoenergetic electron sources are subject to large, unpredictable errors of 0.1−0.5 eV (10−50 kJ/mol) or more.[192] A recent summary[289] of such EI threshold measurements on atoms and small molecules indicates that values within 0.1 eV of photoionization results can be obtained for atoms or small molecules with little geometry change between the neutral and ion. For molecules that change geometries upon ionization, however, the EI threshold energy is unpredictably closer to either the adiabatic or the vertical ionization energy.[289] The prevalence of non-Franck−Condon effects in threshold photoionization processes[195,201] implies that ion production in the Franck−Condon gaps is also likely for electron ionization. Appearance energy measurements on polyatomic molecules are also subject to excess internal energies in the products, and from kinetic and competitive shifts in product ion formation.[109,129,130,146] Low-resolution EI thresholds may be suitable for qualitative predictions of fragmentation patterns from an EI ion source but are not reliable thermochemical values. Nevertheless, many of these results have been carried over from early ion thermochemistry compilations[109,162] into current ones.[106,107]

Modern electron ionization experiments use an electron monochromator to narrow the electron beam energy distribution, and the energy scale is calibrated by measurement of a known ionization energy.[290,291] An electron energy spread of 50−150 meV is typical.[167,290] For atoms and small molecules, modeling the thresholds with a linear threshold law and accounting for the electron energy spread gives ionization energies in excellent agreement with photoionization results.[167] For polyatomic molecules, these experiments are still subject to excess energy in the products and to kinetic and competitive shifts of the thresholds, as described in section V. Appearance energy experiments can provide thermochemically reliable threshold energies if these effects are controlled experimentally or adequately modeled in the data analysis. However, that level of sophistication in the analysis is not uniformly applied in the literature.

A simplified threshold analysis strategy, instead of explicitly accounting for the internal energy distribution as in eq 35, is to treat the apparent threshold onset as the ionization energy or appearance energy as a room-temperature value.[292,293] Holmes[291,292] advocated this approach for appearance energy measurements and questions whether the

internal energy of a polyatomic molecule participates in the dissociation process. Holmes[292] cites the self-consistency of ion enthalpies of formation obtained from appearance energies for the same ion from different precursor molecules as evidence that this approach is valid. However, dissociative photoionization studies[215] show that internal energy effects are important, which suggests that the observed self-consistency in AE measurements[291,292] may rely on cancellation of effects. Figure 5 shows that internal energy effects and kinetic shifts tend to move an apparent threshold in opposite directions. These effects both increase with increasing size of the dissociating molecule, but there is no reason to expect exact cancellation. Ruscic et al.[215] discussed the errors that arise from neglecting the internal energy distribution and thermal corrections in electron ionization.

Locht and co-workers[294−296] employ a dissociative electron ionization method in which the kinetic energies of the product ions are measured using retarding potential analysis. This allows extrapolation of ion appearance energies to zero ion kinetic energy, correcting for cases where a barrier to dissociation causes products to be formed with excess translational energy. Issues of the electron energy spread, internal energies of reactants and products, and kinetics shifts are not addressed by this procedure, however. In the dissociative ionization of acetylene, Locht and Servais[296] obtain dissociation energies of $D$(H−CCH) = 514 ± 22 kJ/mol and $D$(HC≡CH) = 948 ± 10 kJ/mol (no temperature specified), compared with $D_0$(H−CCH) = 551.2 ± 0.1 kJ/mol from photofragment translational spectroscopy[17] and $D_0$(HC≡CH) = 960.1 ± 2.7 kJ/mol from established enthalpies of formation.[79]

Time-resolved appearance energy measurements address the issue of kinetic shifts in electron ionization thresholds.[146,154,297] The concept is identical to time-resolved photoionization discussed in section VII.B. In the work of Lifshitz and co-workers,[146] the ions are stored for a variable residence time following ionization in the ion source using an electron beam trap. Time-resolved ionization has recently been applied to the important problem of the dissociation energy of buckminsterfullerene, $C_{60}$, which has been studied by a variety of techniques as reviewed by Lifshitz and co-workers[297,298] The dissociation energy for $C_2$ loss from $C_{60}^+$ is controversial[298,299] but is now believed to be ≥9.5 eV, higher than earlier estimates.[298] The apparent appearance energy threshold[154] is 45−50 eV, i.e., there is an enormous kinetic shift in this extreme case. The value extracted from the time-resolved ionization and other experiments is highly sensitive to the nature of the transition state that is assumed for the dissociation process, and both radiative relaxation and thermionic emission must be considered as competitive processes.[154,297,298]

Electron ionization experiments have potential for providing accurate ionization and appearance energies, despite their mixed historical record. It is clearly necessary to use a monochromator to narrow the electron energy distribution and to have a reliable electron energy calibration. As with dissociative photoionization, it is necessary to characterize and correct for kinetic and competitive shifts, the internal energy of the neutral precursors, and the internal and kinetic energies of products.

## IX. Direct Photodissociation

This section discusses direct photodissociation experiments for small molecules where the dissociation process is prompt. Photoactivated statistical dissociation processes are treated separately in section X.

### A. Ion Photodissociation Thresholds

Observation of photodissociation imposes an upper limit on the dissociation energy of a molecular ion, which in favorable cases may be near the thermodynamic limit, eq 52.

$$MX^+ + h\nu \rightarrow M^+ + X \qquad D_0(M^+-X) \leq h\nu_0 \quad (52)$$

Dissociation at the thermochemical threshold requires both that the molecule absorbs at the appropriate wavelength and that the excited-state dissociates promptly. For photofragmentation of ions, mass spectrometry allows preselection of the parent ion and detection of the product ion. Ion photodissociation threshold measurements have been made for many systems, including, for example, metal-containing ions.[53,67,300−305] Russon et al.[302] determined photodissociation onsets for transition-metal dimers, $Ti_2^+$, $V_2^+$, and $Co_2^+$ and the trimer $Co_3^+$, which could be compared with dissociation energies measured by threshold collision-induced dissociation experiments.[306−309] An example of the predissociation threshold for $V_2^+$ is shown in Figure 24. The sudden increase in the $V^+$ intensity at 25 326 $cm^{-1}$ gives a bond dissociation energy of $D_0(V^+-V)$ = 303.0 ± 0.2 kJ/mol, in good agreement with the TCID measurement of 302 ± 12 kJ/mol.[302] Spain and Morse[310] give guidelines for the interpretation of these spectroscopic dissociation thresholds as thermochemical

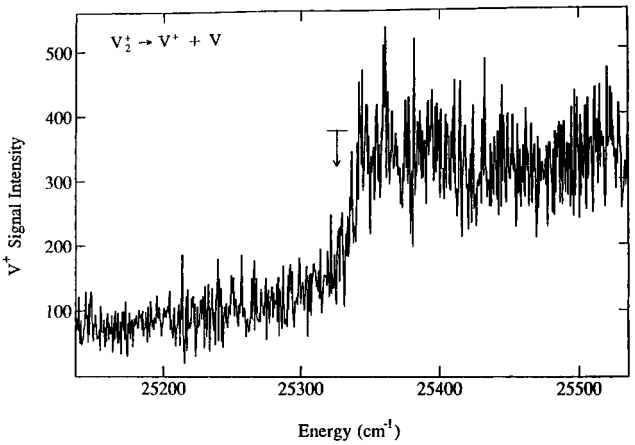


**Figure 24.** Predissociation threshold of $V_2^+$ detected in a photodissociation action spectrum. The threshold energy is marked by an arrow, giving $D_0(V^+-V)$ = 303.0 ± 0.2 kJ/mol. (Reprinted with permission from ref 302. Copyright 1994 American Institute of Physics.)

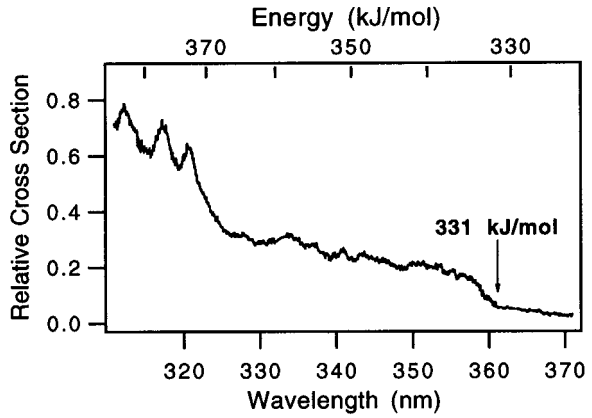


**Figure 25.** Photofragment spectrum of $CoCH_2^+ + h\nu \rightarrow Co^+ + CH_2$. The photodissociation threshold energy at 331 ± 2 kJ/mol is labeled. (Reprinted with permission from ref 304. Copyright 2000 American Chemical Society.)

bond energies—the molecule must have a large density of electronic states near the separated atom limit and this separated atom limit must also connect with repulsive electronic states.

Metz and co-workers[303−305] recently measured photofragment spectra of $FeO^+$ and $MCH_2^+$ (M = Fe, Co, Ni, and Au). The example of $CoCH_2^+$ in Figure 25 shows a sharp increase in $Co^+$ signal at 361 nm, yielding $D_0(Co^+-CH_2) \leq 331 \pm 2$ kJ/mol, which agrees as an upper limit with guided-ion beam results of Armentrout and co-workers[55] of $D_0(Co^+-CH_2) = 317 \pm 5$ kJ/mol. The other metals give thresholds closer to the guided-ion beam results; observation of photodissociation at the thermochemical threshold depends on the Franck−Condon overlap with excited states and their predissociation lifetimes. In the case of $AuCH_2^+$, Metz and co-workers[305] show that the rotational energy of the ions contributes directly toward the dissociation process.

## B. Photofragment Translational Spectroscopy

At energies above the photodissociation threshold, the excess energy goes into either product internal energy or product kinetic energies. Photofragment translational spectroscopy (PTS) measures the product kinetic energies. When the internal energy states can be assigned spectroscopically, a precise measurement of the dissociation energy is obtained by energy balance. Photofragment translational spectroscopy has been carried out on a number of neutral systems.[17,42] For ions, mass spectrometry permits identification of the signal carrier or the product ion.[311−313] For example, Ding et al.[313] measured product recoil velocities in time-of-flight measurements of the photodissociation of $Mg_2^+$ ions via a repulsive state, leading to an estimate of the dissociation energy, $D_0(Mg^+-Mg) = 122 \pm 4$ kJ/mol.

Another experimental approach to photofragment translational spectroscopy of ions is to measure the off-axis translational energy release following photodissociation of a kiloelectronvolt ion beam using a position-sensitive detector.[311,312,314] For negative ions, the process is given by eq 53.

$$XY^- + h\nu \rightarrow X^- + Y \qquad (53)$$

Both products are measured in coincidence, and their positions and times-of-arrival at the detector yield the relative translational energy of the products. If the maximum translational energy release corresponds with products with no internal excitation, then the dissociation energy $D(X^-Y)$ can be deduced by energy conservation. In the photodissociation of $N_2O_2^-$ by Neumark and co-workers,[312] vibrational structure is observed in the translational energy distribution for $O^- + N_2O$ products and assigned to the $N_2O$ bending mode. Assignment of the feature with maximum translational energy release to the ground vibrational level of $N_2O$ allows determination of the bond energy, $D_0(O^-N_2O) = 135 \pm 3$ kJ/mol.

### 1. Fast Radical PTS

Neumark and co-workers[40,315] developed a fast radical beam photofragment translational spectroscopy technique that uses negative-ion photodetachment to prepare a neutral radical, then measures the kinetic energies of the products upon photodissociation in a second step, eq 54.

$$XY^- + h\nu \rightarrow XY + e^- \qquad (54)$$
$$XY + h\nu' \rightarrow X + Y$$

The negative ions are formed by electron attachment in a supersonic expansion source, accelerated to 6−8 keV, mass-selected by a time-of-flight spectrometer, and detached by the first laser pulse creating a fast neutral beam. The neutrals are dissociated by a second laser. The total photodissociation yield as a function of wavelength gives the state-resolved photodissociation spectrum. The example of $CH_3S$ is shown in Figure 26a, with assignments to vibronic transitions in the $A \leftarrow X$ band of $CH_3S$.[40] For nine different transitions, Figure 26b shows the fragment translational energy spectra for $CH_3 + S$, in which the internal energy states of the products are resolved.

Much of the interest in this work is in the spectroscopy and dissociation dynamics of the radicals and ions, but the measurement of photofragment translational energies can also yield accurate dissociation energies. By energy balance, the dissociation energy is equal to the photon energy minus the maximum translational energy of the reactants and the internal energy of the products. The spectroscopic identification of the product vibrational states, and sometimes their rotational states, allow the internal energy to be determined precisely. The internal energy of the reactant ions should also be characterized, because vibrational excitations may not necessarily be completely cooled even in a supersonic expansion. In the case of the fast radical method, the photodetachment wavelength can be set at a near-threshold level to limit the internal excitation of the neutral radical. The maximum photofragment energy is measured in product kinetic energy spectra, as shown for $CH_3S$ in Figure 26b.[40] That work[40] yields the dissociation energy $D_0(CH_3-S) = 293.8 \pm 1.4$ kJ/mol. Using the enthalpies of formation[13,78,79,215] of $CH_3$, H, S, and $CH_3SH$ and integrated heat capacities[78,79] [with $IHC_{298}(CH_3S)$ approximated[9] by the

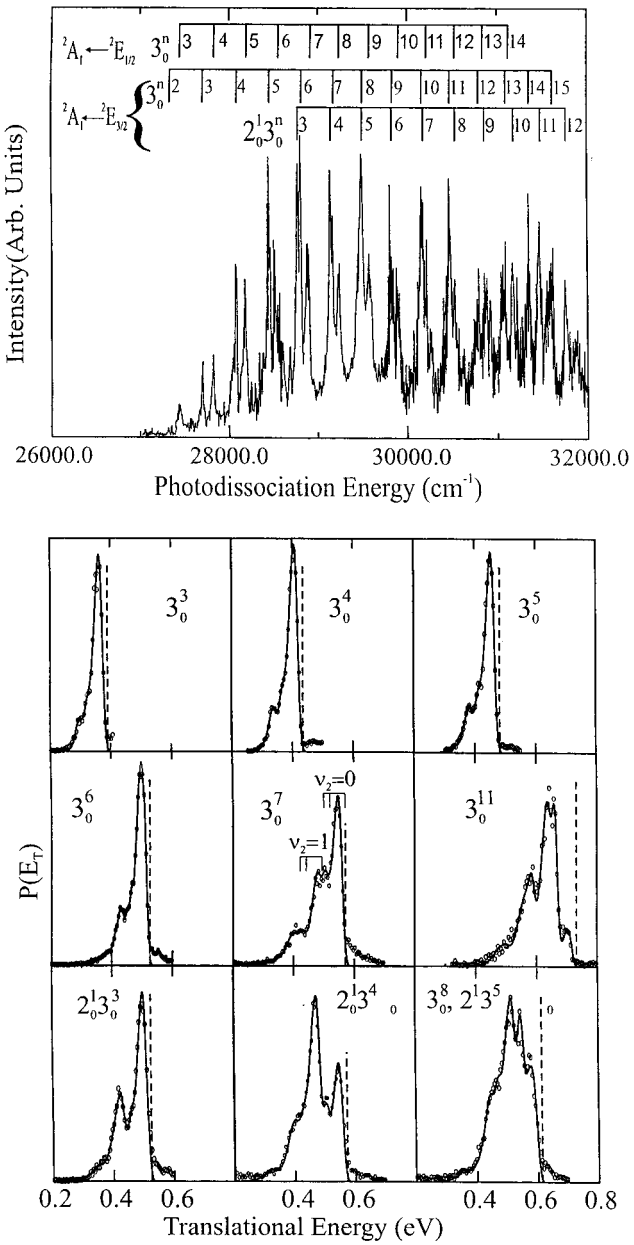


**Figure 26.** Fast radical photofragment translational spectroscopy of $CH_3S$ produced by photodetachment of $CH_3S^-$. (a) Top: photofragment yield spectrum for the $A \leftarrow X$ band of $CH_3S$. (b) Bottom: translational energy distributions of the $CH_3$ + S photofragments for labeled vibrational transitions of the $A \leftarrow X$ band. (Reprinted with permission from ref 40. Copyright 1999 American Institute of Physics.)

value[78,79] for $CH_3Cl$], this value yields the bond dissociation enthalpy of methanethiol, $DH_{298}(CH_3S-H) = 364.2 \pm 1.6$ kJ/mol, in good agreement with the value of $365.5 \pm 1.5$ from radical kinetics measurements.[316]

### 2. Dissociative Photodetachment PTS

A variant of photofragment translational spectroscopy is the dissociative photodetachment experiment of Continetti and co-workers.[314,317] They use multiple coincidence techniques to measure both the photoelectron energy and the kinetic energy release of molecular fragments. An example is the measurement[314] of the process $N_3O_2^- + h\nu \rightarrow NO + N_2O + e^-$ at 266, 355, and 532 nm. From the maximum total energies of the neutral products and with the assumption that at least some neutral products are formed with no internal energy, they estimate the stability of a covalent ion isomer of $N_3O_2^-$ as $190 \pm 20$ kJ/mol relative to $NO + N_2O + e^-$. This strongly bound isomer exists in addition to a loosely bound $NO^-(N_2O)$ complex. However, a recent collision-induced dissociation experiment on $N_3O_2^-$ by de Torchia et al.[318] gives $D_0(NO^- - N_2O) = 73 \pm 10$ kJ/mol. As the electron affinity[319] of NO is small, $EA(NO) = 2.5 \pm 0.5$ kJ/mol, there is a large deviation between these two experiments. The discrepancy could be explained by the unlikely existence of more than one strongly bound isomer of $N_3O_2^-$ or if the dissociative photodetachment process predominantly yields highly excited products.

## X. Unimolecular Dissociation

The basic idea behind unimolecular dissociation methods[320] for measuring thermochemical values is that the rate of dissociation of a molecule or ion with a given internal energy content is strongly dependent upon the energy barrier for dissociation, as given by RRKM/QET theory (section IV). The dissociation rates may be measured directly in time-resolved experiments; otherwise statistical theory is used to correct for kinetic and competitive shifts in threshold energy measurements (section V).

### A. Time-Resolved Photodissociation

In time-resolved photodissociation, the rate of unimolecular dissociation is measured directly by monitoring the ion fragmentation probability as a function of time following photoactivation.[153,321−324] The rate is modeled by statistical theory, preferably for multiple photon energies, to obtain the dissociation energy of the ion. Single-photon or two-photon absorption adds an exactly known amount of energy to the parent ion, which is an advantage over collisional or multiphoton activation. Tandem mass spectrometry allows selection of the ion to be dissociated and identification of the products. ICR or quadrupole ion traps are well suited for time-resolved photodissociation experiments on the 100 $\mu$s or longer time scale. The ions can be made in the trap or injected from an external source, mass-selected, activated in the trap by a laser pulse, then stored for a variable time period before mass analysis.[321,322,324] An alternative arrangement uses a long (1 m) ion beam guide in a tandem mass spectrometer instrument.[153,323] A coaxial laser pulse activates all the ions along the length of the beam guide, and then photofragment product ions are detected as a function of time-of-arrival at the detector. This turns the spatial distribution along the constant-velocity ion beam into a photodissociation time distribution.

Figure 27 shows the time-resolved fragment ion intensity for the dissociation of deuterated naphthalene ion by loss of acetylene after activation by two photons at 355 nm from Ho et al.[322] Losses of $D_2$ and D were also observed as parallel dissociations. Fits to the data use RRKM theory, a convolution over the

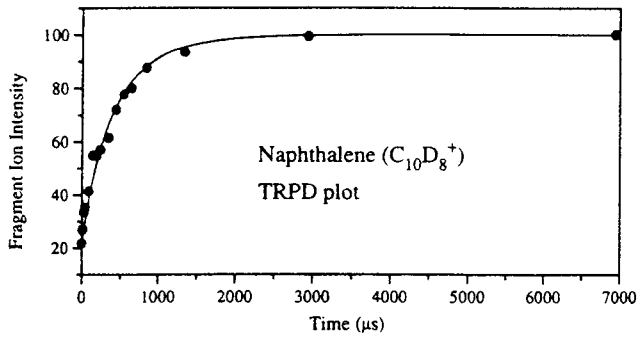


**Figure 27.** Time-resolved photodissociation curve for naphthalene ion, $C_{10}D_8^+ + h\nu \rightarrow C_8D_6^+ + C_2D_2$. The solid line is a simulation from RRKM theory convoluted over the thermal ion internal energy distribution. (Reprinted with permission from ref 322. Copyright 1995 American Chemical Society.)

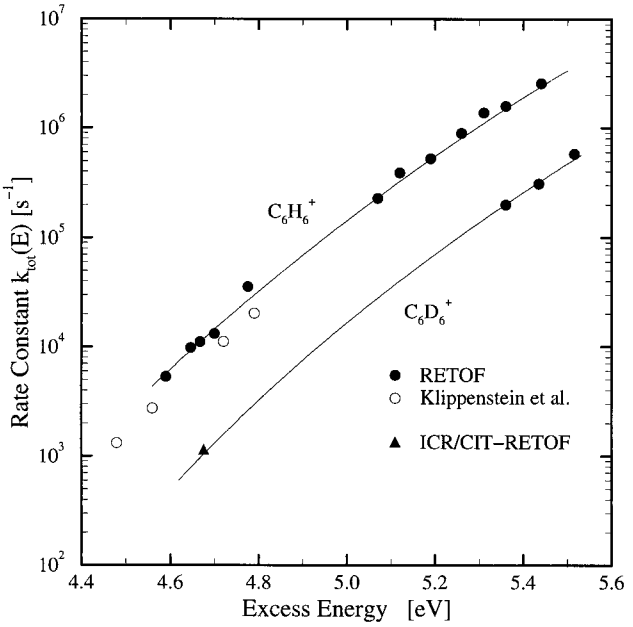


**Figure 28.** Dissociation rate constants $k(E)$ for benzene obtained by time-resolved photodissociation using three different instruments: ICR (○),[327] time-of-flight mass spectrometry (●),[326] and cylindrical ion trap (▲).[325] Solid lines represent the RRKM rate constants. (Reprinted with permission from ref 325. Copyright 1999 Elsevier Science.)

300 K thermal distribution of the naphthalene parent ions, and the instrumental detection probabilities for the ICR. For this system, some of the rates and energetics could also be constrained by independent TPEPICO and TPES experiments, leading to a C−H bond dissociation energy of $D_0(C_{10}H_7^+\text{-H}) = 433 \pm 10$ kJ/mol and an acetylene-loss energy of 426 ± 20 kJ/mol.

The $k(E)$ curves for dissociation of energy-selected benzene ions[325] ($C_6H_6^+$ and $C_6D_6^+$) are presented in Figure 28. Resonantly enhanced multiphoton ionization is used to select the ion internal energy, followed by photodissociation.[325,326] The data in Figure 28 are combined from time-resolved experiments using time-of-flight mass spectrometry,[326] ICR mass spectrometry,[327] and a cylindrical ion trap experiment,[325] covering a range of time regimes and excitation energies. The $k(E)$ data for the total dissociation combined with information on branching ratios for the H-, $H_2$-, $C_2H_2$-, and $C_3H_3$-loss channels are modeled by statistical theory to obtain the transition-state energies (353, 361, 398, and 404 kJ/mol for the four channels, respectively).[325]

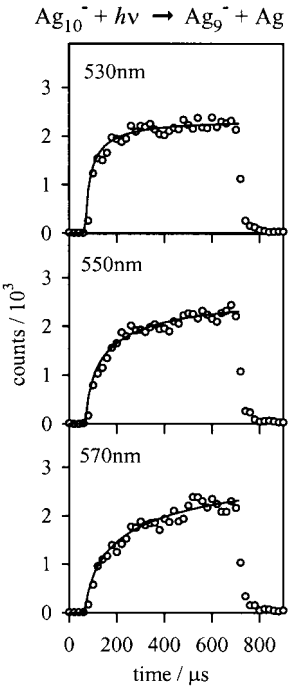


**Figure 29.** Time-resolved photodissociation curves for $Ag_{10}^- + h\nu \rightarrow Ag_9^- + Ag$ measured at three photoactivation wavelengths by guided-ion beam mass spectrometry. Solid lines are RRKM fits using a dissociation energy of $D_0(Ag_9\text{-}Ag) = 176 \pm 4$ kJ/mol. (Adapted with permission from ref 153. Copyright 1999 American Institute of Physics.)

Time-resolved photodissociation has also been applied to metal cluster systems.[153,323,324] Figure 29 shows time-resolved photodissociation curves for a silver cluster anion, $Ag_{10}^-$, from the work of Shi et al.[153] The rise times are slower for longer wavelengths (lower photon energies) as expected. The same dissociation energy is used for the RRKM model of the time profiles at different photon energies, supporting the validity of the RRKM model and estimated transition-state parameters. Shi et al.[153] also observed both prompt photodetachment and delayed electron loss in competition with statistical fragmentation and accounted for the branching ratios in their model. Electron-loss and atom-loss processes are competitive for silver cluster anions because the electron binding energies and dissociation energies happen to be similar.[153] Radiative emission is another possible competitive channel, especially for long dissociation times.[148] Time-resolved photodissociation has been used as a thermometry probe to examine radiative cooling processes.[152,328]

## B. Energy-Resolved Threshold Collision-Induced Dissociation

In the threshold collision-induced-dissociation (TCID) method,[329] a tandem mass spectrometer is used to isolate the parent ion by mass, accelerate or decelerate the ions to a controlled kinetic energy, collide them with an inert target gas under single-collision conditions, and then mass analyze the

fragment ions. The reaction process is given by eq 55

$$AB^+ + Xe \rightarrow [AB^+]^* + Xe \qquad (55)$$

$$[AB^+]^* \rightarrow A^+ + B$$

where xenon is preferred as the target because it is heavy and polarizable, promoting efficient energy transfer.[183] In TCID, the apparent cross section for formation of the fragment ion $A^+$ is measured as a function of the relative ion/target collision energy in the center-of-mass frame. The threshold energy for dissociation, $E_0$, is equal to the 0 K reaction endothermicity of the dissociation $AB^+ \rightarrow A^+ + B$, in the absence of reverse activation energies and when the translational and internal energy distributions and kinetic shifts are accounted for as discussed in section V. The TCID process in eq 55 is shown as two steps to emphasize that although the activation step is bimolecular, it is followed by unimolecular statistical decomposition of the activated ion.

TCID experiments employ tandem mass spectrometers of various types. Guided-ion beam (GIB) instruments[187,329−336] use a radio frequency octopole[337] in the interaction region for high-efficiency collection of scattered products and low-energy ions. These instruments typically use a magnetic sector or Wien filter for initial mass analysis and a quadrupole for postreaction mass analysis,[330,331,333,334] but configurations have been reported using tandem sector,[332] quadrupole,[335,338] or time-of-flight[336] mass spectrometers with an octopole ion beam guide. Commercial triple-quadrupole mass spectrometers have been used for TCID experiments[339−341] as well as for analytic collision-induced dissociation. However, the cross sections in triple quadrupoles may exhibit "tails" in the threshold region[339,340] because of the energy and angular distribution of the ions emerging from the first quadrupole mass filter or the presence of reactant gas in the regions between the quadrupoles. Energy-resolved collision-induced dissociation experiments have also been carried out in ICR traps, where care must be taken to characterize the broad translational energy distributions, multiple collision effects, and mass discrimination effects.[342−346]

Obtaining accurate dissociation energies from TCID requires corrections for kinetic shifts using RRKM theory and convolutions over the internal and translational energy distributions, as outlined in sections IV and V and described in detail elsewhere.[145,187−189,330] The TCID method has been validated for many systems where independent thermochemical information is available.[55,183,345,347] Isolated cases of TCID threshold energies in excess of the thermochemical dissociation energy have been observed, curiously mainly for diatomic species.[348−350] Possible reasons for thresholds in excess of the thermodynamic limit could include a potential energy barrier due to an avoided crossing of electronic surfaces or a required spin change to access ground-state products. Alternatively, for strongly bound species, impulsive mechanisms may not efficiently deposit energy into the reactant ion at the required high collision energies. As with other thermokinetic methods, it is crucial that the reactant ions be prepared with a known internal energy content or temperature. Recent GIB instruments used for TCID experiments employ flow tube reactor ion sources that generally ensure well-thermalized ions via $10^4-10^5$ collisions with a buffer gas.[334,335,351]

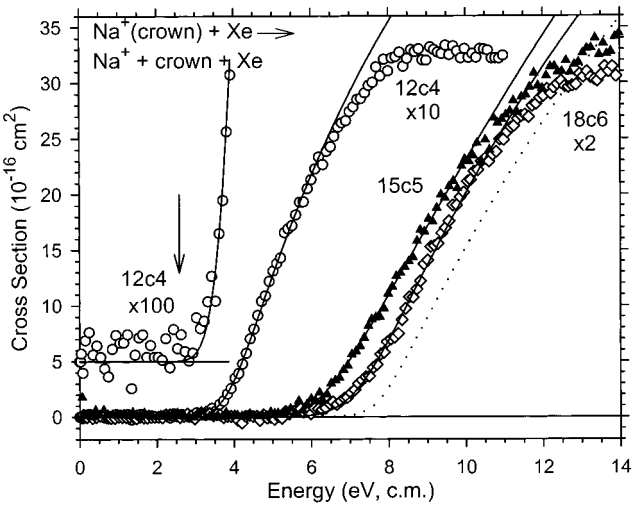


**Figure 30.** Cross sections for threshold collision-induced dissociation (TCID) of crown ethers (12-crown-4, 15-crown-5, and 18-crown-6) complexed with sodium ions as a function of kinetic energy in the center-of-mass frame. Solid lines are the threshold model including the effects of kinetic shifts and internal and translational energy distributions. Dotted line is the model for $Na^+$(18-crown-6) without the convolution over internal energy for comparison. (Reprinted with permission from ref 361. Copyright 1999 Elsevier Science.)

### 1. Single-Channel TCID

The TCID method has been employed to obtain dissociation energies for a variety of systems, including metal and main-group cluster ions,[187,329,352] transition-metal carbonyls,[55,347,353] proton-bound and metal-ion complexes,[28,340,354] polyhalide anions,[355] and $CO_2$ or halide elimination.[339,356] Armentrout and coworkers[357−361] recently studied host−guest interactions of crown ethers with alkali ions using TCID, eq 56.

$$M^+\cdot c\text{-}(C_2H_4O)_n + Xe \rightarrow M^+ + c\text{-}(C_2H_4O)_n + Xe$$
$$E_0 = D_0[M^+ - c\text{-}(C_2H_4O)_n] \qquad (56)$$

These systems present a challenge for TCID because the strong binding of multidentate ligands and the floppy nature of the crown ethers conspire to give large kinetic shifts and internal energy effects. Comparative studies using metal ions complexed with several monodentate or bidentate ether molecules were carried out to evaluate the TCID results on the crown ethers. Figure 30 shows the TCID cross sections for sodium ions complexed with the 12-crown-4, 15-crown-5, and 18-crown-6 ethers (tetra-, penta-, and hexadentate, respectively).[361] The apparent threshold energy for the smallest system, 12-crown-4 ether, matches the derived 0 K dissociation energy of 2.61 ± 0.13 eV relatively closely, but the larger systems have apparent threshold energies substantially higher than the derived dissociation

energies, 3.05 ± 0.19 eV for 15-crown-5 and 3.07 ± 0.20 eV for 18-crown-6. That is, the full RRKM model[145] of the dissociation probabilities as a function of available energy is crucial for obtaining meaningful thermochemical results. The crown ether results were compared with the sums of binding energies for mono- and bidentate ethers and with theoretical calculations to validate the modeling procedures.[361]

### *2. Competitive TCID*

The RRKM model for kinetic shifts in TCID was recently extended by Rodgers and Armentrout[189] to handle the competitive shifts between two or more product channels. The product branching ratio as a function of the available energy is calculated using RRKM theory. The fit to the TCID cross sections for two product channels simultaneously over a range of collision energies above threshold provides an internal test of the statistical model, with the difference in threshold energies as an adjustable parameter. The competitive TCID method has been applied to measure lithium ion affinities,[189] gas-phase acidities,[28,362] proton affinities,[363] hydronium ion affinities,[364] and metal cluster dissociation energies.[350,352] In competitive TCID experiments on proton-bound alkoxide dimer anions, DeTuri and Ervin[28] found excellent agreement with literature values in a ladder of gas-phase acidities from *tert*-butyl alcohol to water. Measuring and modeling the product branching ratio over a wide energy range can test the accuracy of the transition-state model. For example, competitive TCID of the proton-bound complex of $C_4H^-$ with acetaldehyde,[362] eq 57, is shown in Figure 31.

$$[C_4H\cdot\cdot H\cdot\cdot CH_2CHO]^- + Xe \rightarrow HC_4H + {}^-CH_2CHO + Xe \quad (57)$$
$$\rightarrow HC_4^- + {}^-CH_3CHO + Xe$$

The cross section for the lower-energy $HC_4^-$ product channel crosses the higher-energy $^-CH_2CHO$ channel at about 0.9 eV. This is a clear indication that the two dissociation channels have dissimilar transition states, i.e., a tight transition state for the lower-energy channel and a loose transition state for the higher channel. Ab initio calculations[362] confirm this and indicate that the proton transfer surface is a double-well potential with the more stable well corresponding to the complex of $HC_4H$ with $^-CH_2CHO$. RRKM theory is used to model the energy-dependent product branching ratio as a function of available energy, which accounts for both kinetic shifts and competitive shifts.[189] Using ab initio parameters for the dissociation transition states in eq 57, the crossing of the two product channels is reproduced (Figure 31).[362] The threshold energy difference of the two channels, 18 ± 3 kJ/mol, gives the gas-phase acidity of diacetylene relative to acetaldehyde. Using literature values for the gas-phase acidity of acetaldehyde[73] and the electron affinity[365] of $C_4H$, the previously unmeasured bond dissociation energy $D_0(HC_4-H) = 539 \pm 12$ kJ/mol is obtained,[362] making it the same as or slightly smaller than the acetylene bond energy,[17] $D_0(HCC-H) = 551.2 \pm 0.1$ kJ/mol.

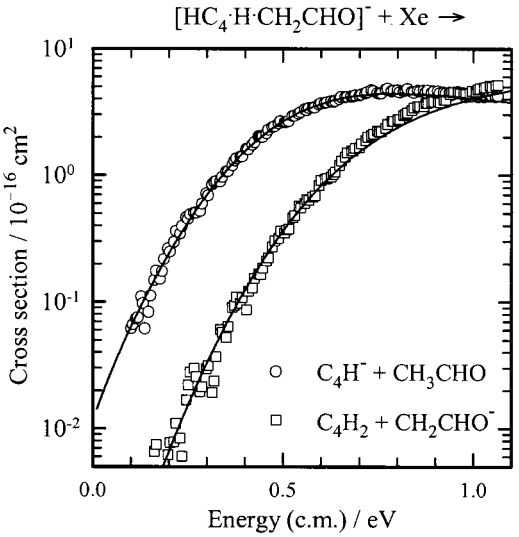


**Figure 31.** Cross sections for competitive TCID of $C_4H^-$(acetaldehyde) complexes as a function of kinetic energy in the center-of-mass frame. Solid lines are the fits using RRKM theory to calculate the product branching ratio as a function of available energy, with convolutions over internal and translational energy distributions. (Reprinted with permission from ref 362. Copyright 2000 Elsevier Science.)

## C. "Slow Heating" Activation

Various "slow heating" methods can be described as near-thermal activation. They include multiple-collision activation in ion cyclotron resonance or other ion traps and multiphoton dissociation from cw infrared lasers or blackbody radiation.[366−374] A shared characteristic of these methods is that multiple activation and deactivation steps occur on roughly the same time scale as the dissociation lifetime.

### *1. Blackbody Infrared Activation*

Under collision-free conditions and at long reaction times, absorption of ambient infrared radiation may become a significant source of activation and unimolecular dissociation.[369,371−373] Ion cyclotron resonance (ICR) mass spectrometers can achieve these conditions, with background pressures below $10^{-8}$ mbar and ion trapping times of milliseconds or longer. In blackbody infrared dissociation (BIRD) experiments,[372,373,375] also called zero-pressure thermal radiation-induced dissociation (ZTRID),[328] the infrared radiation from a temperature-variable ICR cell is employed for unimolecular dissociation rate measurements. Blackbody radiation may also be supplied from a glowing filament source.[370,371] For large molecules and relatively high activation energies, the ions reach equilibrium at the chamber temperature because in that case radiative absorption and emission are faster than dissociation. Under these conditions, the simple Arrhenius rate equation may be applied, eq 58

$$k(E) = A\, e^{-E_{act}/RT} \quad (58)$$

where $E_{act}$ is the activation energy for dissociation. Using the thermodynamic form of RRKM theory, eq 32, the preexponential factor may be related to the

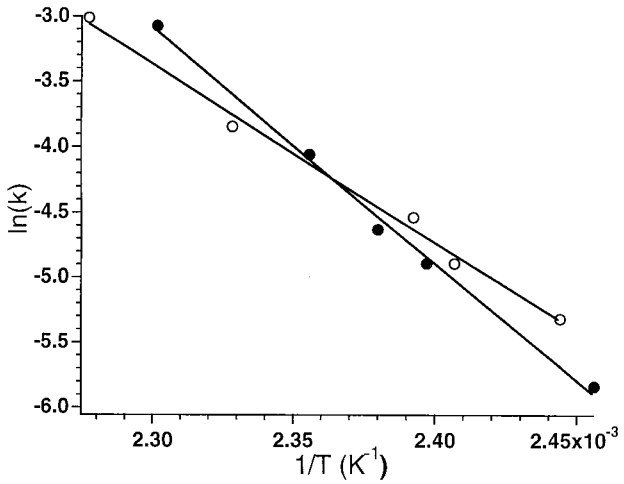


**Figure 32.** Arrhenius plot for blackbody infrared dissociation (BIRD) of $[ubiquitin]^{5+}$, $E_{act} = 120$ kJ/mol and $A = 10^{12}$ $s^{-1}$ (○), and $[ubiquitin]^{11+}$, $E_{act} = 150$ kJ/mol and $A = 10^{17}$ $s^{-1}$ (●). (Reprinted with permission from ref 372. Copyright 1996 American Chemical Society.)

entropy of activation,[133] $A = (kT/h)\exp(1 + \Delta^{\ddagger}S/R)$. Observed $A$-factors range from about $10^{13}$ $s^{-1}$ for small systems to $10^{18}$ $s^{-1}$ for large biomolecular ions with a loosening of the molecular geometry upon dissociation.[369] Figure 32 shows the Arrhenius plot from Price et al.[372] for blackbody infrared dissociation of multiply protonated ubiquitin in its 5+ and 11+ charge states. The activation energy (slope) is 120 and 150 kJ/mol for the two charge states, respectively, while the preexponential factors differ by 5 orders of magnitude ($A \approx 10^{12}$ $s^{-1}$ for 5+ and $A \approx 10^{17}$ $s^{-1}$ for 11+). The high preexponential factor for the 11+ charge state is attributed to an extended salt-bridge structure that enhances free rotations in the transition state, resulting in a highly entropically favored dissociation.[372]

For smaller molecules, the simple Arrhenius relationship does not apply because the high-energy tail of the Boltzmann distribution becomes depleted when unimolecular dissociation rates are faster than the radiative establishment of equilibrium. In that case, the Tolman theorem can be applied to relate the apparent activation energy with the thermodynamic value.[369] In intermediate cases or for more accurate results, it is necessary to apply a master-equation analysis, which treats the individual rates for activation and deactivation explicitly as a function of photon frequency,[372,376] or alternatively to use a Monte Carlo simulation.[370,371] The master-equation approach requires theoretical calculation or a model for absorption and emission rates to account for activation and deactivation as a function of frequency and RRKM theory for the energy-dependent dissociation rates.[372,373]

### 2. Multiphoton Infrared Laser Activation

Infrared multiphoton dissociation (IRMPD) at low powers using an infrared laser bears similarities with blackbody infrared activation.[366,367] Typically, a $CO_2$ laser with a photon frequency of 944 $cm^{-1}$ is used.[53,368] To obtain quantitative information on dissociation energies, the rate of multiphoton absorption must be modeled along with competing dissociation and radiative emission rates.[369,371,376] Unlike blackbody infrared activation, which provides a thermal photon energy distribution, multiphoton infrared activation cannot be modeled using an Arrhenius analysis even for large, long-lived molecules because it is a nonequilibrium activation technique. Uechi and Dunbar[376] used a 440-nm photodissociation probe laser to examine the internal energy distributions in *n*-butylbenzene ions heated by a $CO_2$ laser. They successfully used a master-equation approach to model the photoactivation, radiative emission, and unimolecular dissociation processes but found that a simple harmonic-oscillator model for the transition strengths was inadequate to model the data.[376]

### 3. Multiple Collision Activation

Ions stored in an ICR or quadrupole ion trap in the presence of a background gas undergo multiple collisions that can lead to dissociation. In these experiments, the activation energy is varied either by changing the pressure (number of collisions) or by changing the ion kinetic energies.[374,377−380] In the sustained off-resonance irradiation (SORI) method,[381] ions in an ICR cell undergo collisions during multiple acceleration and deceleration cycles. SORI yields similar fragmentation patterns as infrared multiphoton dissociation.[53,368,381] Resolving the energy dependence of collision-induced dissociation under these conditions requires that both the distribution of the number of collisions and the collision energy distribution be well characterized as a function of trapping parameters and pressure. Modeling dissociation probabilities in multiple-collision processes is more difficult than for single-collision experiments. In ICR traps, for example, the ion kinetic energy oscillates with time because of on-resonance or off-resonance cyclotron excitation and is also damped via collisions.[377] Laskin et al.[377] modeled the CID breakdown curves for bromobenzene cation in an ICR experiment using RRKM theory and various functional forms for the energy deposition function as a function of pressure. Monte Carlo simulations have also been employed.[378] In a more simplified analysis, the dissociation rate versus the estimated mean collision energy is fit to a threshold function of the form of eq 34.[379,380]

Use of slow heating methods for thermochemical determinations requires that the temperature or energy distributions be well characterized. For blackbody infrared activation methods, the photon energy distribution is well characterized and the absorption efficiency can be estimated using molecular vibrational parameters. For multiple collisions or multiphoton laser activation, the nonequilibrium energy distribution is a complex function of instrumental parameters and pressure. Although the sophistication of the modeling methods is improving for multicollision activation,[377,378] their general applicability for accurate absolute thermochemical measurements is yet to be established. An advantage of multiphoton and multicollision methods, at least for relative dissociation energy measurements, is that large biomolecules can be efficiently activated to high

internal energies,[379] which is difficult by single-collision methods because the energy transfer becomes inefficient at high impact energies.

## D. Cooks Kinetic Method

The Cooks "kinetic method" is a widely used procedure developed by Cooks and co-workers for obtaining relative ion affinities from the dissociation of a ion-bound heterodimer.[382−385] The competitive dissociation of the ion-bound dimer is given by eq 59

$$\begin{aligned} A{\cdot}M^+{\cdot}B &\rightarrow AM^+ + B \quad k_1 \\ &\rightarrow A + BM^+ \quad k_2 \end{aligned} \tag{59}$$

where $M^+$ may be a proton, a metal ion, or a polyatomic ion such as $NH_4^+$ or $H_3O^+$. The same method applies to anionic systems, proton-bound dimer anions, $AHB^-$, or electron-bound dimers, $AB^-$, for example. Figure 33 shows a schematic energy diagram of the dissociation process. The ion-bound dimer is mass-selected, and then relative intensities of the two products are measured for either metastable ion dissociation or collision-induced dissociation. If the dissociation is treated as a quasi-equilibrium process, the intensity ratio $I_2/I_1$ can be approximated as the rate constant ratio given by the canonical form of RRKM/QET theory (eq 32), which yields eq 60

$$\ln \frac{I_2}{I_1} \approx \ln \frac{k_2}{k_1} = \frac{\Delta_1^{\ddagger}G - \Delta_2^{\ddagger}G}{RT_{\text{eff}}} = \frac{\Delta_1^{\ddagger}H - \Delta_2^{\ddagger}H}{RT_{\text{eff}}} - \frac{\Delta_1^{\ddagger}S - \Delta_2^{\ddagger}S}{R} \tag{60}$$

where the effective temperature $T_{\text{eff}}$ is not a true thermodynamic temperature because the ions are not in thermal equilibrium but rather should be treated as a kinetic correlation parameter. The intensity ratio is a kinetic quantity that depends on the internal energies of the ions, the instrumental time window for dissociation, and the densities of states of the ion-bound dimer and the transition states for the two channels, as well as on the dissociation energies.[141,386]

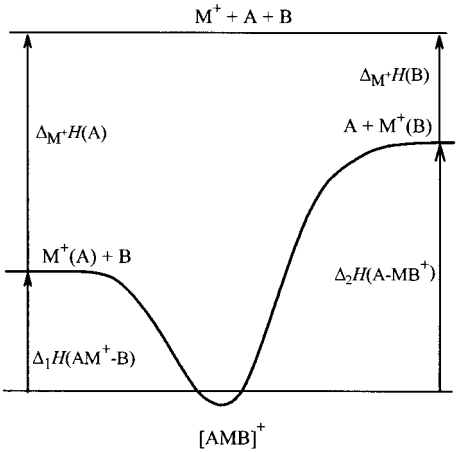


**Figure 33.** Schematic energy diagram for determination of $M^+$ ion affinities by the Cooks kinetic method.

If the two product channels are structurally similar and there are no reverse activation energies for the dissociation process, then the enthalpy difference will be the major factor affecting the intensity ratio. In that case, it can also be assumed that the entropies of activation of the two channels are the same and that the activation enthalpies ($\Delta_j^{\ddagger}H$) can be replaced by thermodynamic dissociation enthalpies ($\Delta_j H$). Using the relationship $\Delta_1 H(AM^+\text{-}B) - \Delta_2 H(A\text{-}MB^+) = \Delta_{M^+}H(A) - \Delta_{M^+}H(B)$ gives eq 61.

$$\ln \frac{I_2}{I_1} \approx \frac{\Delta_{M^+}H(B) - \Delta_{M^+}H(A)}{RT_{\text{eff}}} \tag{61}$$

Alternative derivations of this expression and the criteria for its applicability have been discussed in detail.[141,383−389] In practice, the metastable or collision-induced dissociation intensity ratios are measured for a series of ion-bound dimers composed of the unknown A and a series of molecules B with known ion affinities. A plot of $\ln(I_2/I_1)$ versus $\Delta_{M^+}H(B)$ has a slope of $1/RT_{\text{eff}}$ and an $x$-intercept of $\Delta_{M^+}H(A)/RT_{\text{eff}}$, giving a direct relative measure of the $M^+$-affinity of the unknown. Although the derivation is not rigorous because the ions are not in thermal equilibrium, for similar compounds a near-linear kinetic correlation is obtained. The Cooks kinetic method is attractive because it is conceptually simple, is relatively easy to apply, and gives reproducible results. The kinetic method has been shown to give reasonable results for a variety of chemical systems.[383−385] If the ion-bound dimer can be prepared in a mass spectrometer source, the corresponding neutral does not need to be a stable, volatile molecule. Several calibration schemes have been described employing single or multiple references.[383,384] Various mass spectrometer instruments can be used, including sectors, triple quadrupoles, guided-ion beams, quadrupole ion traps, and ICR. Metastable ion dissociation, single-collision dissociation, multiple collision dissociation (SORI), and blackbody infrared dissociation have all been employed with the Cooks kinetic method.[383−385,390] The empirical correlation with thermochemical quantities of reference species avoids the need for detailed modeling of the ion energy distributions and unimolecular dissociation rates or kinetic shifts.

Because the ions in a mass spectrometer are isolated species with fixed internal energies, not in thermal equilibrium, a proper analysis of the product branching ratio uses the microcanonical form of statistical rate theory, eq 31, to calculate the dissociation probabilities, eq 33, rather than the thermodynamic formulation.[140,141,386,391] An analysis of metastable ion dissociation by Ervin[141] using classical RRK theory, eq 30, shows that the microcanonical rates yield a near-linear relationship for plots of $\ln(I_2/I_1)$ versus $\Delta_{M^+}H(B)$ but with some curvature especially for small, rapidly dissociating systems because of threshold effects. For metastable ion dissociation, an approximate analytical expression for the "effective temperature" can be derived[141]

$$T_{\text{eff}} \approx \frac{[\Delta_1^{\ddagger}H + \Delta_2^{\ddagger}H]/2}{R(s-1)[(2\nu\tau)^{1/(s-1)} - 1]} \tag{62}$$

where the numerator is the average well depth of the $M^+$-ion-bound dimer for dissociation in the two directions, $s$ is its number of vibrational degrees of freedom, $R$ is the gas constant, $\nu$ is the reaction frequency in the RRK model, and $\tau$ is the characteristic experimental detection time. This expression is valid for metastable ion dissociation and high ion source temperatures; the effective temperature never exceeds the actual ion source temperature for metastable ions.[141] Equation 62 shows that the slopes of kinetic method plots for metastable ions depend on kinetic and molecular parameters, not on any thermodynamic temperature. The kinetic correlation with thermochemical energies is valid only if the dimer pairs used in the calibration have similar well depths (complexation energies), number of vibrational degrees of freedom (sizes), and reaction frequency (preexponential factor or entropies of activation). To the extent that these values vary for the references and unknowns, the intensity ratios will deviate from the ideal correlation—variations of 20−40% in apparent $\Delta_{M^+}H(A) - \Delta_{M^+}H(B)$ values are likely.[141] Stated uncertainties based solely on experimental reproducibility are often much smaller. The kinetic method is an approximate correlation that is expected to give reasonable relative energies when applied with care and when the conditions such as zero reverse activation energies are met, but it is not expected to be of the same accuracy as true equilibrium measurements. Recent lively discussions in the literature regarding the applicability of the kinetic method touch upon these and other issues.[385,386,389,392−395]

The work of Seburg and Squires[388] on the cyclopropyl radical nicely illustrates the use of the kinetic method to determine an electron affinity that is not easily determined by other means. The *cyclo*-$C_3H_5^-$ anion is difficult to make in sufficient quantities for photoelectron spectroscopy studies. Seburg and Squires[388] were able to produce thiocarboxylate anions of the form $RC(O)S^-$, where R is cyclopropyl or one of a series of calibrant radicals with known electron affinities. These species are covalently bound, requiring rather high collision energies for dissociation. Collision-induced dissociation at 10−12 eV c.m. in a triple quadrupole produces $R^-$ and $OCS^-$ ions. Using the "single-reference" method, where the unknown ($R = c$-$C_3H_5$) and a series of known calibrants (R = benzyl, vinyl, allyl, acetyl) are each complexed with the single reference OCS to form $R^-(OCS)$, a kinetic method plot of the $\ln(R^-/OCS^-)$ intensity ratio versus the electron affinities yields a linear calibration. The electron affinity of cyclopropyl radical is determined[388] as $EA_0(c\text{-}C_3H_5) = 0.397 \pm 0.069$ eV, in good agreement with values estimated[388] using the negative-ion cycle, eq 5.

Higgins and Bartmess[396] recently reported an instructive case where the kinetic method disagrees with equilibrium measurements. For normal alkanols with 5−9 carbons, kinetic method measurements[397,398] of gas-phase acidities give $\Delta_{acid}G$ values that monotonically decrease with increasing chain length. This behavior might be explained by the stabilization of the anion due to the polarization of the alkyl groups. However, the span of the decrease in $\Delta_{acid}G$ from 1-pentanol to 1-nonanol was 11.3 kJ/mol in metastable dissociation at 6−8 keV ion energy,[397] 9.2 kJ/mol in metastable dissociation in a quadrupole mass spectrometer,[398] and only 4.6 kJ/mol by collision-induced dissociation[398] at 50 eV. These differences already point to deviations due to the different ion energies kinetically sampled under the various instrumental conditions. Higgins and Bartmess[396] carried out equilibrium measurements of the acidities in an ICR experiment and found that the variation is actually nonmonotonic with 1-hexanol being the most acidic. This effect can be explained by equilibrium structures in which the distal end of the alcohol chain can bend back and stabilize the ionic site for chains longer than 5 carbons. The kinetic method is only sensitive to the dissociative transition states, which have geometries similar to the proton-bound complex, while the separated ions are stabilized by intramolecular rearrangement. That is, the requirement of zero reverse activation energies is not met for these systems.

The effective temperature parameter is different for metastable ion dissociation and for CID using various collision gases.[383] Recently, a novel extension of the kinetic method has been employed that uses these variations in effective temperature to extract "apparent entropy" differences from the $y$-intercepts in eq 60.[399−405] An alternative analysis of such data has been proposed[406] and applied[407] to overcome some statistical difficulties with the original procedures. The implicit use of the effective temperature kinetic correlation parameter as a thermodynamic temperature to extract entropy changes is not rigorously valid,[385,389,392,406] however, and it remains to be determined whether this extension of the Cooks kinetic method can provide thermodynamically accurate entropy information.

## E. Kinetic Energy Release Distributions

Measuring the distribution of kinetic energies of products from the dissociation of a metastable ion can be used to infer details of the potential energy surface and to determine dissociation energies.[52,408−410] The reaction mechanism is given by eq 63.

$$A^+ + B \rightarrow [AB]^+* \qquad (63)$$

$$[AB]^+* \rightarrow C^+ + D$$

The metastable adduct ions are formed in the ion source of a sector mass spectrometer, mass-selected in the first sector, then undergo unimolecular dissociation in a field-free region. The kinetic energy release distributions (KERDs) are measured by electrostatic energy analysis of the product ions in the second sector.[52,410] Equation 63 shows the example of formation of decomposition products that are distinct from the adduct-forming reactants, in which case the unimolecular dissociation can be regarded as "chemically activated".[52] KERDs have also been measured using high-resolution time-of-flight spectroscopy in TPEPICO experiments,[261] offering the advantage of spectroscopic energy selection of the ions.

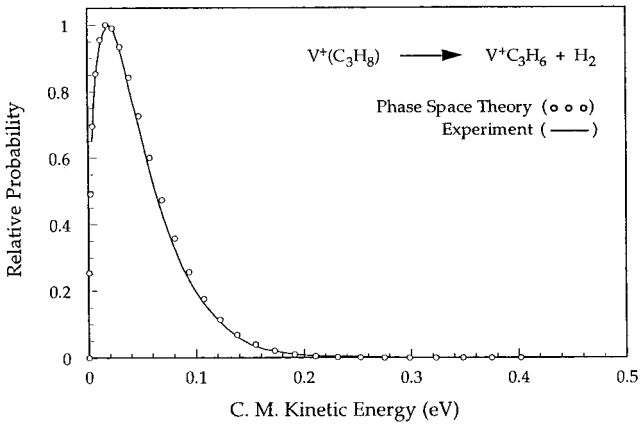


**Figure 34.** Kinetic energy release distribution for metastable loss of $H_2$ from nascent $V^+(C_3H_8)$ collision complexes. The solid line is the experimental distribution resulting from the metastable ion peak shape. The circles are the results of statistical phase space theory calculations. (Reprinted with permission from ref 409. Copyright 1998 American Chemical Society.)

Bowers and co-workers[52,408,409] examined metal-ion adducts with small hydrocarbons by the KERD method, e.g., $V^+$−propane,[409] eq 64.

$$V^+ + C_3H_8 \rightarrow [VC_3H_8]^+ \rightarrow VC_3H_6^+ + H_2 \quad (64)$$

Two types of reaction surfaces[52] characterize the KERDs for metastable adduct ions. The type I surface has no barrier for the reverse association reaction, allows for complete energy randomization with statistical dissociation, and yields a KERD that peaks near zero. The type II surface has an exit channel barrier, which yields a nonstatistical dissociation with higher kinetic energy release. In either case, the maximum kinetic energy places a lower limit on the reaction exothermicity. Thus, the form of the KERD provides qualitative information about the potential energy surface. In the case of type I behavior, the KERD can be modeled statistically using phase space theory (PST) to yield bond dissociation energies.[52] A maximum entropy method has also been used to analyze KERDs.[410] The PST analysis[52] includes the energy distributions of the adduct ions formed in the source and the kinetic selection of those metastable ions with energies that dissociate in the field-free region, as given by eq 33, and the PST dissociation rate. Figure 34 shows the KERD for the elimination of $H_2$ from metastable $V^+(C_3H_8)$ ions.[409] The comparison with phase space theory shows that the $H_2$-loss channel behaves statistically, i.e., on a type I surface. The fit of PST theory allows extraction of the $V^+$−propene complexation energy,[409] $D_0(V^+-C_3H_6) = 128 \pm 8$ kJ/mol, in good agreement with a threshold collision-induced dissociation value[411] of $124 \pm 8$ kJ/mol.

## XI. Bimolecular Ion–Molecule Reactions

## A. Reaction Equilibrium Measurements

Equilibrium concentration measurements represent one of the most accurate ways to measure relative gibbs energies. There are three major ion energetics scales, for gas-phase basicities (proton affinities of neutrals),[84,87] gas-phase acidities (proton affinities of anions),[75,76,86] and electron affinities.[72] Equilibrium measurements for a direct proton loss or electron loss process are usually prohibited by the high endoergicity. Instead, the equilibria of proton transfer (PT), eqs 65 and 66, or electron transfer (ET) reactions, eqs 67 and 68, are studied to obtain relative energetics.

$$B + HA^+ \rightleftarrows HB^+ + A \qquad \Delta_{PT}G = \Delta_{PA}G(A) - \Delta_{PA}G(B) \quad (65)$$

$$HA + B^- \rightleftarrows A^- + HB \qquad \Delta_{PT}G = \Delta_{acid}G(HA) - \Delta_{acid}G(HB) \quad (66)$$

$$A^+ + B \rightleftarrows A + B^+ \quad \Delta_{ET}G = \Delta_I G(B) - \Delta_I G(A) \quad (67)$$

$$A^- + B \rightleftarrows A + B^- \quad \Delta_{ET}G_T = \Delta_{EA}G(A) - \Delta_{EA}G(B) \quad (68)$$

Electron-transfer equilibrium measurements are well suited for obtaining ionization energies or electron affinities of species with very different neutral and ionic geometries,[72,412] for which small Franck−Condon factors make spectroscopic methods difficult. Ion affinity scales have also been established[4,71,75,92,413−418] for metal cations such as $Li^+$, $Na^+$, $Mg^+$, and $Cu^+$ and for halides such as $F^-$ and $Cl^-$. Kebarle and co-workers[419] recently reported hydration energies for doubly charged cations ($Mg^{2+}$, $Ca^{2+}$, $Sr^{2+}$, and $Ba^{2+}$), produced by electrospray ionization, from their equilibria with water. Clustering or solvation equilibria can be measured directly under high-pressure conditions using eq 69[71,420]

$$X^+(L)_{n-1} + L \rightleftarrows X^+(L)_n \quad \Delta_{L,n}G_T(X^+) \quad (69)$$

or relative Gibbs energies can be measured by solvent- or ligand-switching reactions, eq 70.[4,5,416]

$$X^+(L) + M \rightleftarrows X^+(M) + L \qquad \Delta_r G = \Delta_{X^+}G(M) - \Delta_{X^+}G(L) \quad (70)$$

### 1. Direct Equilibrium Measurements

The direct equilibrium measurement involves determining the equilibrium constant, $K_T$, by sampling ion intensities to measure ion concentrations at fixed partial pressures of the neutrals. Using cationic proton transfer (eq 65) as an example gives eqs 71 and 72.

$$K_T^\circ = \frac{(p_{BH^+}/p^\circ)\,(p_A/p^\circ)}{(p_{AH^+}/p^\circ)\,(p_B/p^\circ)} = \frac{I_{BH^+}\,p_A}{I_{AH^+}\,p_B} \quad (71)$$

$$\Delta_r G_T^\circ = -RT \ln K_T^\circ = \Delta_r H_T^\circ - T\Delta_r S_T^\circ \quad (72)$$

Application of eqs 71 and 72 requires that equilibrium be established at a well-defined temperature, that the ion intensities faithfully reproduce the ratio of ion densities, and that the pressure ratio is well determined. If the equilibrium is measured at a single temperature, an estimate of the entropy change

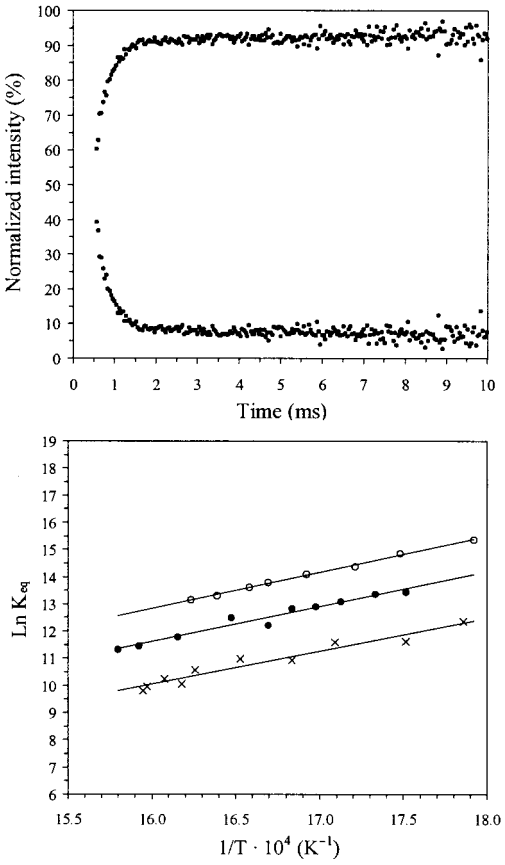


**Figure 35.** (a) Top: Normalized ion intensity profiles for the clustering of sodium ion onto ammonia at 577 K measured by pulsed-ionization high-pressure mass spectrometry. (b) Bottom: van't Hoff plots for the clustering reactions of sodium ion onto methylamine, ammonia, and methanol. (Reprinted with permission from ref 413. Copyright 1999 American Chemical Society.)

from statistical mechanics is required to obtain the reaction enthalpy from the Gibbs energy. If the temperature dependence of the equilibrium constant is measured, then a van't Hoff plot of ln $K_T$ vs $1/T$ yields the entropy change from the slope, $-\Delta_r H/R$, and the entropy change from the $y$-intercept, $\Delta_r S/R$.

Direct equilibrium measurements have been performed most often using either high-pressure mass spectrometry (HPMS)[3,72,421−426] or ion cyclotron resonance (ICR) mass spectrometry.[75,427−433] Equilibria of bimolecular reactions (eqs 65−68, 70) can be investigated by either HPMS or ICR, but the higher pressure conditions of HPMS are required for association reactions (eq 69). In HPMS, because the equilibrium is established at high pressure but the mass spectrometric detection occurs at low pressure, the possibility of loss of solvent molecules before detection needs to be considered.[434] Figure 35a shows experimental data for a recent example, the equilibrium of clustering of ammonia with sodium ion, eq 73, using pulsed-ionization HPMS.[413]

$$Na^+ + NH_3 \rightleftharpoons Na^+(NH_3) \qquad (73)$$

The plot shows the normalized relative intensities of the $Na^+$ and $Na^+(NH_3)$ ions versus reaction time following the electron pulse that generates ions in the high-pressure cell. The absolute total ion intensities decrease over this time period. The ratio of the ion intensities after equilibrium is attained and the $NH_3$ pressure gives the equilibrium constant, eq 74,

$$K_T° = \frac{I_{Na^+(NH_3)}}{I_{Na^+}(p_{NH_3}/p°)} \qquad (74)$$

measured over a range of temperatures. The van't Hoff plots of ln $K$ versus $1/T$ for $Na^+$ clustering with ammonia, methanol, and methylamine are shown in Figure 35b.[413]

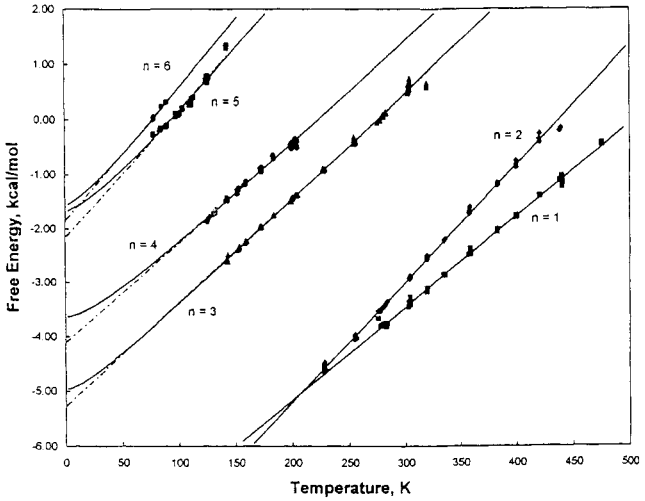


**Figure 36.** Plot of Gibbs energy, $\Delta G_T°$, versus temperature for the reaction $Cr^+(H_2)_{n-1} + H_2 \rightleftharpoons Cr^+(H_2)_n$ for $n = 1-6$. The dashed lines are linear fits to the data yielding values of $\Delta H_T°$ (intercept) and $\Delta S_T°$ (slope) at the average temperature. The solid lines are fits using statistical mechanics, with intercepts $\Delta H_0°$. (Reprinted with permission from ref 425. Copyright 1997 Elsevier Science.)

Bowers and co-workers[424−426] use a different version of high-pressure mass spectrometry for equilibrium measurements of clustering reactions. Ions are formed in an external source, mass-selected, and then injected into a high-pressure (1−50 Torr) drift cell containing the reactant gas. This method avoids side reactions that are possible when ions are formed by electron ionization in a high-pressure cell. The ions are thermalized after a few collisions and reach equilibrium by the time they reach the end of the drift cell. Figure 36 shows a plot of experimentally determined Gibbs energies of clustering as a function of temperature for eq 75.[425]

$$Cr^+(H_2)_{n-1} + H_2 \rightleftharpoons Cr^+(H_2)_n \qquad (75)$$

The measured intensities of reactant and product ions as a function of temperature yield the Gibbs complexation energy, eq 76.

$$\Delta_r G_T°\,(Cr^+) = -RT \ln K_T° = -RT \ln\left(\frac{I_{Cr^+(H_2)_n}}{I_{Cr^+(H_2)_{n-1}}(p_{H_2}/p°)}\right) \qquad (76)$$

The plots of $\Delta_r G_T°$ versus $T$ yield $\Delta_r H_T°$ as the intercept and $\Delta_r S_T°$ as the slope, as shown in Figure 36. Bowers and co-workers[424−426] model the data by using statistical mechanics to calculate the temper-

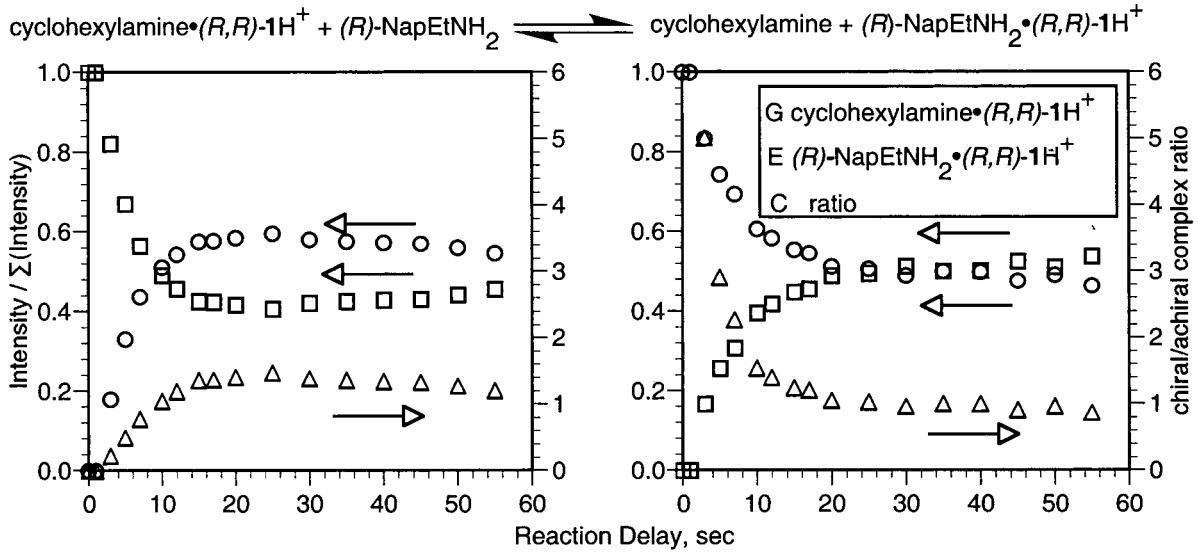


**Figure 37.** Approach to equilibrium in the forward (left) and reverse (right) directions, for exchange of cyclohexylamine and (*R*)-(1-naphthyl)ethylamine on protonated *R*-dimethyldiketopyridino-18-crown-6, measured by Fourier transform ion cyclotron resonance mass spectrometry. (Reprinted with permission from ref 435. Copyright 1997 American Chemical Society.)

ature dependence of $\Delta_r H_T°$and $\Delta_r S_T°$with molecular parameters obtained from ab initio calculations. The entropy change (slope) is sensitive to the calculated vibrational frequencies, which are therefore adjusted along with $\Delta_r H_0°$ to fit the data. The curved lines in Figure 36 show these fits with the 0 K reaction enthalpies, $\Delta_r H_0°$, as the intercepts. This procedure ensures that the results are consistent with calculated entropy changes.

Chiral recognition studies on host−guest complexes of chiral crown ethers by Dearden et al.[435] represent a clever application of ICR equilibrium measurements. Electrospray ionization was used to introduce the involatile chiral crown ether ligand (dimethyldiketopyridino-18-crown-6) into the ICR trap as a protonated host molecule. A neutral chiral amine and an achiral reference amine were introduced as guest species, and equilibrium constants were measured for the exchange of chiral and achiral guests. Figure 37 shows the establishment of equilibrium starting from complex ions with either the chiral or achiral guest.[435] Preferential complexation of the chiral guest with the opposite absolute enantiomeric configuration as the host's stereocenter is observed, with Gibbs energy differences ranging from 0.3 ± 0.4 kJ/mol for *sec*-butylamine to 3.6 ± 0.6 kJ/mol for α-(1-naphthyl)-ethylamine. This work indicates that chiral recognition is intrinsic, not primarily due to solvent effects, and also provides a route for analytical determinations of enantiomeric mixtures.[435]

The sensitivity of equilibrium measurements to small enthalpy changes is demonstrated by the work of Schauer et al.[436] on the not-quite-symmetric charge-transfer process in eq 77.

$$^3He^+ + {}^3He \rightleftarrows {}^3He + {}^4He^+ \quad \Delta_r H_0 = +0.11 \text{ kJ/mol} \quad (77)$$

The small difference in ionization energies of $^3$He and $^4$He is due to the difference in reduced electron−nuclear mass. Schauer et al.[436] measured the forward and reverse rates in a Penning ion trap at 8−80 K. The van't Hoff plot has a slope that closely matches the theoretical endothermicity, and the intercept is zero within experimental uncertainty, matching the expected $\Delta_r S = 0$ assuming nuclear spin is conserved during electron transfer.

Although equilibrium measurements have the potential for high precision and accuracy in relative ion affinities, that is not guaranteed because of experimental difficulties including determining pressures and temperatures and the extrapolation to find entropy changes.[107,421,437] The recent update[84] of the proton affinity scale introduced significant changes to reconcile deviations between equilibrium ladders from different laboratories. Statistical mechanics calculations of entropy changes using ab initio molecular parameters were used to identify poor experimental values and to redetermine the actual temperatures of various experiments.[84] A possible general conclusion from this reassessment of proton affinities[84] is that $\Delta G_T$ values obtained directly in the equilibrium experiments, assuming the temperature is well characterized, are more reliable than are $\Delta H_T$ and $\Delta S_T$ obtained from van't Hoff plots. Small deviations in the slope of a van't Hoff plot can lead to large correlated deviations in the entropy change obtained from the extrapolated intercept.[406,437] Absolute proton affinities from independent measurements for several compounds, as well as a theoretical value for the absolute proton affinity of ammonia,[438,439] were used to anchor the new proton affinity scale.[84] However, a new measurement of the proton affinity of propene by PFI/PEPICO spectroscopy[267] yields $PA_{298}(C_3H_6) = 742.3 \pm 1.5$ kJ/mol, lower than the recommended value in the compilation,[84] $PA_{298}(C_3H_6) = 751.6$ kJ/mol. This implies that there may still be regions of the proton affinity scale of somewhat greater uncertainty than the cited ±8 kJ/mol.

Recent experimental reexaminations of sodium ion affinities by both HPMS equilibrium[413] and

TCID[354,414,440] techniques identify significant errors in previous equilibrium values. Experimental work on sodium ion affinities[413,414] further relies on ab initio calculations to buttress experimental observations, identify trends, and predict values not accessible by experiments. Similarly, a revision and reanchoring[418] of the lithium ion affinity scale from ICR equilibrium[417] and kinetic method[441,442] measurements has been prompted by TCID experiments[443,444] that questioned the accepted $Li^+(H_2O)$ binding energy. The revised lithium ion scale[418] uses the absolute lithium ion affinity from the TCID experiments as the anchoring point.[443,444]

### 2. Measurement of Forward and Reverse Rates

An alternative to the measurement of ion concentrations for a reaction at equilibrium is the separate measurement of the forward and reverse rates of a reaction, for example, for the anionic proton transfer reactions in eq 78.

$$A^- + HB \rightarrow HA + B^- \quad k_1 \qquad (78)$$

$$HA + B^- \rightarrow A^- + HB \quad k_{-1}$$

The principle of detailed balancing gives the relationship between the rates and the equilibrium constant, eq 79

$$\Delta_r G_T^\circ = -RT \ln K_T^\circ = -RT \ln \frac{k_1}{k_{-1}} = \Delta_{acid} G_T^\circ(HB) - \Delta_{acid} G_T^\circ(HA) \qquad (79)$$

which is valid when both reaction rates are measured under conditions of thermal equilibrium of the reactants.[133] Relative gas-phase acidities have been measured from forward and reverse proton transfer rate constants measured by selected ion flow tube (SIFT) experiments.[21,23,242,243] A recent example is the determination of the gas-phase acidity of *tert*-butylhydroperoxide by Clifford et al.[243] The forward and reverse rates for the proton transfer reaction with phenyl acetylene, eq 80

$$(CH_3)_3COOH + C_6H_5C{\equiv}C^- \rightleftarrows (CH_3)_3COO^- + C_6H_5C{\equiv}CH \qquad (80)$$

were measured in the SIFT apparatus at 300 K, giving $k_1 = (6.12 \pm 0.63) \times 10^{-10}$ cm$^3$ s$^{-1}$ and $k_{-1} = (8.50 \pm 0.18) \times 10^{-10}$ cm$^3$ s$^{-1}$, which translates to *tert*-butylhydroperoxide being a weaker acid by 0.81 ± 0.26 kJ/mol than phenylacetylene,[243] yielding $\Delta_{acid}H_{300}[(CH_3)_3COOH] = 1552 \pm 8$ kJ/mol after entropy corrections. This work also measured the acidity of *tert*-butyl hydroperoxide using the Cooks kinetic method via the hydrogen-bound complexes of the peroxide anions with several alcohols as reference acids, and agreement within 1.3 kJ/mol was found. Finally, Clifford et al.[243] used negative-ion photoelectron spectroscopy to measure the electron affinity of the *tert*-butylperoxy radical, $EA_0[(CH_3)_3COO] = 1.196 \pm 0.011$ eV, allowing determination of the ROO−H bond dissociation energy, $D_0[(CH_3)_3COO{-}H] = 356 \pm 8$ kJ/mol via the negative-ion cycle, eq 5. The predominant source of uncertainty arises from the ±8 kJ/mol uncertainty of the acidities of phenylacetylene and the alcohol reference acids from the ICR equilibrium acidity scale.[75,86,428]

## B. Bimolecular Reaction Threshold Energies

The translational energy threshold of an endoergic bimolecular ion−molecule reaction, eq 81, is equal to its endoergicity if there is no excess barrier to reaction.

$$A^+ + B \rightarrow C^+ + D \qquad E_0 \geq \Delta_r H_0 \qquad (81)$$

Although ion−molecule reactions often proceed at the thermochemical threshold, barriers can result when the passage from reactants to products requires a spin change or a nonadiabatic transition to a different electronic potential energy surface[183] or for double-well potentials.[334] The tandem mass spectrometry techniques used to measure kinetic threshold energies for bimolecular endoergic ion−molecule reactions are the same as those discussed above for threshold collision-induced dissociation experiments (section X.B). The threshold analysis is also identical, except that kinetic shifts are not usually at issue because transient ion complexes formed in a bimolecular collision typically have short lifetimes compared with the detection times in a tandem mass spectrometer. Large systems might exhibit a kinetic shift, in which case the long-lived adduct of the reactant ion and neutral could be detected directly. Higher-energy fragmentation channels might also exhibit competitive shifts.

A large number of bimolecular reaction threshold energies have been measured by guided-ion beam techniques,[35,174,183,445−447] as well as in triple-quadrupole[339] and ICR[342] instruments. The hydrogen-atom affinities of atomic cations for a large portion of the periodic table have been measured by guided beam techniques using the endoergic reactions of the metal cations with molecular hydrogen.[448] Both positive-ion and negative-ion proton transfer experiments have been carried out.[445,449,450] Endoergic charge-transfer reactions can be used to determine ionization energies, including situations where poor Franck−Condon factors make photoionization or electron ionization threshold measurements difficult, for $NO_2$ for example.[451] Selected examples of metal and nonmetal systems are described here.

### 1. Metal–Ligand Dissociation Energies

Many ion beam reaction experiments have been devoted to the study of the reactivity and energetics of metal-ion species.[55,329,347,450,452−455] These experiments along with ion association equilibrium, photodissociation, TCID, and KERD measurements have yielded a large database of the metal-ion−ligand dissociation energies,[54,55,453] including metal−hydride, metal−methyl, metal−oxide, metal−carbonyl, and metal−hydrocarbon systems. Threshold energy measurement for the endoergic bimolecular reaction of a metal-ion $M^+$ with a ligand donor, eq 82, yields the

**Table 5. Experimental Endoergicity or Activation Energy of $N^+ + H_2 \rightarrow NH^+ + H$**

| method | $E_0^{\ddagger}$ or $\Delta_r H_0$ (meV) | ref |
|---|---|---|
| SIFT/drift | $11 \pm 3$ | 456 |
| low-$T$ ion trap (10 K) | 4 (22[a]) | 457 |
| low-$T$ jet (8−70 K) | $7.4 \pm 0.8$ (18.5[a]) | 458 |
| guided-ion beam/gas cell at 305 K | $33 \pm 24$ (empirical threshold)<br>$18 \pm 5$ (PST fit) | 186 |
| low-$T$ jet (<163 K) | $18 \pm 2$ | 459 |
| low-$T$ ion trap at 15−300 K; merged beam | $17 \pm 2$ | 460,461 |
| guided-ion beam/gas cell at 105 and 305 K | 12−15 | 462 |
| guided-ion beam/crossed molecular beam; merged beam | $11 \pm 3$ | 446 |

[a] Experimental activation energy corrected to 0 K by adding the average $H_2$ rotational energy at the experimental temperature.[186]

$M^+$−L binding energy when $D$(R−L) is known.

$$M^+ + RL \rightarrow ML^+ + R \qquad (82)$$

Experiments of this type to obtain $M^+$−H, $M^+$−$CH_x$ ($x = 1-3$), $M^+$−$NH_x$ ($x = 1-2$), $M^+$−O, and other bond dissociation energies have been thoroughly reviewed.[55,448] In cases where ionization energies of the metal-ion−ligand complex are known, eq 1 can be used to derive the corresponding neutral metal−ligand dissociation energy.[55] Periodic trends for the transition metals have been explained in terms of the atomic electronic configurations and promotion energies.[55,448,453]

### 2. $N^+ + H_2$

A simple bimolecular ion−molecule reaction that has received considerable experimental attention[186,338,446,456−462] is the near thermoneutral hydrogen-atom abstraction, eq 83

$$N^+ + H_2 \rightarrow NH^+ + H \qquad (83)$$

and its isotopic variants with $D_2$ and HD. This reaction may be involved in ammonia synthesis in interstellar space,[461] and the reaction enthalpy is related to the bond dissociation energy of NH, which is not precisely characterized spectroscopically.[463] Table 5 lists activation energies for eq 82 found by various experiments. Corrected to 0 K by adding the $H_2$ rotational energy where appropriate, the activation energies are from 11 to 33 meV, a range of 2.1 kJ/mol. Despite this apparent general agreement for a small endoergicity, the values have been somewhat controversial. By comparing $H_2$, $D_2$, and HD, early experiments found the variation of the activation energies agreed well with the expectation based on the different zero-point energies[186,456,458] and concluded that the measured activation energy was the true reaction endoergicity. These were either thermal experiments or beam/gas experiments where the $H_2$ rotational energy was significant compared with the measured activation energies. A variety of effects can influence the measured threshold energy and threshold behavior at the meV level—including the rotational states of $H_2$, spin−orbit splittings in $N^+(^2P_J)$ reactants and $NH^+$ ($^2\Pi_J$) products, the low-lying $^4\Sigma^-$ excited state of $NH^+$, and the ion−quadrupole potential of hydrogen.[186] Ervin and Armentrout[186] assumed that the rotational and spin−orbit energy of the reactants was equally as effective as translational energy and ignored product excited states to obtain $\Delta_r H_0 = 33 \pm 24$ meV using the empirical threshold law or $\Delta_r H_0 = 18 \pm 5$ meV using a classical phase space theory (PST) fit of threshold cross section. In cold ion trap and merged ion beam−molecular beam experiments, which achieve higher energy resolution than the beam/gas experiments, Gerlich[460,461] used *p*- and *n*-hydrogen and dynamic PST calculations to show that rotational energy does indeed promote the reaction as well as translational energy. Guided-beam experiments by Sunderlin and Armentrout[462] using a temperature-variable gas cell also indicate that rotational energy drives the reaction; they obtained a threshold energy of 12−15 meV as a best fit using classical PST with an explicit sum over all fine-structure states. In a collaboration between the Freiburg group and the Trento group, which uses a crossed guided-ion beam−molecular beam arrangement, Tosi et al.[338,446] found good agreement between the two high-resolution experiments. The cross section for eq 82 from the merged beam experiments is presented in Figure 38.[446] Because the Trento ion source is expected to produce a statistical mixture of $N^+(^2P_J)$ spin−orbit states, while the Freiburg group

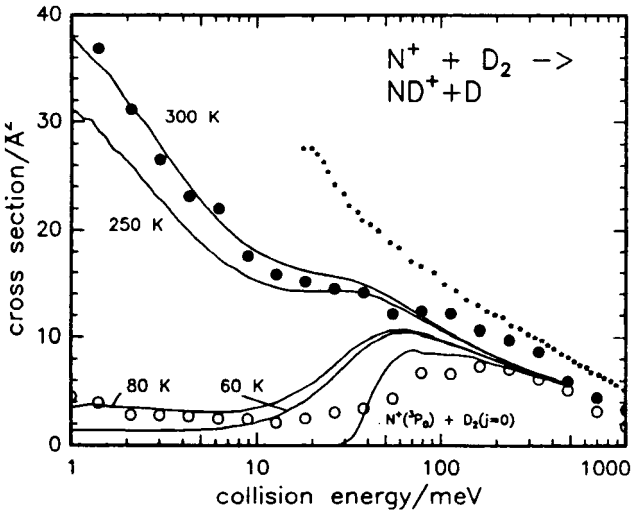


**Figure 38.** Cross section for the reaction $N^+ + D_2 \rightarrow ND^+ + D$ as a function of collision energy in the center-of-mass frame measured with a merged ion/neutral beam apparatus[446] for two different nozzle temperatures (80 K, ○; 300 K, ●). The small symbols represent results from a guided-ion beam/gas cell apparatus at 305 K.[186] Lines are phase space theory calculations for $\Delta_r H_0 = 35$ meV at the indicated temperatures; the lowest curve is for 0 K. (Reprinted with permission from ref 446. Copyright 1994 American Institute of Physics.)

allows the ions to relax in a cooled ion trap, the agreement suggests that spin−orbit energy is not available to promote reaction. Tosi et al.[446] also observed that their threshold energy for $D_2$ is only 18 meV higher than that of $H_2$, less than the expected 28 meV zero-point energy difference. That implies that the threshold energy may not be the true endoergicity after all, i.e., that there may be an isotope-dependent barrier. Therefore, Tarroni et al.[464] treat the threshold energy[446] as strictly a lower limit to the endoergicity. To resolve these issues, reactant spin−orbit and rotationally state-selective experiments and preferably product-state specific experiments would need to be carried out.

The threshold energy for eq 82 can be used to derive $D_0$(N−H) for comparison with independent measurements. Using $IE_0(NH) = 13.476 \pm 0.002$ eV determined by REMPI/PES spectroscopy[465] and other well-established quantities,[78] Tosi et al.[464] obtain $D_0(NH) \geq 329.9 \pm 1.0$ kJ/mol from the $N^+ + D_2$ threshold energy from PST fits[446] treated as a limit (using the $N^+ + H_2$ threshold energy[446] of 11± 3 meV gives $D_0(NH) \geq 328.9 \pm 0.6$ kJ/mol). At the other end of the range in Table 5, the empirical threshold-law value of Ervin and Armentrout,[186] $\Delta_r H_0 = 33 \pm 24$ meV for $N^+ + H_2$, gives $D_0(NH) = 326.8 \pm 2.4$ kJ/mol where the error bars reflect the uncertainties of the threshold model parameters. The value of $D_0$(NH) can be independently derived from $IE_0(NH_2) = 11.14 \pm 0.01$ eV and $AE_0(NH^+,NH_2) = 17.440 \pm 0.002$ eV from threshold photoionization,[466,467] $AE_0(NH_2^+,NH_3) = 15.768 \pm 0.004$ eV from photoionization,[202] $IE_0$(NH) given above from REMPI/PES,[465] and ammonia and atomic enthalpies of formation from Gurvich et al.[78] These values yield $D_0(NH) = 328.9 \pm 1.3$ kJ/mol, which conversely would correspond with a $N^+ + H_2 \rightarrow NH^+ + H$ reaction enthalpy of $\Delta_r H_0 = +11 \pm 14$ meV. This derivation involves two applications of the appearance energy cycle to obtain $D_0(H-NH_2) = 446.5 \pm 1.1$ kJ/mol and $D_0(HN-H) = 382.5 \pm 0.3$ kJ/mol as intermediate results. The first N−H bond energy agrees well with the value obtained independently from the negative-ion cycle,[36,37,39] $D_0(H-NH_2) = 445.8 \pm 1.3$ kJ/mol, but less well with a recent value from photofragment translational spectroscopy,[38] $D_0(H-NH_2) = 444.0 \pm 0.2$ kJ/mol. Using these latter two values for $D_0(H-NH_2)$ instead would yield reaction enthalpies $\Delta_r H_0 = 4 \pm 16$ meV and $\Delta_r H_0 = -15 \pm 6$ meV, respectively, i.e., eq 83 could actually be slightly exothermic. Nevertheless, the relative small range of these derived reaction energies compared with the experimental threshold energies (Table 5) indicates that any excess energy barrier above the reaction enthalpy is smaller than about 3 kJ/mol.

### 3. Phenol Ions

One of the issues in collisionally activated reactions is the role of reactant internal energies in promoting the reaction.[445,468] A recent study by Anderson and co-workers[35] uses MATI techniques to prepare vibrationally state-selected ions for subsequent guided-ion beam cross section measurements. A two-photon process prepares phenol, $C_6H_5OH$, in a Rydberg state corresponding with a core phenol ion in a specific vibrational state. Pulsed-field ionization then creates $C_6H_5OH^+$ in the same vibrational state. The proton transfer reaction of ground-state phenol ions with $ND_3$, eq 84, exhibits a 19 ± 4 kJ/mol threshold energy.[35]

$$C_6H_5OH^+ (v=0) + ND_3 \rightarrow C_6H_5O + ND_3H^+ \quad (84)$$

Correcting for zero-point energy differences and thermal corrections and using $PA_{298}(NH_3) = 853.6$ kJ/mol,[84] Anderson and co-workers[35] obtain the proton affinity of phenoxy radical, $PA_{298}(C_6H_5O) = 873.2 \pm 4$ kJ/mol, significantly higher than the value of 858 ± 8 kJ/mol of Hunter and Lias.[84] Combining this new proton affinity[35] with the ionization energy of phenol from ZEKE experiments,[469] $IE_0(C_6H_5OH) = 820.97 \pm 0.05$ kJ/mol, using the proton affinity cycle (eq 4) leads to $DH_{298}(C_6H_5O-H) = 381 \pm 4$ kJ/mol, which is significantly higher than a recent evaluation[32] that recommended $DH_{298}(C_6H_5O-H) = 371.3 \pm 2.3$ kJ/mol. Another recent but less precise value is $DH_{298}(C_6H_5O-H) = 377 \pm 13$ kJ/mol, determined from the gas-phase acidity of phenol obtained by the endoergic proton transfer threshold energy for $Cl^- + C_6H_5OH$ in a guided beam experiment[33] and the electron affinity of $C_6H_5O$ from photoelectron spectroscopy.[34] All three values are higher than earlier values from neutral radical kinetics (Table 1).

## C. Radiative Association Kinetics

The mechanism for radiative association is given by eqs 85.[470]

$$A^+ + B \rightleftarrows [AB]^+* \qquad k_1, k_{-1} \quad (85)$$

$$[AB]^+* \rightarrow AB^+ \qquad k_r$$

$$[AB]^+* + M \rightarrow AB^+ + M \qquad k_c$$

At low pressures where collisional stabilization ($k_c$) of the intermediate complex is negligible, the overall reaction rate is due to radiative association, given by the effective bimolecular rate coefficient, $k_{ra}$.

$$k_{ra} = \frac{k_1 k_r}{k_{-1} + k_r} \quad (86)$$

The radiative association rate is sensitive to the lifetime of the intermediate ($1/k_{-1}$) and therefore to the binding energy, $D(A^+-B)$. To obtain thermochemical information from measured radiative association rates, the various rate constants in eq 86 are modeled as described by Dunbar, Klippenstein, and co-workers.[149,156,471] The models employ collision theory or transition-state theory for complex formation ($k_1$), statistical RRKM theory for unimolecular dissociation ($k_{-1}$), and a radiative emission model using the infrared transition strengths and vibrational frequencies of the metastable complex ($k_r$).

The radiative association method has been applied by Dunbar and co-workers to estimate, for example, the binding energies of aromatic molecules with $NO^+$ and metal ions.[148,149,472,473] The low pressures required

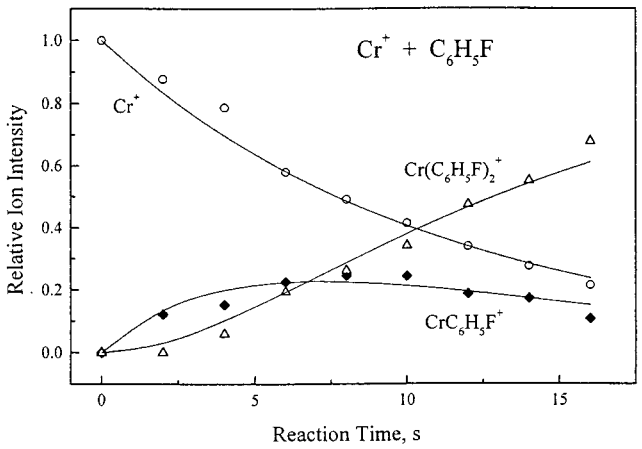


**Figure 39.** Ion intensities as a function of time for radiative association of $Cr^+$ with fluorobenzene at $1.1 \times 10^{-8}$ Torr in an ICR mass spectrometer cell. Lines represent a fit using sequential binding kinetics. (Reprinted with permission from ref 470. Copyright 1999 Elsevier Science.)

to avoid competition by collisional processes are obtained by measuring the radiative association rates in an ICR trap. Figure 39 shows the sequential radiative association of $Cr^+$ with two $C_6H_5F$ molecules.[470] The reaction time is more than 15 s at a reagent pressure of $10^{-8}$ mbar, with little loss of total ion intensity from the ion trap. Modeling yields a binding energy for the first ligand of 164 kJ/mol for fluorobenzene, compared with 186 kJ/mol for benzene and 79 kJ/mol for hexafluorobenzene.[470] The binding energy decreases with additional fluorine substitution on the benzene ring, consistent with a $\pi$-bonding interaction with the metal ion and the electron-withdrawing nature of the halogen.[470]

## D. Kinetic Bracketing

Bracketing experiments provide relative measurements of gas-phase ion affinities. In bracketing experiments, the rates are measured for an unknown ion reacting with a series of reference molecules. Strongly endergonic ($\Delta_r G \gg 0$) reactions will have undetectably small rate coefficients, while strongly exergonic ($\Delta_r G \ll 0$) ion−molecule reactions often have rates near the collision rate because of their low activation energies.[144,217,474] Slightly endergonic reactions may have detectable rates but usually only for $\Delta_r G \lesssim 10$ kJ/mol. Bracketing experiments have been used to determine gas-phase acidities, gas-phase basicities, electron affinities, and other ion affinities[475−482] and can use any technique to measure rate constants, typically SIFT or ICR. Under thermal, high-pressure conditions, kinetic bracketing provides relative orderings of Gibbs energies, but in single-collision experiments the method yields relative energies or enthalpies.[217] The bracketing technique is a method of first and last resort—first to obtain a quick estimate of the ion affinity of an unknown and last if more quantitative methods are not applicable, because of unstable or involatile reagents for instance. The method relies on exergonic ion−molecule reactions having a zero or very small activation energy and the availability of suitable reference species. Proton-transfer reactions often have no barriers,[475] and the gas-phase acidity and basicity scales[84,86] provide large databases of reference acids and bases for use in bracketing studies.

Despite the qualitative nature of bracketing studies, they are useful for systems where equilibrium methods are not feasible. For example, Natterer et al.[483] recently used bracketing to estimate the gas-phase acidity of hexatriyne, $C_6H_2$, an explosive and unstable compound. The anion $C_6H^-$ was produced by chemical ionization of acetylene in the external ion source of an ICR mass spectrometer.[483] Proton transfer of $C_6H^-$ with acetylene, acetone, $Si(OH)(CH_3)_3$, and $[(CH_3)_3Si]_2NH$ is not observed, but proton transfer is observed with 4-methylpyrazole, hydrogen sulfide, and formic acid. This bracketing gives an estimate for the acidity of $\Delta_{acid}G_{298}(C_6H_2) = 1452 \pm 13$ kJ/mol. At the time of the work of Natterer et al.,[483] the electron affinity of $C_6H$ was not known but theoretical estimates of the bond dissociation energy, $D_0(HC_6-H) \approx 530.5 \pm 6.7$ kJ/mol, and electron affinity, $EA_0(C_6H) \approx 3.69 \pm 0.05$ eV, were consistent with the experimental bracketed acidity.[483] The recent experimental value of the electron affinity from negative-ion photoelectron spectroscopy[365] is $EA_0(C_6H) = 3.809 \pm 0.015$ eV. The experimental EA can be combined (eq 5) with the gas-phase acidity from bracketing to yield an experimental estimate of the bond dissociation energy of $D_0(HC_6-H) \approx 543 \pm 13$ kJ/mol (using thermal corrections from Natterer et al.[483]). That value is consistent with the bond dissociation energies of acetylene, $D_0(HCC-H) = 551.2 \pm 0.1$ kJ/mol, measured by photofragment translational spectroscopy,[17] and of diacetylene, $D_0(HC_4-H) = 539 \pm 12$ kJ/mol, measured by competitive TCID[362] (section X.B).

## E. Bouchoux Thermokinetic Method

Bouchoux et al.[484−486] recently refined the bracketing method by quantifying the correlation between the reaction efficiency and the Gibbs energy change for bimolecular proton transfer (PT) reactions, eq 87.

$$MH^+ + B \xrightarrow{k_{exp}} M + BH^+ \qquad \Delta_{PT}G = \Delta_{PA}G(M) - \Delta_{PA}G(B) \quad (87)$$

The reaction efficiency for this reaction relative to the calculated collision rate, $R = k_{exp}/k_c$, is measured for unknown base M and a series of reference bases B and plotted vs $\Delta_{PA}G(B)$, as shown in Figure 40. The correlation between kinetics (reaction efficiency) and $\Delta_r G$ is well-known[487] and has been demonstrated in the past for proton transfer reactions, for example, by Bohme and co-workers.[474,488] Bouchoux et al.[484] derive a theoretical basis for the correlation beginning with a Lindemann-type mechanism for the proton transfer reaction via a single intermediate, eq 88.

$$MH^+ + B \underset{k_{-1}}{\overset{k_c}{\rightleftharpoons}} [MHB]^+ \xrightarrow{k_1} M + BH^+ \quad (88)$$

Applying the steady-state approximation for the

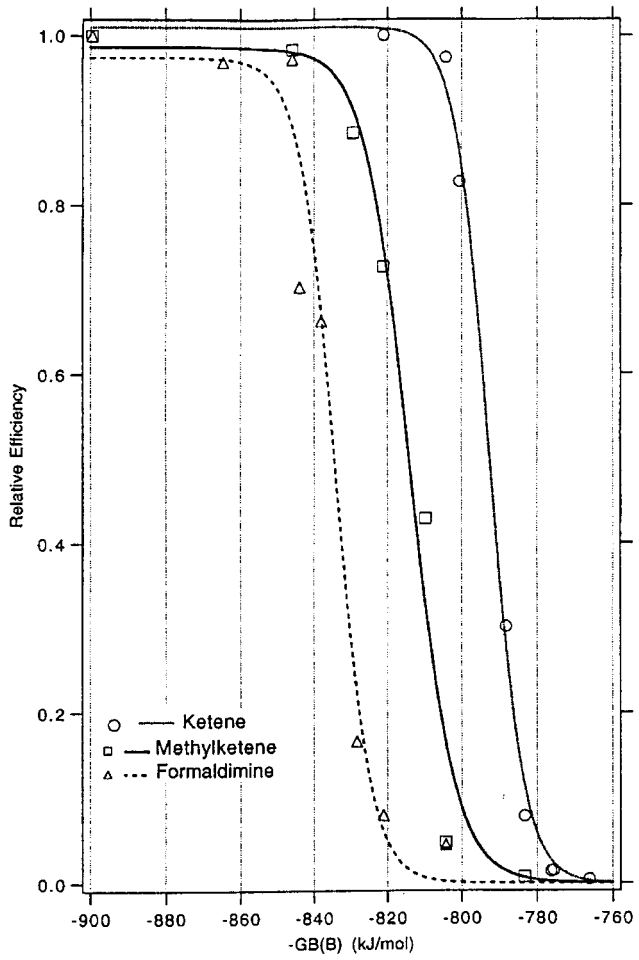


**Figure 40.** Calibration curves for the Bouchoux thermokinetic method. Reaction efficiencies for proton transfer of ketene, methylketene, and formaldimine with various reference bases versus the gas-phase basicities of the references. (Reprinted with permission from ref 485. Copyright 1996 American Chemical Society.)

intermediate proton-bound dimer, the reaction efficiency $R$ can be expressed by eq 89.

$$R = \frac{k_{\mathrm{exp}}}{k_{\mathrm{c}}} = \frac{1}{1 + (k_{-1}/k_1)} \tag{89}$$

The rates for the unimolecular decomposition of the intermediate are approximated by the canonical thermodynamic form of transition-state theory, eq 32. Canonical transition-state theory does not exactly hold for mechanism 88 because the transient intermediate complex, $[MHB]^+$, is not necessarily in thermal equilibrium. Using an effective temperature $T_{\mathrm{eff}}$, the rate ratio may be expressed as eq 90

$$\frac{k_{-1}}{k_1} = \exp[-(\Delta^{\ddagger}_{-1}G - \Delta^{\ddagger}_{1}G)/RT_{\mathrm{eff}}] \approx \exp(-\Delta_{\mathrm{PT}}G/RT_{\mathrm{eff}}) \tag{90}$$

where $\Delta_{\mathrm{PT}}G = \Delta_{\mathrm{PA}}G(\mathrm{B}) - \Delta_{\mathrm{PA}}G(\mathrm{M}) \approx \Delta_{-1}{}^{\ddagger}G - \Delta_{1}{}^{\ddagger}G$ assuming there are no reverse activation energies. Substituting the rate ratio into eq 89 yields eq 91

$$R \propto \frac{1}{1 + \exp[b(c - \Delta_{\mathrm{PT}}G)]} \tag{91}$$

where $b$ and $c$ are correlation parameters obtained by fits to the data plotted as $R$ vs $\Delta_{\mathrm{PA}}G(\mathrm{B})$. The parameter $c$ is an apparent Gibbs activation energy for the bimolecular reaction. For five different sets of reaction efficiency data on various compounds (four sets from rate measurements in ICR mass spectrometers and one set using flow tube data), Bouchoux et al.[484] found fairly uniform values of $b = 1/RT_{\mathrm{eff}}$ corresponding to $T_{\mathrm{eff}} \approx 550 \pm 130$ K (higher than the nominal experimental temperatures of 300 K) and $c = 4.8 \pm 1.4$ kJ/mol for the effective Gibbs energy barrier. In other words, on average the reactions must be slightly exergonic, $\Delta_{\mathrm{PT}}G \approx -5$ kJ/mol $\approx RT_{\mathrm{eff}}$, before the proton transfer rates reach the expected 50% of the collision rate for a thermoneutral process. In subsequent work, Bouchoux and Salpin[484,486] adopt $c = RT_{\mathrm{eff}}$. The generality of this result is untested for systems other than proton transfer. An elevated effective temperature is reasonable for association complexes that undergo no or only a few stabilizing collisions before decomposing either to products or back to reactants. The effective temperature might be expected to depend on the well depth of the proton-bound complex, in analogy with eq 62 for the Cooks kinetic method. The source of the apparent Gibbs activation energy has not been definitively explained.

The fit of eq 91 to the reaction efficiency data for M = ketene, methylketene, and formaldimine is shown in Figure 40, taken from Bouchoux and Salpin.[485] The resulting gas-phase basicity of ketene after recalibration[486] to the new proton affinity scale,[84] $\Delta_{\mathrm{PA}}G(CH_2CO) = 790.1 \pm 3$ kJ/mol, is in good agreement with equilibrium measurements, while new values are obtained for methylketene, $\Delta_{\mathrm{PA}}G(CH_3CHCO) = 809.6 \pm 3$ kJ/mol, and formaldimine, $\Delta_{\mathrm{PA}}G(CH_2{=}NH) = 829.7 \pm 3$ kJ/mol. Decker et al.[479] recently employed the Bouchoux thermokinetic method to measure the gas-phase basicity and proton affinity of $HS_2{\cdot}$. They obtain $\Delta_{\mathrm{PA}}G_{298}(HS_2) = 710.4 \pm 10$ kJ versus $707 \pm 13$ kJ/mol using simple bracketing.

The Bouchoux thermokinetic method improves on simple kinetic bracketing by parametrizing the dependence of the reaction efficiency on $\Delta_{\mathrm{PT}}G$. It is applicable when a series of gas-phase reference bases with similar structures and basicities are available to make a reaction efficiency calibration curve. It can be applied to cases where the ion $MH^+$ can be produced even if the neutral base M is unstable or unavailable. Bouchoux et al.[484] showed that the correlation using $\Delta_{\mathrm{PA}}G(\mathrm{B})$ is statistically better than using $\Delta_{\mathrm{PA}}H(\mathrm{B})$, presumably because entropy effects on the relative reaction efficiencies are included in the Gibbs energy. The thermochemical correlation used by the Bouchoux thermokinetic method is conceptually similar to the Cooks kinetic method and is subject to the same general cautions.

## F. Competitive Reactivity Correlations

The competition between two similar product channels in a bimolecular reaction is sensitive to the

relative energies of the transition states for the two channels. If the transition states for the two product channels are both loose, i.e., product-like, then they may have zero reverse activation energies or at least similar reverse activation energies. In that case, the branching ratio may be correlated with the energy difference of the two channels.[489−492]

The DePuy silane-cleavage method[489−491] correlates the branching ratio of reaction of $OH^-$ with trimethylsilyl-substituted compounds, $RSiMe_3$, to form RH or $CH_4$, eq 92,

$$\begin{aligned} HO^- + Me_3SiR &\rightarrow [Me_3Si(OH)(R)]^- \\ [Me_3Si(OH)(R)]^- &\rightarrow RH + Me_3SiO^- \quad k_{RH} \\ &\rightarrow CH_4 + RMe_2SiO^- \quad k_{CH_4} \end{aligned} \tag{92}$$

with the relative gas-phase acidities of RH and methane using the correlation formula given in eq 93,

$$\ln\left(\frac{3I_{Me_3SiO^-}}{I_{RMe_2SiO^-}}\right) \approx \ln\left(\frac{k_{RH}}{k_{CH_4}}\right) = -\beta[\Delta_{acid}H(RH) - \Delta_{acid}H(CH_4)] \tag{93}$$

where the factor of 3 corrects statistically for the number of methyl groups versus R-groups[491] and $\beta$ is the correlation parameter. A calibration curve is obtained for a two or more known acids RH. This method requires synthesis of the trimethylsilyl compound for each of the calibrants and unknowns. DePuy and co-workers[489,490] used the silane-cleavage method to determine the gas-phase acidities of alkanes, whose acidities are difficult to measure by bimolecular proton transfer methods because of the lack of reagent anions with sufficiently strong basicities. Wenthold and Squires[491] applied the procedure to the measurement of the gas-phase acidities of a series of halogen-substituted aromatic compounds, where the proton of interest is not necessarily the most acidic site, an implicit requirement in direct proton transfer studies. Hare et al.[476] attempted to apply the silane-cleavage method to measure the acidity of cubane but found that the kinetic correlation does not agree with bracketing experiments. It was postulated that rehybridization upon forming the cubyl anion retards the formation of cubane relative to the reference acids.[476] This behavior emphasizes the necessity of using reference compounds that are functionally similar to the unknowns in any thermokinetic correlation method.

Holman et al.[492] recently applied a similar competitive reactivity method correlating product branching ratios with the relative enthalpies of HY and HZ elimination in eq 93

$$\begin{aligned} X^- + YCH_2CH_2CH_2Z &\rightarrow Y^- + CH_2{=}CHCH_2Z + HX \\ &\rightarrow YCH_2CH{=}CH_2 + Z^- + HX \end{aligned} \tag{94}$$

where $X^-$ is a base such as $F^-$ or $CH_3O^-$ and $Y^-$ and $Z^-$ are halides, alkyl carboxylates, or halo-substituted methyl carboxylates. The 1,3-disubstituted propanes were chosen to reveal intrinsic leaving group abilities without interference from other structural effects.[492] Linear relationships were found between $\ln(Y^-/Z^-)$ intensity ratios in ICR experiments and the relative elimination enthalpies for a series of $Y(CH_2)_3Z$ compounds with different Y and the same Z.

As with the Cooks kinetic method and the Bouchoux thermokinetic method, competitive reactivity correlations may be expected to give reasonable relative energetics when leaving groups of similar structure, functionality, and size are used as calibrants and unknowns. Side reactions, structural rearrangements, and clustering reactions should be avoided. These kinetic correlation methods are useful in cases where equilibrium measurements are not possible but must be used with due care.

## G. Temperature-Dependent Kinetics Measurements

When the ion−molecule reaction rates for an endothermic reaction are measured as a function of temperature, the data may be analyzed using the Arrhenius equation, eq 58.[456−458] In recent work, Viggiano and co-workers[493−495] studied the temperature and kinetic energy dependence of ion−molecule reactions using a variable-temperature selected-ion flow/drift tube instrument. The effects of changing the ion kinetic temperature by increasing the drift field versus changing the thermal temperature can be compared, leading to information about rotational and vibrational energy effects.[493] For example, Hierl et al.[494] recently reported the temperature-dependence of eq 95,

$$C^+(^2P) + H_2 \rightarrow CH^+ + H \qquad \Delta_rH_0^\circ = +37.94 \pm 0.06 \text{ kJ/mol} \tag{95}$$

which has served as a benchmark for the measurement of endoergic ion-molecular reactions.[462,494,496−503] When these experiments were performed, the reaction endoergicity was believed to be $\Delta_rH_0^\circ = 38.4 \pm 0.3$ kJ/mol based on a spectroscopic determination[504] of $D_0(C^+-H) = 32907 \pm 23$ cm$^{-1}$, but a new measurement[505] of $D_0(C^+-H) = 32947 \pm 5$ cm$^{-1}$ reduces it to $\Delta_rH_0^\circ = 37.94 \pm 0.06$ kJ/mol. Hierl et al.[494] recently measured the thermal rate coefficients over the temperature range 400−1300 K. Phase space theory (PST) rate constants[503] fit the experimental rates well over the entire temperature range[494] (although the PST model used the older endoergicity). Comparisons between the thermal rate constants and drift tube and beam data as a function of translational energy show that rotational and vibrational modes are fully available to promote the reaction.[462,494,503] The Arrhenius plot[494] of the rate data is shown in Figure 41. The Arrhenius fit gives $E_{act} = 37.7 \pm 1.0$ kJ/mol, in excellent agreement with the new value of $\Delta_rH_0$.

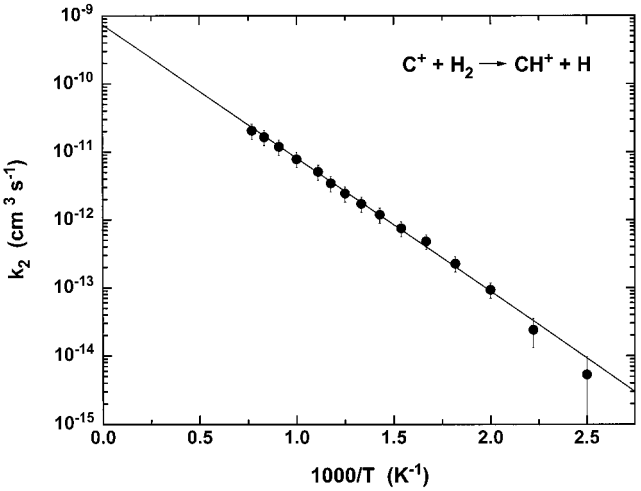


**Figure 41.** Arrhenius plot for the reaction $C^+ + H_2 \rightarrow CH^+ + H$ measured using a variable-temperature selected ion flow tube apparatus. The straight line is a linear regression fit to the data. (Reprinted with permission from ref 494. Copyright 1997 American Institute of Physics.)

## *XII. Electron–Molecule Reactions*

The electron capture detector (ECD) kinetics method[506−511] has been used to estimate electron affinities, including those of many aromatic organic molecules whose anions are bound by less than 1 eV. In the ECD experiments, thermal electrons from a radioactive $\beta$ source are captured by the analtye in the effluent from a gas chromatograph. The fractional depletion of the electron current is measured as a function of temperature and modeled using the kinetic scheme[511] in eq 96.

$$\begin{aligned} AB + e^- &\rightleftarrows AB^- && k_1/k_{-1} \\ AB^- &\rightarrow A + B^- && k_2 \\ AB^- + M^+ &\rightarrow \text{neutrals} && k_N \\ e^- + M^+ &\rightarrow \text{neutrals} && k_D \end{aligned} \qquad (96)$$

Treating the two neutralization processes as pseudo-first-order and temperature independent and obtaining their rate coefficients from calibration experiments, fits to the data are used to obtain Arrhenius activation energies and preexponential factors for the other three reaction rates, a total of six adjustable parameters.[511] Electron affinities are obtained as the difference between the activation energies for the forward and reverse directions of the first reaction in eq 96.[511] In some cases, additional reactions involving putative excited states of the anions are added to the kinetic scheme.[512] The ECD kinetics method can analyze closed-shell aromatic molecules for which the molecular anions are difficult to produce in the gas phase and also can examine systems with poor Franck−Condon overlap between the anion and neutral. Unless combined with negative-ion mass spectrometry,[513] however, the chemical identities of molecular anions present in the ECD sampling region are uncertain. The EA values from ECD often agree with electron-transfer equilibria studies[72] within the larger stated uncertainties (±0.1 eV) of the latter. Table 6 compares all EAs found (in a literature search primarily of the NIST negative-ion database[86]) with values both from ECD[506−511,514,515] and from laser photoelectron spectra with resolved and assigned 0−0 origin transitions.[164,226−229,245,252,319,516−518] Some of the values agree very well, but the mean absolute deviation is 0.11 eV and three of seven deviate outside stated uncertainty limits. This limited comparison implies that caution should be used in adopting electron affinities obtained by the ECD method and that an uncertainty of ±0.1 eV or greater is more appropriate.

Electron attachment rates at thermal energies can be measured by the flowing afterglow Langmuir probe (FALP) technique.[519] Temperature-dependent rates of electron detachment can also be measured in some cases, but the forward activation energy alone does not give the electron affinity because there may be an activation energy for the reverse thermal electron attachment. For example, the activation

**Table 6. Comparison of Electron Affinities from ECD and PES Experiments (eV)[a]**

| molecule | EA (ECD) | ref | $EA_0$ (PES) | ref | $\delta^b$ |
|---|---|---|---|---|---|
| $I_2$ | 2.33 | 506 | 2.524 ± 0.005 | 252 | −0.19 |
| $O_2$ | 0.451 ± 0.052 | 507 | 0.450 ± 0.002 | 226 | 0.001 ± 0.05 |
| | | | 0.451 ± 0.007 | 319 | |
| | | | 0.440 ± 0.008 | 516 | |
| $NO_2$ | 2.11 ± 0.18 | 507 | 2.273 ± 0.005 | 228 | −0.16 ± 0.18 |
| | | | 2.36 ± 0.1 | 517 | |
| NO | 0.1 ± 0.1 | 507 | 0.026 ± 0.005 | 319 | 0.07 ± 0.1 |
| | | | 0.024 ± 0.010 | 518 | |
| $C_{10}H_8$ (azulene) | 0.69 ± 0.04 | 509 | 0.757 ± 0.005 | 164 | −0.07 ± 0.04 |
| | 0.69 ± 0.05 | 508 | | | |
| | 0.519 ± 0.011 | 515 | | | |
| | 0.656 ± 0.008 | 514 | | | |
| $C_6H_5NO_2$ | 1.00 ± 0.02 | 509 | 1.00 ± 0.01 | 229 | 0.00 ± 0.02 |
| | >0.9 ± 0.1 | 508 | | | |
| $C_{14}H_{10}$ (anthracene) | 0.660 ± 0.080 | 510 | 0.530 ± 0.005 | 227 | 0.13 ± 0.08 |
| | 0.56 ±0.05 | 508 | | | |
| | 0.480 ± 0.004 | 515 | | | |
| | 0.556 ± 0.008 | 514 | | | |
| $CH_3NO_2$ | 0.50 ± 0.02 | 511 | 0.26 ± 0.08 | 245 | 0.24 ± 0.08 |
| | 0.45 ± 0.10 | 508 | | | |

[a] ECD, electron capture detector method; PES, photoelectron spectroscopy. [b] $\delta$ = EA(ECD) − EA(PES) for most recent reports.

energy[520] for electron attachment to $C_{60}$ is 25 kJ/mol. Besides the ECD kinetics measurements, there are few examples of measurement of forward and reverse rates to obtain equilibrium constants in reactions involving electrons as reactants or products.[111,519,521,522] Miller et al.[522] used the FALP technique to measure the thermal detachment and attachment rates for perfluorocyclobutane, eq 97.

$$cyclo\text{-}C_4F_8 + e^- \rightleftarrows cyclo\text{-}C_4F_8^- \quad k_a, k_d \quad (97)$$

The extraction of the attachment and detachment rate constants ($k_a$ and $k_d$, respectively) from electron density measurements in the flow tube requires modeling of electron and ion diffusion rates. In this case, the anion does not undergo dissociative detachment and does not react with precursors, simplifying the kinetic analysis and allowing determination of the attachment and detachment rates. Miller et al.[522] obtain $k_a = (1.6 \pm 0.5) \times 10^{-8}$ cm$^3$ s$^{-1}$ and $k_d = 1010 \pm 300$ s$^{-1}$ at 375 K, leading to $\Delta_{EA}G_{375}°$(cyclo-$C_4F_8$) $= 61 \pm 2$ kJ/mol. To correct this value to a 0 K electron affinity, Miller et al.[522] use the classical Boltzmann description for the entropy and integrated heat capacity of the electron, which gives $EA_0$(*cyclo*-$C_4F_8$) $= 61 \pm 2$ kJ/mol (the cancellation of $T\Delta S$ and $H_T - H_0$ at 375 K is accidental). If instead one uses quantum Fermi−Dirac statistics[104] (see section II.D), the result is $EA_0$(*cyclo*-$C_4F_8$) $= 64 \pm 2$ kJ/mol. The 3 kJ/mol difference is significant compared with the ±2 kJ/mol experimental precision. If the electron affinity of *cyclo*-$C_4F_8$ could be accurately measured independently, this system might provide an experimental test for the correct treatment of the thermodynamics of the electron.[104,111]

## XIII. Concluding Remarks

A wide variety of experimental methods are available for examination of thermochemical and spectroscopic properties of gas-phase ions. This review has attempted to subdivide them into categories based on the physical or chemical processes involved rather than the specific mass spectrometry instruments or laser methods used. Use of different instrumentation can often provide complementary information. Key characteristics for evaluating various mass spectrometric methods are the internal energies of the ions, the number and frequency of collisions of the ions with neutral gases, the method of activation (chemical, collisional, or photon absorption), and the lifetimes of the ions between activation and detection.

An implicit theme of this work is that detailed theoretical analysis of experimental results, especially employing statistical rate models for activated decomposition processes and accounting for ion internal energies, is critically important for obtaining accurate thermochemical results and is de rigueur for precise experimental work. The increasing accuracy and affordability of theoretical methods including ab initio molecular orbital theory and density functional theory have revolutionized experimental chemistry in general and ion thermochemistry in particular. Because mass spectrometry methods do not directly measure ion structures, theoretical calculation of geometries and vibrational frequencies combined with statistical analysis of reaction kinetics, for example, provide enormous synergistic benefit for determination of ion energetics.

The high activity in the field of gas-phase ion thermochemistry is evident in some of the new techniques introduced in the past decade for determination of energetic properties of ions. These include blackbody infrared dissociation, SORI multicollision activation, photofragment translational spectroscopy, threshold ion-pair production spectroscopy, competitive threshold collision-induced dissociation, the Bouchoux thermokinetic method, and extensions of the Cooks kinetic method to examine apparent entropies and different kinds of complexes. Undoubtedly some of these new techniques will prove themselves and become permanent additions to the ion thermochemistry repertoire. Established techniques including photoelectron spectroscopy, photoionization mass spectrometry, threshold photoelectron−photoion coincidence, ICR and HPMS equilibrium measurements, guided ion beam threshold measurements, and flow tube reaction kinetics are being applied to increasingly complex systems and with increasing precision. High-resolution ZEKE/PFI photoelectron spectroscopy, introduced in the 1980s, is continuing to evolve with applications to more complex systems.

Although this review is nominally about *ion* thermochemistry, much of it concerns determinations of *neutral* thermochemistry. The distinction between the two is rather arbitrary given the wide use of mass spectrometry detection techniques in spectroscopic and kinetic experiments on neutrals. The thermochemical cycles of eqs 1−6 allow the use of ion energetics measurements to obtain neutral thermochemistry. Confidence in thermochemical quantities is achieved by multiple determinations by completely independent methods. Ion chemistry and spectroscopy techniques can provide reliable thermochemical determinations independent of traditional calorimetric and neutral kinetics methods.

## XIV. Acknowledgments

I thank my colleagues in the ion chemistry community for their contributions cited in the references and for making this area enjoyable and stimulating. I would especially like to thank P. B. Armentrout, W. C. Lineberger, and G. B. Ellison for many discussions and support. Ion chemistry research in the Ervin group at the University of Nevada, Reno, is supported by the Department of Energy (Office of Basic Energy Sciences), the National Science Foundation (Experimental Physical Chemistry Program), and the donors of the Petroleum Research Fund (administered by the American Chemical Society), and has been carried out with the help of undergraduate and graduate students and postdoctoral co-workers as also cited in the references.

## XV. Note Added in Proof

A downward revision of the accepted enthalpy of formation of OH and bond dissociation energy of $H_2O$ has been recommended on the basis of positive-ion cycle experiments and high-level calculations.[523] This affects values for $D$(HO−H) in Tables 1 and 4.

Several valuable reviews related to experimental techniques discussed here have appeared in Volume 200 special issue of the *International Journal of Mass Spectrometry*.[524]

## XVI. References


(1) Ngoka, L. C. M.; Gross, M. L. Multistep Collisionally Activated Decomposition in an Ion Trap for the Determination of the Amino-Acid Sequence and Gas-Phase Ion Chemistry of Lithium-Coordinated Valinomycin. *Int. J. Mass Spectrom.* **2000**, *194*, 247−259.

(2) Brauman, J. I.; Blair, L. K. Gas-Phase Acidities of Alcohols. *J. Am. Chem. Soc.* **1970**, *92*, 5986−5992.

(3) Castleman, A. W., Jr. Solvated Cluster Ions. In *Clusters of Atoms and Molecules II*; Haberland, H., Ed.; Springer: Berlin, 1994; pp 77−133.

(4) Hiraoka, K.; Yamabe, S. Gas-Phase Cluster Ions: Stability, Structure, and Solvation. In *Dynamics of Excited Molecules*; Kuchitsu, K., Ed.; Elsevier: Amsterdam, 1994; pp 399−475.

(5) Takashima, K.; Riveros, J. M. Gas-Phase Solvated Ions. *Mass Spectrom. Rev.* **1998**, *17*, 409−430.

(6) Berkowitz, J.; Ellison, G. B.; Gutman, D. Three Methods to Measure RH Bond Energies. *J. Phys. Chem.* **1994**, *98*, 2744−2765.

(7) Traeger, J. C.; Kompe, B. M. Thermochemical Data for Free Radicals from Studies of Ions. In *Energetics of Organic Free Radicals*; Simões, J. A., Greenberg, A., Liebman, J. F., Eds.; Blackie Academic and Professional: London, 1996; pp 59−109.

(8) Cohen, N.; Benson, S. W. Estimation of Heats of Formation of Organic Compounds by Additivity Methods. *Chem. Rev.* **1993**, *93*, 2419−2438.

(9) Benson, S. W. *Thermochemical Kinetics*, 2nd ed.; John Wiley and Sons: New York, 1976.

(10) Cohen, N.; Benson, S. W. The Thermochemistry of Alkanes and Cycloalkanes. In *The Chemistry of Alkanes and Cycloalkanes*; Patai, S., Rappoport, Z., Eds.; Wiley: Chichester, 1992; pp 215−287.

(11) Benson, S. W.; Cohen, N. Current Status of Group Additivity. In *Computational Thermochemistry. Prediction and Estimation of Molecular Thermodynamics*; Irikura, K. K., Frurip, D. J., Eds.; American Chemical Society: Washington, DC, 1998; pp 21−46.

(12) Domalski, E. S.; Hearing, E. D. Estimation of the Thermodynamics Properties of Carbon−Hydrogen−Nitrogen−Oxygen−Sulfur−Halogen Compounds at 298.15 K. *J. Phys. Chem. Ref. Data* **1993**, *22*, 805−1159.

(13) Pedley, J. B. *Thermochemical Data and Structures of Organic Compounds*; Thermodynamics Research Center: College Station, TX, 1994; Vol. 1.

(14) McMillen, D. F.; Golden, D. M. Hydrocarbon Bond Dissociation Energies. *Annu. Rev. Phys. Chem.* **1982**, *33*, 493−532.

(15) Tsang, W. Heats of Formation of Organic Free Radicals by Kinetic Methods. In *Energetics of Organic Free Radicals*; Martinho Simões, J. A., Greenberg, A., Liebman, J. F., Eds.; Blackie Academic and Professional: London, 1996; pp 22−58.

(16) Litorja, M.; Ruscic, B. Evidence of Rotational Autoionization in the Threshold Region of the Photoionization Spectrum of $CH_3$. *J. Chem. Phys.* **1997**, *107*, 9852−9856.

(17) Mordaunt, D. H.; Ashfold, M. N. Near Ultraviolet Photolysis of $C_2H_2$: A Precise Determination of $D_0$(HCC−H). *J. Chem. Phys.* **1994**, *101*, 2630−2631.

(18) Pilgrim, J. S.; Taatjes, C. A. Infrared Absorption Probing of the Cl + $C_2H_4$ Reaction: Direct Measurement of Arrhenius Parameters for Hydrogen Abstraction. *J. Phys. Chem. A* **1997**, *101*, 4172−4177. Erratum. *J. Phys. Chem. A* **1997**, *101*, 8741.

(19) Knyazev, V. D.; Slagle, I. R. Experimental and Theoretical Study of the $C_2H_3$ = H + $C_2H_2$ Reaction. Tunneling and the Shape of the Falloff Curves. *J. Phys. Chem.* **1996**, *100*, 16899−16911.

(20) Kaiser, E. W.; Wallington, T. J. Kinetics of the Reactions of Chlorine Atoms with $C_2H_4$ ($k_1$) and $C_2H_2$ ($k_2$): A Determination of $\Delta H_{f,298}°$ for $C_2H_3$. *J. Phys. Chem.* **1996**, *100*, 4111−4119.

(21) Davico, G. E.; Bierbaum, V. M.; DePuy, C. H.; Ellison, G. B.; Squires, R. R. The C−H Bond Energy of Benzene. *J. Am. Chem. Soc.* **1995**, *117*, 2590−2599.

(22) Seetula, J. A. Kinetics and Thermochemistry of the $C_3H_5$ + HBr ⇌ $C_3H_6$ + Br Equilibrium. *Phys. Chem. Chem. Phys.* **1999**, *1*, 4727−4731.

(23) Ellison, G. B.; Davico, G. E.; Bierbaum, V. M.; DePuy, C. H. Thermochemistry of the Benzyl and Allyl Radicals and Ions. *Int. J. Mass Spectrom. Ion Processes* **1996**, *156*, 109−131.

(24) Becerra, R.; Carpenter, I. W.; Walsh, R. Time-Resolved Studies of the Kinetics of the Reactions of CHO with HI and HBr: Thermochemistry of the CHO Radical and the C−H Bond Strengths in $CH_2O$ and CHO. *J. Phys. Chem. A* **1997**, *101*, 4185−4190.

(25) Dóbé, S.; Bérces, T.; Turányi, T.; Márta, F.; Grussdorf, J.; Temps, F.; Wagner, H. G. Direct Kinetic Studies of the Reactions of Br + $CH_3OH$ and $CH_2OH$ + HBr: The Heat of Formation of $CH_2OH$. *J. Phys. Chem.* **1996**, *100*, 19864−19873.

(26) Johnson, R. D., III.; Hudgens, J. W. Structural and Thermochemical Properties of Hydroxymethyl ($CH_2OH$) Radicals and Cations Derived from Observations of B $^2A'(3p)$ ← X $^2A''$ Electronic Spectra. *J. Phys. Chem.* **1996**, *100*, 19874−19890.

(27) Osborn, D. L.; Leahy, D. J.; Ross, E. M.; Neumark, D. M. Study of the Predissociation of $CH_3O$ $\tilde{A}(^2A_1)$ by Fast Beam Photofragment Translational Spectroscopy. *Chem. Phys. Lett.* **1995**, *235*, 484−489.

(28) DeTuri, V. F.; Ervin, K. M. Competitive Threshold Collision-Induced Dissociation: Gas-Phase Acidities and Bond Dissociation Energies for a Series of Alcohols. *J. Phys. Chem. A* **1999**, *103*, 6911−6920.

(29) Ramond, T. M.; Davico, G. E.; Schwartz, R. L.; Lineberger, W. C. Vibronic Structure of Alkoxy Radicals Via Photoelectron Spectroscopy. *J. Chem. Phys.* **2000**, *112*, 1158−1169.

(30) Dobois, O.; Benson, S. W. Temperature Coefficients and Rates of Ethyl Radical Reactions with HBr and Br in the 228−368 K Temperature Range at Millitorr Pressures. *J. Phys. Chem. A* **1997**, *101*, 6030−6042.

(31) Seetula, J. A.; Slagle, I. R. Kinetics and Thermochemistry of the R + HBr = RH + Br (R = *n*-$C_3H_7$, Iso$C_3H_7$, *n*-$C_4H_9$, iso$C_4H_9$, sec-$C_4H_9$ or tert-$C_4H_9$) Equilibrium. *J. Chem. Soc., Faraday Trans.* **1997**, *93*, 1709−1719.

(32) Borges dos Santos, R. M.; Martinho Simões, J. A. Energetics of the O−H Bond in Phenol and Substituted Phenols: A Critical Evaluation of Literature Data. *J. Phys. Chem. Ref. Data* **1998**, *27*, 707−739.

(33) DeTuri, V. F.; Ervin, K. M. Proton-Transfer Between $Cl^-$ and $C_6H_5OH$. O−H Bond Energy of Phenol. *Int. J. Mass Spectrom.* **1998**, *175*, 123−132.

(34) Gunion, R. F.; Gilles, M. K.; Polak, M. L.; Lineberger, W. C. Ultraviolet Photoelectron Spectroscopy of the Phenide, Benzyl and Phenoxide Anions, with Ab Initio Calculations. *Int. J. Mass Spectrom. Ion Processes* **1992**, *117*, 601−620.

(35) Kim, H.-T.; Green, R. J.; Qian, J.; Anderson, S. L. Proton Transfer in the $[Phenol\text{-}NH_3]^+$ System: An Experimental and Ab Initio Study. *J. Chem. Phys.* **2000**, *112*, 5717−5721.

(36) Bohme, D. K.; Hemsworth, R. S.; Rundle, H. W. Chemical Equilibrium of $NH_2^-$ + $H_2$ ⇌ $H^-$ + $NH_3$ and the Determination of $D_0(NH_2-H)$. *J. Chem. Phys.* **1973**, *59*, 77−81.

(37) Wickham-Jones, C. T.; Ervin, K. M.; Ellison, G. B.; Lineberger, W. C. $NH_2$ Electron Affinity. *J. Chem. Phys.* **1989**, *91*, 2762−2763.

(38) Mordaunt, D. H.; Ashfold, M. N. R.; Dixon, R. N. Photodissociation Dynamics of $\tilde{A}$ State Ammonia Molecules. I. State Dependent $\mu$-$v$ Correlation in the $NH_2$ ($ND_2$) Products. *J. Chem. Phys.* **1996**, *104*, 6460−6471.

(39) Lykke, K. R.; Murray, K. K.; Lineberger, W. C. Threshold Photodetachment of $H^-$. *Phys. Rev. A* **1991**, *43*, 6104−6107.

(40) Bise, R. T.; Choi, H.; Pedersen, H. B.; Mordaunt, D. H.; Neumark, D. M. Photodissociation Spectroscopy and Dynamics of the Methylthio Radical ($CH_3S$). *J. Chem. Phys.* **1999**, *110*, 805−816.

(41) Robinson, M. S.; Polak, M. L.; Bierbaum, V. M.; DePuy, C. H.; Lineberger, W. C. Experimental Studies of Allene, Methylacetylene, and the Propargyl Radical: Bond Dissociation Energies, Gas-Phase Acidities, and Ion−Molecule Chemistry. *J. Am. Chem. Soc.* **1995**, *117*, 6766−6778.

(42) Wilson, S. H. S.; Howe, J. D.; Ashfold, M. N. R. On the Near Ultraviolet Photodissociation of Hydrogen Sulphide. *Mol. Phys.* **1996**, *88*, 841−858.

(43) Rempala, K.; Ervin, K. M. Collisional Activation of the Endoergic Hydrogen Atom Transfer Reaction $S^-(^2P)$ + $H_2$ → $SH^-$ + H. *J. Chem. Phys.* **2000**, *112*, 4579−4590.

(44) Cook, P. A.; Langford, S. R.; Ashfold, M. N. R.; Dixon, R. N. Angular Resolved Studies of the Lyman-α Photodissociation of HCN and DCN: New Dynamical Insights. *J. Chem. Phys.* **2000**, *113*, 994−1004.

(45) Shiell, R. C.; Hu, X. K.; Hu, Q. J.; Hepburn, J. W. A Determination of the Bond Dissociation Energy ($D_0$(H−SH)): Threshold Ion-Pair Production Spectroscopy (TIPPS) of a Triatomic Molecule. *J. Phys. Chem. A* **2000**, *104*, 4339−4342.

(46) Doering, W. v. E. Impact of Upwardly Revised $\Delta H_f°$ of Primary, Secondary, and Tertiary Radicals on Mechanistic Constructs in Thermal Reorganizations. *Proc. Natl. Acad. Sci. U.S.A.* **1981**, *78*, 5279−5283.

(47) Smith, B. J.; Radom, L. Heat of Formation of the *tert*-Butyl Radical. *J. Phys. Chem. A* **1998**, *102*, 10787−10790.
(48) Benson, S. W.; Dobis, O. Existence of Negative Activation Energies in Simple Bimolecular Metathesis Reactions and Some Observations on Too-Fast Reactions. *J. Phys. Chem. A* **1998**, *102*, 5175−5181.
(49) Marshall, P. Thermochemistry of the Ethyl Radical and the C−H Bond Strength in Ethane. *J. Phys. Chem. A* **1999**, *103*, 4560−4563.
(50) Tsang, W. Shock Tube Studies on the Stability of Polyatomic Molecules and the Determination of Bond Energies. In *Energetics of Stable Molecules and Reactive Intermediates*; Minas da Piedade, M. E., Ed.; Kluwer Academic: Dordrecht, 1999; pp 323−352.
(51) Martinho Simões, J. A. *Energetics of Organometallic Species*; Kluwer: Dordrecht, 1992.
(52) van Koppen, P. A. M.; Bowers, M. T.; Beauchamp, J. L.; Dearden, D. V. Organometallic Reaction Energetics from Product Kinetic Energy Release Distributions. In *Bonding Energetics in Organometallic Compounds*; Marks, T. J., Ed.; American Chemical Society: Washington, 1990; pp 34−54.
(53) Ranasinghe, Y. A.; Surjasasmita, I. B.; Freiser, B. S. Gas-Phase Organometallic Ion Photochemistry. In *Organometallic Ion Chemistry*; Freiser, B. S., Ed.; Kluwer Academic: Dordrecht, 1996; pp 229−258.
(54) Freiser, B. S. Table of Bond Energies. In *Organometallic Ion Chemistry*; Freiser, B. S., Ed.; Kluwer Academic: Dordrecht, 1996; pp 283−332.
(55) Armentrout, P. B.; Kickel, B. L. Gas-Phase Thermochemistry of Transition Metal Ligand Systems: Reassessment of Values and Periodic Trends. In *Organometallic Ion Chemistry*; Freiser, B. S., Ed.; Kluwer Academic: Dordrecht, 1996; pp 1−45.
(56) Pilcher, G. Combustion Calorimetry of Organometallic Compounds. In *Energetics of Organometallic Species*; Martinho Simões, J. A., Ed.; Kluwer: Dordrecht, 1992; pp 9−34.
(57) Carrington, A.; Softley, T. P. High-Resolution Infrared Spectroscopy of Molecular Ions. In *Molecular Ions: Spectroscopy, Structure, and Chemistry*; Miller, T. A., Bondybey, V. E., Eds.; North-Holland: Amsterdam, 1983; pp 49−72.
(58) Oka, T. Infrared Spectroscopy of Molecular Ions. In *Frontiers of Laser Spectroscopy of Gases*; Alves, A. C. P., Brown, J. M., Hollas, J. M., Eds.; Kluwer Academic: Dordrecht, 1988; pp 353−377.
(59) Saykally, R. J. Infrared Laser Spectroscopy of Molecular Ions. *Science* **1988**, *239*, 157−161.
(60) Davies, P. B. Infrared Laser and Microwave Spectroscopy of Electric Discharges. *Chem. Soc. Rev.* **1995**, *24*, 151−157.
(61) Lugez, C. L.; Forney, D.; Jacox, M. E.; Irikura, K. K.; Thompson, W. E. Infrared Spectra of Molecular Ions Derived from the Hydrogen and Methyl Halides Trapped in Solid Neon. *J. Mol. Struct.* **1998**, *449*, 111−118.
(62) Szczepanski, J.; Hodyss, R.; Vala, M. Isotopic Infrared Absorption Study of $C_5^-$, $C_7^-$, and $C_9^-$ Carbon Cluster Anions in Ar Matrices. *J. Phys. Chem. A* **1998**, *102*, 8300−8304.
(63) Zhou, M.; Andrews, L. Reactions of Laser-Ablated Cu with NO: Infrared Spectra and Density Functional Calculations of $CuNO^+$, CuNO, $Cu(NO)_2$, and $Cu(NO)_2^-$ in Solid Neon and Argon. *J. Phys. Chem. A* **2000**, *104*, 2618−2625.
(64) Grutter, M.; Wyss, M.; Maier, J. P. Electronic Absorption Spectra of $C_{2n}H^-$, $C_{2n-1}N^-$ ($n$ = 4−7), and $C_{2n-1}N$ ($n$ = 3−7) Chains in Neon Matrices. *J. Chem. Phys.* **1999**, *110*, 1492−1496.
(65) Carrington, A.; Shaw, A. M.; Taylor, S. M. Ion-Beam Spectroscopy of Long-Range Complexes. *J. Chem. Soc., Faraday Trans.* **1995**, *91*, 3725−3740.
(66) Angel, L.; Stace, A. J. Reappraisal of the Contribution from $[O_2(H_2O)_n]^+$ Cluster Ions to the Chemistry of the Ionosphere. *J. Phys. Chem. A* **1999**, *103*, 2999−3005.
(67) France, M. R.; Pullins, S. H.; Duncan, M. A. Photodissociation of $Mg^+(CH_3OH)_n$ Complexes: Evidence for the Onset of Solvation. *Chem. Phys.* **1998**, *239*, 447−457.
(68) Moore, C. E. *Atomic Energy Levels—As Derived from the Analyses of Optical Spectra*; Natl. Stand. Ref. Data Series 35; National Bureau of Standards: Washington, DC, 1971; Vol. I−III.
(69) Huber, K. P.; Herzberg, G. *Constants of Diatomic Molecules*; Van Nostrand-Reinhold: New York, 1979.
(70) Hotop, H.; Lineberger, W. C. Binding Energies in Atomic Negative Ions: II. *J. Phys. Chem. Ref. Data* **1985**, *14*, 731−750.
(71) Keesee, R. G.; Castleman, A. W., Jr. Thermochemical Data on Gas-Phase Ion−Molecule Association and Clustering Reactions. *J. Phys. Chem. Ref. Data* **1986**, *15*, 1011−1071.
(72) Kebarle, P.; Chowdhury, S. Electron Affinities and Electron-Transfer Reactions. *Chem. Rev.* **1987**, *87*, 513−534.
(73) Lias, S. G.; Bartmess, J. E.; Liebman, J. F.; Holmes, J. L.; Levin, R. D.; Mallard, W. G. Gas-Phase Ion and Neutral Thermochemistry. *J. Phys. Chem. Ref. Data* **1988**, *17* (Suppl. 1).
(74) Morse, M. D. Clusters of Transition Metal Atoms. *Chem. Rev.* **1986**, *86*, 6, 1049−1109.
(75) Bartmess, J. E. Gas-Phase Equilibrium Affinity Scales and Chemical Ionization Mass Spectrometry. *Mass Spectrom. Rev.* **1989**, *8*, 297−343.
(76) Bartmess, J. E. *NIST Negative Ion Database*, Ver. 3.01; NIST Standard Reference Database 19B; National Institute of Standards and Technology: Washington, DC, 1991.
(77) Cox, J. D.; Wagman, D. D.; Medvedev, V. A. *CODATA Key Values for Thermodynamics*; Hemisphere: New York, 1989 (http://www.codata.org/codata/databases/key1.html).
(78) Gurvich, L. V.; Veyts, I. V.; Alcock, C. B. *Thermodynamic Properties of Individual Substances*, 4th ed.; Hemisphere Publishing Corporation: New York, 1989; Vol. 1 (Elements O, H (D, T), F, Cl, Br, I, He, Ne, Ar, Kr, Xe, Rn, S, N, P and Their Compounds), Parts 1−2.
(79) Gurvich, L. V.; Veyts, I. V.; Alcock, C. B. *Thermodynamic Properties of Individual Substances*, 4th ed.; Hemisphere: New York, 1991; Vol. 2 (Elements C, Si, Ge, Sn, Pb, and Their Compounds), Parts 1−2.
(80) Curtiss, L. A.; Raghavachari, K.; Redfern, P. C.; Pople, J. A. Assessment of Gaussian-2 and Density Functional Theories for the Computation of Enthalpies of Formation, *J. Chem. Phys.* **1997**, *106*, 1063−1079.
(81) Curtiss, L. A.; Redfern, P. C.; Raghavachari, K.; Pople, J. A. Assessment of Gaussian-2 and Density Functional Theories for the Computation of Ionization Potentials and Electron Affinities. *J. Chem. Phys.* **1998**, *109*, 42−55.
(82) Curtiss, L. A.; Raghavachari, K.; Redfern, P. C.; Pople, J. A. Assessment of Gaussian-3 and Density Functional Theories for a Larger Experimental Test Set. *J. Chem. Phys.* **2000**, *112*, 7374−7383.
(83) Chase, M. W., Jr. NIST-JANAF Thermochemical Tables, 4th ed.; *J. Phys. Chem. Ref. Data* **1998** (Monograph No. 9).
(84) Hunter, E. P. L.; Lias, S. G. Evaluated Gas-Phase Basicities and Proton Affinities of Molecules: An Update. *J. Phys. Chem. Ref. Data* **1998**, *27*, 413−656.
(85) Schlag, E. W. *ZEKE Spectroscopy*; Cambridge University Press: Cambridge, 1998.
(86) Bartmess, J. E. Negative Ion Energetics Data. In *NIST Chemistry WebBook, NIST Standard Reference Database Number 69*; Mallard, W. G., Linstrom, P. J., Eds.; National Institute of Standards and Technology: Gaithersburg, MD, Jan 2000 (http://webbook.nist.gov).
(87) Hunter, E. P.; Lias, S. G.; Proton Affinity Evaluation. In *NIST Chemistry WebBook, NIST Standard Reference Database Number 69*; Mallard, W. G., Linstrom, P. J., Eds.; National Institute of Standards and Technology: Gaithersburg, MD, Jan 2000 (http://webbook.nist.gov).
(88) Lias, S. G. Ionization Energy Evaluation. In *NIST Chemistry WebBook, NIST Standard Reference Database Number 69*; Mallard, W. G., Linstrom, P. J., Eds.; National Institute of Standards and Technology: Gaithersburg, MD, Jan 2000 (http://webbook.nist.gov).
(89) Lias, S. G.; Bartmess, J. E.; Liebman, J. F.; Holmes, J. L.; Levin, R. D.; Mallard, W. G. Ion Energetics Data. In *NIST Chemistry WebBook, NIST Standard Reference Database Number 69*; Mallard, W. G., Linstrom, P. J., Eds.; National Institute of Standards and Technology: Gaithersburg, MD, Jan 2000 (http://webbook.nist.gov).
(90) Martinho Simões, J. A. Organometallic Thermochemistry Data. In *NIST Chemistry WebBook, NIST Standard Reference Database Number 69*; Mallard, W. G., Linstrom, P. J., Eds.; National Institute of Standards and Technology: Gaithersburg, MD, Feb 2000 (http://webbook.nist.gov).
(91) Afeefy, H. Y.; Liebman, J. F.; Stein, S. E. Neutral Thermochemical Data. In *NIST Chemistry WebBook, NIST Standard Reference Database Number 69*; Mallard, W. G., Linstrom, P. J., Eds.; National Institute of Standards and Technology: Gaithersburg, MD, Jan 2000 (http://webbook.nist.gov).
(92) Mautner, M. Binding Energies Between Ions and Molecules, and the Thermochemistry of Cluster Ions. In *NIST Chemistry WebBook, NIST Standard Reference Database Number 69*; Mallard, W. G., Linstrom, P. J., Eds.; National Institute of Standards and Technology: Gaithersburg, MD, Jan 2000 (http://webbook.nist.gov).
(93) Rienstra-Kiracofe, J. C.; Nandi, S.; Ellison, G. B.; Schaefer, H. F., III Atomic and Molecular Electron Affinities: Theory and Photoelectron Experiments. *Chem. Rev.*, submitted for publication.
(94) Irikura, K. K.; Frurip, D. J. *Computational Thermochemistry. Prediction and Estimation of Molecular Thermodynamics*; American Chemical Society: Washington, DC, 1998.
(95) Farrar, J. M.; Saunders, W. H., Jr., Eds. *Techniques for the Study of Ion−Molecule Reactions*. Techniques of Chemistry, vol. 20; John Wiley & Sons: New York, 1988.
(96) Curtiss, L. A.; Raghavachari, K.; Trucks, G. W.; Pople, J. A. Gaussian-2 Theory for Molecular Energies of First- and Second-Row Compounds, *J. Chem. Phys.* **1991**, *94*, 7221−7230.
(97) Nicolaides, A.; Rauk, A.; Glukhovtsev, M. N.; Radom, L. Heats of Formation from G2, G2(MP2), and G2(MP2, SVP) Total Energies, *J. Phys. Chem.* **1996**, *100*, 17460−17464.
(98) Curtiss, L. A.; Raghavachari, K.; Redfern, P. C.; Rassolov, V.; Pople, J. A. Gaussian-3 (G3) Theory for Molecules Containing

First and Second Row Atoms, *J. Chem. Phys.* **1998**, *109*, 7764−7776. (Supporting Information at http://chemistry.anl.gov/compmat/comptherm.htm).
(99) Irikura, K. K. Extracting Thermochemical Information from Ab Initio Data. In *Energetics of Stable Molecules and Reactive Intermediates*; Minas da Piedada, M. E., Ed.; Kluwer: Dordrecht, 1999; pp 353−372.
(100) Irikura, K. K. Essential Statistical Thermodynamics. In *Computational Thermochemistry. Prediction and Estimation of Molecular Thermodynamics*; Irikura, K. K., Frurip, D. J., Eds.; American Chemical Society: Washington, DC, 1998; pp 402−418.
(101) Scott, A. P.; Radom, L. Harmonic Vibrational Frequencies: An Evaluation of Hartree−Fock, Møller−Plesset, Quadratic Configuration Interaction, Density Functional Theory, and Semiempirical Scale Factors. *J. Phys. Chem.* **1996**, *100*, 16502−16513.
(102) East, A. L. L.; Radom, L. Ab Initio Statistical Thermodynamical Models for the Computation of Third-Law Entropies. *J. Chem. Phys.* **1997**, *106*, 6655−6674.
(103) Lias, S. G.; Rosenstock, H. M.; Su, T. Thermochemistry of Polyatomic Cations. In *Kinetics of Ion−Molecule Reactions*; Ausloos, P., Ed.; Plenum: New York, 1979; pp 223−254.
(104) Bartmess, J. E. Thermodynamics of the Electron and the Proton. *J. Phys. Chem.* **1994**, *98*, 6420−6424. Erratum, *ibid.* **1995**, *99*, 6755.
(105) Bartmess, J. E.; Pittman, J. L.; Aeschleman, J. A.; Deakyne, C. A. The Temperature Dependence of Absolute Gas-Phase Acidities. *Int. J. Mass Spectrom.* **2000**, *195/196*, 215−223.
(106) *NIST Chemistry WebBook, NIST Standard Reference Database Number 69*; Mallard, W. G., Linstrom, P. J., Eds.; National Institute of Standards and Technology: Gaithersburg, MD, Jan 2000 (http://webbook.nist.gov).
(107) Lias, S. G.; Bartmess, J. E. Gas-Phase Ion Thermochemistry. In *NIST Chemistry WebBook, NIST Standard Reference Database Number 69*; Mallard, W. G., Linstrom, P. J., Eds.; National Institute of Standards and Technology: Gaithersburg, MD, Jan 2000 (http://webbook.nist.gov).
(108) Franklin, J. L.; Dillard, J. G.; Rosenstock, H. M.; Herron, J. T.; Draxl, K.; Field, F. H. *Ionization Potentials, Appearance Potentials, and Heats of Formation of Gaseous Positive Ions*; Natl. Stand. Ref. Data Ser. 26; Washington, DC: National Bureau of Standards, 1969.
(109) Field, F. H.; Franklin, J. L. *Electron Impact Phenomena and the Properties of Gaseous Ions*, Revised ed.; Academic: New York, 1970.
(110) Lias, S. G.; Liebman, J. F.; Levin, R. D. Evaluated Gas-Phase Basicities and Proton Affinities of Molecules; Heats of Formation of Protonated Molecules. *J. Phys. Chem. Ref. Data* **1984**, *13*, 695−808.
(111) Henchman, M. Thermodynamic Properties of the Electron. In *Linking the Gaseous and Condensed Phases of Matter*; Christophorou, L. G., Ed.; Plenum: New York, 1994; pp 455−460.
(112) Mohr, P. J.; Taylor, B. N. CODATA Recommended Values of the Fundamental Constants: 1998. *J. Phys. Chem. Ref. Data* **1999**, *28*, 1713−1852 (http://physics.nist.gov/cuu/Constants/).
(113) Bevington, P. R. *Data Reduction and Error Analysis for the Physical Sciences*; McGraw-Hill: New York, 1969.
(114) Shoemaker, D. P.; Garland, C. W.; Nibler, J. W. *Experiments in Physical Chemistry*, 6th ed.; McGraw-Hill: New York, 1996.
(115) Taylor, J. R. *An Introduction to Error Analysis*, 2nd ed.; University Science Books: Sausilito, CA, 1997.
(116) Taylor, B. N.; Kuyatt, C. *Guidelines for Evaluating and Expressing the Uncertainty of NIST Measurement Results*; NIST Technical Note 1297; Washington, DC: National Institute of Standards and Technology, 1994 (http://physics.nist/gov/Document/tn1297.pdf).
(117) Martin, W. C.; Zalubas, R.; Hagan, L. *Atomic Energy Levels—The Rare Earth Elements*; National Standards Reference Data Series 60; National Bureau of Standards: Washington, DC, 1978.
(118) Martin, W. C.; Zalubas, R. Energy Levels of Magnesium, Mg I through Mg XII. *J. Phys. Chem. Ref. Data* **1980**, *9*, 1−58.
(119) Martin, W. C.; Zalubas, R. Energy Levels of Sodium, Na I through Na XI. *J. Phys. Chem. Ref. Data* **1981**, *10*, 153−196.
(120) Martin, W. C.; Zalubas, R. Energy Levels of Silicon, Si I through Si XIV. *J. Phys. Chem. Ref. Data* **1983**, *12*, 323−380.
(121) Martin, W. C.; Zalubas, R.; Musgrove, A. Energy Levels of Phosphorus, P I through P XV. *J. Phys. Chem. Ref. Data* **1985**, *14*, 751−802.
(122) Sugar, J.; Corliss, C. Atomic Energy Levels of the Iron-Period Elements, Potassium through Nickel. *J. Phys. Chem. Ref. Data* **1985**, *14* (Suppl. 2).
(123) Sugar, J.; Musgrove, A. Energy Levels of Molybdenum, Mo I through Mo XLII. *J. Chem. Phys. Ref. Data* **1988**, *17*, 155−239.
(124) Sugar, J.; Musgrove, A. Energy Levels of Copper, Cu I through Cu XXIX. *J. Chem. Phys. Ref. Data* **1990**, *19*, 527−616.
(125) Martin, W. C.; Zalubas, R.; Musgrove, A. Energy Levels of Sulfur, S I through S XVI. *J. Phys. Chem. Ref. Data* **1990**, *19*, 821−880.
(126) Sugar, J.; Musgrove, A. Energy Levels of Zinc, Zn I through Zn XXX. *J. Chem. Phys. Ref. Data* **1995**, *24*, 1803−1872.
(127) Kramida, A.; Martin, W. A Compilation of Energy Levels and Wavelengths for the Spectrum of Neutral Beryllium (Be I). *J. Phys. Chem. Ref. Data* **1997**, *26*, 1185−1194.
(128) Kelleher, D. E.; Martin, W. C.; Wiese, W. L.; Sugar, J. R.; Fuhr, K.; Olsen, A.; Musgrove, A.; Mohr, P. J.; Reader, J.; Dalton, G. R. The New NIST Atomic Spectra Database. *Phys. Scr. A* **1999**, *T83*, 158−161 (http://physics.nist.gov/asd).
(129) Chupka, W. A. Effect of Unimolecular Decay Kinetics on the Interpretation of Appearance Potentials. *J. Chem. Phys.* **1959**, *30*, 191−211.
(130) Lifshitz, C.; Long, F. A. Influence of Competitive Decomposition Processes on Ionization Efficiency Curves from Electron Impact. *J. Chem. Phys.* **1964**, *41*, 2468−2471.
(131) Lorquet, J. C. Basic Questions in Mass Spectrometry, *Org. Mass Spectrom.* **1981**, *16*, 469−482.
(132) Baer, T.; Mayer, P. M. Statistical Rice-Ramsperger-Kassel-Marcus Quasiequilibrium Theory Calculations in Mass Spectrometry. *J. Am. Soc. Mass Spectrom.* **1997**, *8*.
(133) Steinfeld, J. I.; Francisco, J. S.; Hase, W. L. *Chemical Kinetics and Reaction Dynamics*, 2nd ed.; Prentice Hall: Upper Saddle River, NJ, 1998.
(134) Baer, T.; Hase, W. L. *Unimolecular Reaction Dynamics: Theory and Experiments*; Oxford University Press: New York, 1996.
(135) Forst, W. *Theory of Unimolecular Reactions*; Academic: New York, 1973.
(136) Gilbert, R. G.; Smith, S. C. *Theory of Unimolecular and Recombination Reactions*; Blackwell Scientific: Boston, 1990.
(137) Holbrook, K. A.; Pilling, M. J.; Robertson, S. H. *Unimolecular Reactions*, 2nd ed.; Wiley: New York, 1996.
(138) Truhlar, D. G.; Garret, B. C.; Klippenstein, S. J. Current Status of Transition-State Theory. *J. Phys. Chem.* **1996**, *100*, 12771−12800.
(139) Klippenstein, S. J.; Allen, W. D. Variable Reaction Coordinate Direct RRKM Theory. *Ber. Bunsen-Ges. Phys. Chem.* **1997**, *101*, 423−437.
(140) Bojesen, G.; Breindahl, T. On the Proton Affinity of Some α-Amino Acids and the Theory of the Kinetic Method. *J. Chem. Soc., Perkin Trans. 2* **1994**, 1029−1037.
(141) Ervin, K. M. Microcanonical Analysis of the Kinetic Method: Meaning of the 'Effective Temperature'. *Int. J. Mass Spectrom.* **2000**, *195/196*, 271−284.
(142) Chesnavich, W. J.; Bowers, M. T. Statistical Phase Space Theory of Polyatomic Systems: Rigorous Energy and A.M. Conservation in Reactions of Symmetric Polyatomics. *J. Chem. Phys.* **1977**, *66*, 2306−2315.
(143) Chesnavich, W. J.; Bowers, M. T. Theory of Ion−Neutral Interactions: Applications of Transition State Theory Concepts to Both Collisional and Reactive Properties of Simple Systems. *Prog. React. Kinet.* **1982**, *11*, 137−267.
(144) Talrose, V. L.; Vinogradov, P. S.; Larin, I. K. On the Rapidity of Ion−Molecule Reactions. In *Gas-Phase Ion Chemistry*; Bowers, M. T., Ed.; Academic: New York, 1979; pp 305−347.
(145) Rodgers, M. T.; Ervin, K. M.; Armentrout, P. B. Statistical Modeling of Collision-Induced Dissociation Thresholds. *J. Chem. Phys.* **1997**, *106*, 4499−4508.
(146) Lifshitz, C. Time-Resolved Appearance Energies, Breakdown Graphs, and Mass Spectra: The Elusive 'Kinetic Shift'. *Mass Spectrom. Rev.* **1982**, *1*, 309−348.
(147) Yi, S. S.; Blomberg, M. R. A.; Siegbahn, P. E. M.; Weisshaar, J. C. Statistical Modeling of Gas-Phase Organometallic Reactions Based on Density Functional Theory: $Ni^+ + C_3H_8$. *J. Phys. Chem. A* **1998**, *102*, 395−411.
(148) Dunbar, R. C. Infrared Radiative Cooling of Gas-Phase Ions. *Mass Spectrom. Rev.* **1992**, *11*, 309−339.
(149) Dunbar, R. C. Modeling Radiative Association Kinetics. *Int. J. Mass Spectrom. Ion Processes* **1997**, *160*, 1−16.
(150) Amrein, A.; Simpson, R.; Hackett, P. Multiphoton Excitation, Ionization, and Dissociation Decay Dynamics of Small Clusters of Niobium, Tantalum, and Tungsten: Time-Resolved Thermionic Emission. *J. Chem. Phys.* **1991**, *95*, 1781−1800.
(151) Ganteför, G.; Eberhardt, W.; Weidele, H.; Kreisle, D.; Recknagel, E. Energy Dissipation in Small Clusters: Direct Photoemission, Dissociation, and Thermionic Emission. *Phys. Rev. Lett.* **1996**, *77*, 4524−4527.
(152) Walther, C.; Dietrich, G.; Dostal, W.; Hansen, K.; Krückeberg, S.; Lützenkirchen, K.; Schweikhard, L. Radiative Cooling of a Small Metal Cluster: The Case of $V_{13}^+$. *Phys. Rev. Lett.* **1999**, *83*, 3816−3819.
(153) Shi, Y.; Spasov, V. A.; Ervin, K. M. Competitive Fragmentation and Electron Loss Kinetics of Photoactivated Silver Cluster Anions. Dissociation Energies of $Ag_n^-$ ($n = 7-11$). *J. Chem. Phys.* **1999**, *111*, 938−949.
(154) Lifshitz, C. Energetics and Dynamics through Time-Resolved Measurements in Mass Spectrometry: Aromatic Hydrocarbons, Polycylic Aromatic Hydrocarbons and Fullerenes. *Int. Rev. Phys. Chem.* **1997**, *16*, 113−139.

(155) Klots, C. E. Quasiequilibrium Rate Constants for Thermionic Emission from Small Particles. *Chem. Phys. Lett.* **1991**, *186*, 73−76.
(156) Klippenstein, S. J.; Yang, Y.-C.; Ryzhov, V.; Dunbar, R. C. Theory and Modeling of Ion-Molecule Radiative Association Kinetics. *J. Chem. Phys.* **1996**, *104*, 4502−4516.
(157) Chupka, W. A.; Klots, C. E. Radiative Energy Loss from Hot $C_{60}$ Molecules. *Int. J. Mass Spectrom. Ion Processes* **1997**, *167/168*, 595−603.
(158) Hansen, K.; Campbell, E. E. B. Thermal Radiation from Small Particles. *Phys. Rev. E* **1998**, *58*, 5477−5482.
(159) Campbell, E. E. B.; Levine, R. D. Delayed Ionization and Thermionic Emission in Hot Clusters and Molecules. *Comments Mod. Phys. D. Comments At. Mol. Phys.* **1999**, *1*, 155−169.
(160) Wigner, E. P. On the Behavior of Cross Sections Near Thresholds. *Phys. Rev.* **1948**, *73*, 1002−1009.
(161) Berkowitz, J. *Photoabsorption, Photoionization, and Photoelectron Spectroscopy*; Academic: New York, 1979.
(162) Rosenstock, H. M.; Draxl, K.; Steiner, B. W.; Herron, J. T. Energetics of Gaseous Ions. *J. Phys. Chem. Ref. Data* **1977**, *6*(Suppl. 1).
(163) Parr, A. C.; Inghram, M. G. Threshold Behavior for Photo Double Ionization. *J. Chem. Phys.* **1970**, *52*, 4916−4917.
(164) Boesl, U.; Knott, W. J. Negative Ions, Mass Selection, and Photoelectrons. *Mass Spectrom. Rev.* **1998**, *17*, 275−305.
(165) Dessent, C. E. H.; Johnson, M. A. Fundamentals of Negative Ion Photoelectron Spectroscopy. In *Fundamentals and Applications of Gas-Phase Ion Chemistry*; Jennings, K. R., Ed.; Kluwer Academic: Dordrecht, 1999; pp 287−306.
(166) Wannier, G. H. The Threshold Law for Single Ionization of Atoms or Ions by Electrons. *Phys. Rev.* **1953**, *90*, 817−825.
(167) Winkler, C.; Märk, T. D. Experimental Investigation of the Electron Impact Ionization Cross Section Behavior Near Threshold. *Int. J. Mass Spectrom. Ion Processes* **1994**, *133*, 157−164.
(168) Dorman, F. H.; Morrison, J. D.; Nicholson, A. J. C. Threshold Law for the Probability of Excitation by Electron Impact. *J. Chem. Phys.* **1960**, *32*, 378−384.
(169) Bilodeau, R. C.; Scheer, M.; Haugen, H. K.; Brooks, R. L. Near-Threshold Laser Spectroscopy of Iridium and Platinum Negative Ions: Electron Affinities and the Threshold Law. *Phys. Rev. A* **1999**, *61*, 012505.
(170) Smith, J. R.; Kim, J. B.; Lineberger, W. C. High-Resolution Threshold Photodetachment Spectroscopy of $OH^-$. *Phys. Rev. A* **1997**, *55*, 2036−2043.
(171) Ruscic, B.; Berkowitz, J. Heat of Formation of $CH_2OH$ and $D_0(H-CH_2OH)$. *J. Phys. Chem.* **1993**, *97*, 11451−11455.
(172) Armentrout, P. B. Energy Dependences of Ion−Molecule Reactions. *Comments At. Mol. Phys.* **1988**, *22*, 133−144.
(173) González Ureña, A. Experimental Methods for Reaction Threshold Determination Using Molecular Beam and Laser Techniques. *J. Phys. Chem.* **1992**, *96*, 8212−8219.
(174) Armentrout, P. B. Kinetic Energy Depdendence of Ion−Molecule Reactions: Guided Ion Beams and Threshold Measurements. *Int. J. Mass Spectrom.* **2000**, *200*, in press.
(175) Levine, R. D.; Bernstein, R. B. *Molecular Reaction Dynamics and Chemical Reactivity*; Oxford University Press: New York, 1987.
(176) Mahan, B. H. Impulsive Collisional Excitation. *J. Chem. Phys.* **1970**, *52*, 5221−5225.
(177) Levine, R. D.; Bernstein, R. B. CID: A Simplistic Optical Model Analysis. *Chem. Phys. Lett.* **1971**, *11*, 552−536.
(178) Levine, R. D.; Bernstein, R. B. Post-Threshold Energy Dependence of the Cross Section for Endoergic Processes: Vibrational Excitation and Reactive Scattering. *J. Chem. Phys.* **1972**, *56*, 2281−2287.
(179) Rebick, C.; Levine, R. D. CID: A Statistical Theory. *J. Chem. Phys.* **1973**, *58*, 3942−3952.
(180) Chesnavich, W. J.; Bowers, M. T. Threshold Behavior of Endoergic Bimolecular Reactions: A Statistical Phase Space Approach. *J. Chem. Phys.* **1978**, *68*, 901−903.
(181) Chesnavich, W. J.; Bowers, M. T. Theory of Translationally Driven Reactions. *J. Phys. Chem.* **1979**, *83*, 900−905.
(182) Ervin, K. M. Orientational Effects in the Direct $Cl^- + CH_3Cl$ $S_N2$ Reaction at Elevated Collision Energies: Hard-Ovoid Line-of-Centers Collision Model. *Int. J. Mass Spectrom.* **1999**, *185/186/187*, 343−350.
(183) Armentrout, P. B. Thermochemical Measurements by Guided Ion Beam Mass Spectrometry. In *Advances in Gas-Phase Ion Chemistry*; Adams, N. G., Babcock, L. M., Eds.; JAI Press: Greenwich, CT, 1992; Vol. 1, pp 83−119.
(184) Chantry, P. J. Doppler Broadening in Beam Experiments. *J. Chem. Phys.* **1971**, *55*, 2746−2759.
(185) Lifshitz, C.; Wu, R.; Tiernan, T. O.; Terwilleger, D. T. Negative Ion−Molecule Reactions of Ozone and Their Implications on the Thermochemistry of $O_3^-$. *J. Chem. Phys.* **1978**, *68*, 247−260.
(186) Ervin, K. M.; Armentrout, P. B. Energy Dependence, Kinetic Isotope Effects and Thermochemistry of the Nearly Thermoneutral Reactions $N^+(^3P) + H_2$ (HD, $D_2$) → $NH^+$ ($ND^+$) + H (D). *J. Chem. Phys.* **1987**, *86*, 2659−2673.
(187) Sowa-Resat, M. B.; Hintz, P. A.; Anderson, S. L. Dissociation Energies for Small Carbon Cluster Ions ($C_{2-19}^+$) Measured by Collision-Induced Dissociation. *J. Phys. Chem.* **1995**, *99*, 10736−10741.
(188) Khan, F. A.; Clemmer, D. E.; Schultz, R. H.; Armentrout, P. B. Sequential Bond Energies of $Cr(CO)_x^+$, $x = 1-6$. *J. Phys. Chem.* **1993**, *97*, 7978−7987.
(189) Rodgers, M. T.; Armentrout, P. B. Statistical Modeling of Competitive Threshold Collision-Induced Dissociation. *J. Chem. Phys.* **1998**, *109*, 1787−1800.
(190) White, H. E. *Introduction to Atomic Spectra*; McGraw-Hill: New York, 1934.
(191) Lotz, W. Ionization Potentials of Atoms and Ions from Hydrogen to Zinc. *J. Opt. Soc. Am.* **1967**, *57*, 873−878.
(192) Rosenstock, H. M. The Measurement of Ionization and Appearance Potentials. *Int. J. Mass Spectrom. Ion Phys.* **1976**, *20*, 139−190.
(193) Martin, W. C. Series Formulas for the Spectrum of Atomic Sodium (Na I). *J. Opt. Soc. Am.* **1980**, *70*, 784−788.
(194) Beattie, D. A.; Donovan, R. J. Advances in Photoionisation Techniques. *Prog. React. Kinet.* **1998**, *23*, 281−296.
(195) Baer, T.; Guyon, P.-M. Historical Introduction to Threshold Photoionization. In *High-Resolution Laser Photoionization and Photoelectron Studies*; Powis, I., Baer, T., Ng, C.-Y., Eds.; John Wiley & Sons: Chichester, 1995; pp 1−20.
(196) Müller-Dethlefs, K. High-Resolution Spectroscopy with Photoelectrons: ZEKE Spectroscopy of Molecular Systems. In *High-Resolution Laser Photoionization and Photoelectron Studies*; Powis, I., Baer, T., Ng, C.-Y., Eds.; John Wiley & Sons: Chichester, 1995; pp 21−78.
(197) Linton, C.; Simard, B.; Loock, H. P.; Wallin, S.; Rothschopf, G. K.; Gunion, R. F.; Morse, M. D.; Armentrout, P. B. Rydberg and Pulsed Field Ionization−Zero Electron Kinetic Energy Spectra of YO. *J. Chem. Phys.* **1999**, *111*, 5017−5026.
(198) Berkowitz, J.; Ruscic, B. Photoionization Mass Spectrometric Studies of Free Radicals. In *Vacuum Ultraviolet Photoionization and Photodissociation of Molecules and Clusters*; Ng, C. Y., Ed.; World Scientific: Singapore, 1991; pp 1−41.
(199) *High-Resolution Laser Photoionization and Photoelectron Studies*; Powis, I., Baer, T., Ng, C.-Y., Eds.; John Wiley & Sons: Chichester, 1995.
(200) Baer, T.; Lafleur, R.; Mazyar, O. The Role of Ion Dissociation Dynamics in the Study of Ion and Neutral Thermochemistry. In *Energetics of Stable Molecules and Reactive Intermediates*; Minas da Piedade, M. E., Ed.; Kluwer Academic: Dordrecht, 1999; pp 303−322.
(201) Lifshitz, C.; Gotkis, Y.; Laskin, J.; Ioffe, A.; Shaik, S. Threshold Formation of Benzylium ($Bz^+$) and Tropylium ($Tr^+$) from Toluene. Nonstatistical Behavior in Franck−Condon Gaps. *J. Phys. Chem.* **1993**, *97*, 12291−12295.
(202) McCulloh, K. E. Energetics and Mechanisms of Fragment Ion Formation in the Photoionization of Normal and Deuterated Water and Ammonia. *Int. J. Mass Spectrom. Ion Phys.* **1976**, *21*, 333−342.
(203) Berkowitz, J. Photoion-Pair Formation. In *VUV and Soft X-ray Photoionization*; Becker, U., Shirley, D. A., Eds.; Plenum: New York, 1996; pp 263−289.
(204) Ng, C. Y. Photoionization, Photoelectron and Photodissociation Studies: Combining Theory and Experiment. In *The Structure, Energetics and Dynamics of Organic Ions*; Baer, T., Ng, C. Y., Powis, I., Eds.; John Wiley & Sons: Chichester, 1996; pp 35−124.
(205) Rühl, E.; Rockland, U.; Baumgärtel, H.; Lösking, O.; Binnewies, M.; Willner, H. Photoionization Mass Spectrometry of Chlorine Oxides. *Int. J. Mass Spectrom* **1999**, *185/186/187*, 545−558.
(206) Thorn, R. P., Jr.; Monks, P. S.; Stief, L. J.; Kuo, S.-C.; Zhang, Z.; Ross, S. K.; Klemm, R. B. Photoionization-Efficiency Spectrum and Ionization Energy of the Cyanomethyl Radical $CH_2CN$ and Products of the $N(^4S) + C_2H_3$ Reaction. *J. Phys. Chem. A* **1998**, *102*, 846−851.
(207) Litorja, M.; Ruscic, B. A Photoionization Study of the Hydroperoxyl Radical, $HO_2$, and Hydrogen Peroxide. *J. Electron Spectrosc. Relat. Phenom.* **1998**, *97*, 131−146.
(208) Blondel, C. Recent Experimental Achievements with Negative Ions. *Phys. Scr.* **1995**, *T58*, 31−42.
(209) Valli, C.; Blondel, C.; Delsart, C. Measuring Electron Affinities with the Photodetachment Microscope. *Phys. Rev. A* **1999**, *59*, 3809−3815.
(210) Yokoyama, K.; Leach, G. W.; Kim, J. B.; Lineberger, W. C.; Boldyrev, A. I.; Gutowski, M. Autodetachment Spectroscopy and Dynamics of Vibrationally Excited Dipole-Bound States of $H_2CCC^-$. *J. Chem. Phys.* **1996**, *105*, 10706−10718.
(211) Drzaic, P. S.; Marks, J.; Brauman, J. I. Electron Photodetachment from Gas-Phase Molecular Anions. In *Gas-Phase Ion Chemistry: Ions and Light*; Bowers, M. T., Ed.; Academic: Orlando, 1984; Vol. 3, pp 167−211.
(212) Römer, B.; Janaway, G. A.; Brauman, J. I. Cyclopentadienyl, Indenyl, and Fluorenyl Anions: Gas-Phase and Solvation Energy

Contributions to Electron Detachment Energies. *J. Am. Chem. Soc.* **1997**, *119*, 2249−2254.
(213) Berkowitz, J.; Rühl, E.; Baumgärtel, H. Valence Ionization Processes in the VUV Region. In *VUV and Soft X-ray Photoionization*; Becker, U., Shirley, D. A., Eds.; Plenum: New York, 1996; pp 221−261.
(214) Litorja, M.; Ruscic, B. Direct Observation of the Ionization Threshold of Triplet Methylene by Photoionization Mass Spectrometry. *J. Chem. Phys.* **1998**, *108*, 6748−6755.
(215) Ruscic, B.; Litorja, M.; Asher, R. L. Ionization Energy of Methylene Revisited: Improved Values of the Enthalpy of Formation of $CH_2$ and the Bond Dissociation Energy of $CH_3$ via Simultaneous Solution of the Local Thermochemical Network. *J. Phys. Chem. A* **1999**, *103*, 8625−8633. Erratum. *J. Phys. Chem. A* **2000**, *104*, 8600.
(216) Asher, R. L.; Ruscic, B. On the Heats of Formation of Trifluoromethyl Radical $CF_3$ and Its Cation $CF_3^+$. *J. Chem. Phys.* **1997**, *106*, 210−221.
(217) Irikura, K. K. The Ionization Energy of $CF_3$: When Does Entropy Matter in Gas-Phase Reactions? *J. Am. Chem. Soc.* **1999**, *121*, 7689−7695.
(218) Gotkis, I.; Lifshitz, C. Time-Dependent Mass Spectra and Breakdown Graphs. 16−The Methylnaphthalenes. *Org. Mass Spectrom.* **1993**, *28*, 372−377.
(219) Ervin, K. M.; Lineberger, W. C. Photoelectron Spectroscopy of Molecular Anions. In *Advances in Gas-Phase Ion Chemistry*; Adams, N. G., Babcock, L. M., Eds.; JAI: Greenwich, CT, 1992; Vol. 1, pp 121−166.
(220) Wenthold, P. G.; Squires, R. R. Bond Dissociation Energies of $F_2^-$ and $HF_2^-$. A Gas−Phase Experimental and $G_2$ Theoretical Study. *J. Phys. Chem.* **1995**, *99*, 2002−2005.
(221) Ho, J.; Ervin, K. M.; Lineberger, W. C. Photoelectron Spectroscopy of Metal Cluster Anions: $Cu_n^-$, $Ag_n^-$ and $Au_n^-$. *J. Chem. Phys.* **1990**, *93*, 6987−7002.
(222) Tiggesbäumeker, J.; Köller, L.; Meiwes-Broer, K.-H. Bound-Free Collective Electron Excitations in Negatively Charged Silver Clusters. *Chem. Phys. Lett.* **1996**, *260*, 428−432.
(223) Wang, L.-S.; Wu, H.; Cheng, H. Photoelectron Spectroscopy of Small Chromium Clusters: Observation of Even−Odd Alternations and Theoretical Interpretation. *Phys. Rev. B* **1997**, *55*, 12884−12887.
(224) Han, S. Y.; Song, J. K.; Kim, J., Hyun; Oh, H. B.; Kim, S. K. Photoelectron Spectroscopy of Pyridine Cluster Anions, $(Py)_n^-$ ($n$ = 4−13). *J. Chem. Phys.* **1999**, *111*, 4041−4050.
(225) Wenthold, P.; Lineberger, W. C. Negative Ion Photoelectron Spectroscopy Studies of Organic Reactive Intermediates. *Acc. Chem. Res.* **1999**, *32*, 597−603.
(226) Shiedt, J.; Weinkau, R. Spin−Orbit Coupling in the $O_2^-$ Anion. *Z. Naturforsch. A* **1995**, *50*, 1041−1044.
(227) Schiedt, J.; Weinkauf, R. Photodetachment Photoelectron Spectroscopy of Mass Selected Anions: Anthracene and the Anthracene−$H_2O$ Cluster. *Chem. Phys. Lett.* **1997**, *266*, 201−205.
(228) Ervin, K. M.; Ho, J.; Lineberger, W. C. Ultraviolet Photoelectron Spectrum of $NO_2^-$. *J. Phys. Chem.* **1988**, *92*, 5405−5412.
(229) Desfançois, C.; Périquet, V.; Lyapustina, S. A.; Lippa, T. P.; Robinson, D. W.; Bowen, K. H.; Nonaka, H.; Compton, R. N. Electron Binding to Valence and Multipole States of Molecules: Nitrobenzene, para- and meta-Dinitrobenzenes. *J. Chem. Phys.* **1999**, *111*, 4569−4576.
(230) Klopcic, S. A.; Moravec, V. D.; Jarrold, C. C. Anion Photoelectron Spectroscopy of $PdCO^-$ and PdCN: Reactivity of $Pd^-$. *J. Chem. Phys.* **1999**, *110*, 8986−8991.
(231) Duncan, M. A.; Knight, A. M.; Negishi, Y.; Nagao, S.; Nakamura, Y.; Kato, A.; Nakjima, A.; Kaya, K. Production of Jet-Cooled Coronene and Coronene Cluster Anions and Their Study with Photoelectron Spectroscopy. *Chem. Phys. Lett.* **1999**, *309*, 49−54.
(232) Arnold, C. C.; Neumark, D. M. Study of Small Carbon and Silicon Clusters Using Negative Ion Photodetachment Techniques. In *Advances in Metal and Semiconductor Clusters*; Duncan, M. A., Ed.; JAI: Greenwich, CT, 1995; Vol. 3, pp 113−148.
(233) Marcy, T. P.; Leopold, D. G. A Vibrationally Resolved Negative Ion Photoelectron Spectrum of $Nb_8$. *Int. J. Mass Spectrom.* **2000**, *195/196*, 653−666.
(234) Luder, C.; Meiwes-Broer, K. H. Electron Detachment Energies of $Pb_N^-$ ($N$ = 24−204). *Chem. Phys. Lett.* **1998**, *294*, 391−396.
(235) Kietzmann, H.; Morenzin, J.; Bechthold, P. S.; Ganteför, G.; Eberhardt, W. Photoelectron Spectra of $Nb_n^-$ Clusters: Correlation Between Electronic Structure and Hydrogen Chemisorption. *J. Chem. Phys.* **1998**, *109*, 2275−2278.
(236) Sarkas, H. W.; Arnold, S. T.; Hendricks, J. H.; Bowen, K. H. Photoelectron Spectroscopy of Alkali Metal Tetramer Anions: The Anomalous Spectrum of $Li_4^-$. *J. Chem. Phys.* **1995**, *102*, 2653−2656.
(237) Wang, L.-S.; Wu, H. Probing the Electronic Structures of Transition Metal Clusters from the Molecular to Bulk-Like Using Photoelectron Spectroscopy. In *Advances in Metal and Semiconductor Clusters*; Michael A. Duncan, Ed.; JAI: Greenwich, CT, 1998; Vol. 4, pp 299−343.
(238) Bengali, A. A.; Casey, S. M.; Cheng, C.-L.; Dick, J. P.; Fenn, P. T.; Villalta, P. W.; Leopold, D. G. Negative Ion Photoelectron Spectroscopy of Coordinatively Unsaturated Group VI Metal Carbonyls: $Cr(CO)_3$, $Mo(CO)_3$, and $W(CO)_3$. *J. Am. Chem. Soc.* **1992**, *114*, 5257−5268.
(239) Xu, C.; Burton, G. R.; Taylor, T. R.; Neumark, D. M. Photoelectron Spectroscopy of $C_4^-$, $C_6^-$, and $C_8^-$. *J. Chem. Phys.* **1997**, *107*, 3428−3436.
(240) Casey, S. M.; Leopold, D. G. Negative Ion Photoelectron Spectroscopy of $Cr_2H$ and $Cr_2D$. *Chem. Phys. Lett.* **1993**, *201*, 205−211.
(241) Davico, G. E.; Schwartz, R. L.; Ramond, T. M.; Lineberger, W. C. Photoelectron Spectroscopy of Benzoquinonide and Dehydrobenzoquinone Anions. *J. Am. Chem. Soc.* **1999**, *121*, 6047−6054.
(242) Ervin, K. M.; Gronert, S.; Barlow, S. E.; Gilles, M. K.; Harrison, A. G.; Bierbaum, V. M.; DePuy, C. H.; Lineberger, W. C.; Ellison, G. B. Bond Strengths of Ethylene and Acetylene. *J. Am. Chem. Soc.* **1990**, *112*, 5750−5759.
(243) Clifford, E. P.; Wenthold, P. G.; Gareyev, R.; Lineberger, W. C.; DePuy, C. H.; Bierbaum, V. M.; Ellison, G. B. Photoelectron Spectroscopy, Gas-Phase Acidity, and Thermochemistry of *tert*-Butyl Hydroperoxide: Mechanisms for the Rearrangement of Peroxyl Radicals. *J. Chem. Phys.* **1998**, *109*, 10293−10310.
(244) Wenthold, P. G.; Squires, R. R.; Lineberger, W. C. Ultraviolet Photoelectron Spectroscopy of the *o*-, *m*-, and *p*-Benzyne Negative Ions. Electron Affinities and Singlet−Triplet Splittings for *o*-, *m*-, and *p*-Benzyne. *J. Am. Chem. Soc.* **1998**, *120*, 5279−5290.
(245) Compton, R. N.; Carman, H. S., Jr.; Desfrancois, C.; Abdoul-Carmine, H.; Schermann, J. P.; Hendricks, J. H.; Lyapustina, S. A.; Bowen, K. H. On the Binding of Electrons to Nitromethane: Dipole and Valence Bound Anions. *J. Chem. Phys.* **1996**, *105*, 3472−3478.
(246) Hendricks, J. H.; de Clercq, H. L.; Lyapustina, S. A.; Fancher, C. A.; Lippa, T. P.; Collins, J. M.; Arnold, S. T.; Lee, G. H.; Bowen, K. H. Photoelectron Spectroscopy of Small Cluster Anions: Dipole Bound, Ground-State Systems. *Front. Sci. Ser.* **1996**, *16 (Structures and Dynamics of Clusters)*, 321−328.
(247) Wang, L.-S.; Wang, X.-B. Probing Free Multiply Charged Anions Using Photodetachment Photoelectron Spectroscopy. *J. Phys. Chem. A* **2000**, *104*, 1978−1990.
(248) Haberland, H.; Bowen, K. H. Solvated Electron Clusters. In *Clusters of Atoms and Molecules II*; Haberland, H., Ed.; Springer: Berlin, 1994; pp 134−153.
(249) Lyapustina, S.; Xu, S.; Nilles, J. M.; Bowen, K. H., Jr. Solvent-Induced Stabilization of the Naphthalene Anion by Water Molecules: A Negative Cluster Ion Photoelectron Spectroscopic Study. *J. Chem. Phys.* **2000**, *112*, 6643−6648.
(250) Burrow, P. D.; Michejda, J. A.; Jordan, K. D. Electron Transmission Study of the Temporary Negative Ion States of Selected Benzenoid and Conjugated Aromatic Hydrocarbons. *J. Chem. Phys.* **1987**, *86*, 9−24.
(251) Heinis, T.; Chowdhury, S.; Kebarle, P. Electron Affinities of Naphthalene, Anthracene and Substituted Naphthalenes and Anthracenes, *Org. Mass Spectrom.* **1993**, *28*, 358.
(252) Zanni, M. T.; Taylor, T. R.; Greenblatt, B. J.; Soep, B.; Neumark, D. M. Characterization of the $I_2^-$ Anion Ground State Using Conventional and Femtosecond Photoelectron Spectroscopy. *J. Chem. Phys.* **1997**, *107*, 7613−7619.
(253) Turner, D. W.; Baker, C.; Baker, A. D.; Brundle, C. R. *Molecular Photoelectron Spectroscopy*; Wiley-Interscience: New York, 1970.
(254) Lichtenberger, D. L.; Kellogg, G. E. Experimental Quantum Chemistry: Photoelectron Spectroscopy of Organotransition-Metal Complexes. *Acc. Chem. Res.* **1987**, *20*, 379−387.
(255) Tomoda, S.; Kimura, K. Proton Transfer in Ionic States of Hydrogen-Bonded Dimers. A Photoelectron Spectroscopic Approach. In *Vacuum Ultraviolet Photoionization and Photodissociation of Molecules and Clusters*; Ng, C. Y., Ed.; World Scientific: Singapore, 1991; pp 101−168.
(256) Chen, P. Photoelectron Spectroscopy of Reactive Intermediates. In *Unimolecular and Bimolecular Reactions Dynamics*; Ng, C.-Y., Baer, T., Powis, I., Eds.; John Wiley & Sons: Chichester, 1994; pp 371−425.
(257) Logan, C., F.; Ma, J. C.; Chen, P. The Photoelectron Spectrum of the α,3-Dehydrotoluene Biradical. *J. Am. Chem. Soc.* **1994**, *116*, 2137−2138.
(258) West, J. B.; Dyke, J. M.; Morris, A.; Wright, T. G.; Gamblin, S. D. Photoelectron Spectroscopy of Short-Lived Molecules Using Synchrotron Radiation. *J. Phys. B: At., Mol. Opt. Phys.* **1999**, *32*, 2763−2782.
(259) Zhu, Z.; Ge, M.; Qiao, C.; Sun, Z.; Wang, D. A He I Photoelectron Spectrum of the $(CH_3CH_2CH_2)_2N$ Radical. *Chem. Phys. Lett.* **2000**, *319*, 85−88.
(260) Yencha, A. J.; Cormack, A. J.; Donovan, R. J.; Lawley, K. P.; Hopkirk, A.; King, G. C. Threshold Photoelectron Spectroscopy of HBr and DBr. *Chem. Phys.* **1998**, *238*, 133−151.
(261) Güthe, F.; Locht, R.; Leyh, B.; Baumgärtel, H.; Weitzel, K.-M. Kinetic Energy Release Distributions in the Dissociation of

Energy-Selected Fluoroethene and 1,1-Difluoroethene Ions. *J. Phys. Chem. A* **1999**, *103*, 8404−8412.
(262) Lafleur, R. D.; Szátary, B.; Baer, T. A Photoelectron-Photoion Coincidence Study of $ICH_2CN$ Ion Dissociation: Thermochemistry of $\cdot CH_2CN$, $^+CH_2CN$, and $ICH_2CN$. *J. Phys. Chem. A.* **2000**, *104*, 1450−1455.
(263) Zhu, L.; Johnson, P. Mass Analyzed Threshold Ionization Spectroscopy. *J. Chem. Phys.* **1991**, *94*, 5769−5771.
(264) Neuhauser, R. G.; Siglow, K.; Neusser, H. J. High *n* Rydberg Spectroscopy of Benzene: Dynamics, Ionization Energy and Rotational Constants of the Cation. *J. Chem. Phys.* **1997**, *106*, 896−907.
(265) Neusser, H. J.; Drause, H. Decay Energetics of Molecular Clusters Studied by Multiphoton Mass Spectrometry and Pulsed Field Threshold Ionization. *Int. J. Mass Spectrom.* **1994**, *131*, 211−232.
(266) Blush, J. A.; Chen, P.; Wiedmann, R. T.; White, M. G. Rotationally Resolved Threshold Photoelectron Spectrum of the Methyl Radical. *J. Chem. Phys.* **1993**, *98*, 3557−3559.
(267) Baer, T.; Song, Y.; Ng, C. Y.; Liu, J.; Chen, W. The Heat of Formation of 2-$C_3H_7^+$ and Proton Affinity of $C_3H_6$ Determined by Pulsed Field Ionization−Photoelectron Photoion Coincidence Spectroscopy. *J. Phys. Chem. A* **2000**, *104*, 1959−1964.
(268) Kitsopoulos, T. N.; Waller, I. M.; Loeser, J. G.; Neumark, D. M. High Resolution Threshold Photodetachment Spectroscopy of Negative Ions. *Chem. Phys. Lett.* **1989**, *159*, 300−308.
(269) Gantefor, G. F.; Cox, D. M.; Kaldor, A. Zero Electron Kinetic Energy Spectroscopy of $Au_6^-$. *J. Chem. Phys.* **1992**, *96*, 4102−4105.
(270) Burton, G. R.; Xu, C.; Arnold, C. C.; Neumark, D. M. Photoelectron Spectroscopy and Zero Electron Kinetic Energy Spectroscopy of Germanium Cluster Ions. *J. Chem. Phys.* **1996**, *104*, 2757−2764.
(271) Drechsler, G.; Boesl, U.; Bässmann, C.; Schlag, E. W. Mass Selected Anion-Zero Kinetic Energy Photoelectron Spectroscopy (Anion-ZEKE): Ground and Low Excited States of FeO. *J. Chem. Phys.* **1997**, *107*, 2284−2291.
(272) Ruscic, B.; Berkowitz, J. Photoion-Pair Formation and Photoelectron-Induced Dissociative Attachment in $C_2H_2$: $D_0$(HCC−H). *J. Chem. Phys.* **1990**, *93*, 5586−5593.
(273) Ervin, K. M.; Lineberger, W. C. Photoelectron Spectra of $C_2^-$ and $C_2H^-$. *J. Phys. Chem.* **1991**, *95*, 1167−1177.
(274) Martin, J. D. D.; Hepburn, J. W. Electric Field Induced Dissociation of Molecules in Rydberg-Like Highly Vibrationally Excited Ion-Pair States. *Phys. Rev. Lett.* **1997**, *79*, 3154−3157.
(275) Martin, J. D. D.; Hepburn, J. W. Determination of Bond Dissociation Energies by Threshold Ion-Pair Production Spectroscopy: An Improved $D_0$(HCl). *J. Chem. Phys.* **1998**, *109*, 8139−8142.
(276) Martin, J. D. D. Experimental Investigations of Negative Ion Collisions: Electron Detachment and Ion−Molecule Collisions. Ph.D. Dissertation. University of Waterloo, Waterloo, Ontario, 1998.
(277) Berkowitz, J.; Chupka, W. A.; Walker, T. A. Photoionization of HCN: The Electron Affinity and Heat of Formation of CN. *J. Chem. Phys.* **1967**, *50*, 1497−1500.
(278) Berkowitz, J.; Mayhew, C. A.; Ruscic, B. Photoion-Pair Formation in $Cl_2$. *Chem. Phys.* **1988**, *123*, 317−328.
(279) Pratt, S. T.; McCormack, E. F.; Dehmer, J. L.; Dehmer, P. M. Field-Induced Ion-Pair Formation in Molecular Hydrogen. *Phys. Rev. Lett.* **1992**, *68*, 584−587.
(280) Yencha, A. J.; Kela, D. K.; Donovan, R. J.; Hopkirk, A.; Kavaran, A. Ion-Pair ($Br^+ + Br^-$) Formation from Photodissociation of $Br_2$ Near the First Ionisation Limit. *Chem. Phys. Lett.* **1990**, *165*, 283−288.
(281) Kavaran, A.; Yencha, A. J.; Kela, D. K.; Donovan, R. J.; Hopkirk, A. Vibrationally Resolved Excitation Functions for Direct Ion-Pair ($I^+ + I^-$) Formation from Photodissociation of $I_2$. *Chem. Phys. Lett.* **1991**, *170*, 263−267.
(282) Oertel, H.; Schenk, H.; Baumgärtel, H. Ion Pair Formation from Photon Irradiation of $O_2$, NO, and CO. *Chem. Phys.* **1988**, *46*, 251−262.
(283) Zemke, W. T.; Stwalley, W. C.; Coxon, J. A.; Hijigeorgiou, P. G. Improved Potential Energy Curves and Dissociation Energies for HF, DF, and TF. *Chem. Phys. Lett.* **1991**, *177*, 412−418.
(284) Neumark, D. M.; Lykke, K. R.; Andersen, T.; Lineberger, W. C. Laser Photodetachment Measurement of the Electron Affinity of Atomic Oxygen. *Phys. Rev. A* **1985**, *32*, 1890−1892.
(285) Berzinsh, U.; Gustafsson, M.; Hanstorp, D.; Klinkmüller, A.; Ljungblad, U.; Mårtensson-Pendrill, A.-M. Isotope Shift in the Electron Affinity of Chlorine. *Phys. Rev. A* **1995**, *51*, 231−238.
(286) Bradforth, S.; Kim, E.; Arnold, D.; Neumark, D. Photoelectron Spectroscopy of $CN^-$, $NCO^-$, and $NCS^-$. *J. Chem. Phys.* **1993**, *98*, 800−810.
(287) Larson, D. J.; Edge, C. J.; Elmquist, R. E.; Mansour, N. B.; Trainham, R. Physics with Negative Ions in Traps. *Phys. Scr. T* **1988**, *22*, 183−190.
(288) Breyer, F.; Frey, P.; Hotop, H. High-Resolution Photoelectron Spectrometry of Negative Ions: Rotational Transitions in Laser-Photodetachment of $OH^-$, $SH^-$, and $SD^-$. *Z. Phys. A* **1981**, *300*, 7.
(289) Hildenbrand, D. L. Electron Impact Ionization Energies. *Int. J. Mass Spectrom.* **2000**, *197*, 237−242.
(290) Holmes, J. L.; Lossing, F. P. Heats of Formation of Organic Radicals from Appearance Energies. *Int. J. Mass Spectrom. Ion Processes* **1984**, *58*, 113−120.
(291) Holmes, J. L. The Present State and Utility of Ion Thermochemistry. *Int. J. Mass Spectrom. Ion Processes* **1992**, *118−119*, 381−394.
(292) Holmes, J. L.; Lossing, F. P.; Mayer, P. M. Heats of Formation of Oxygen-Containing Organic Free Radicals from Appearance Energy Measurements. *J. Am. Chem. Soc.* **1991**, *113*, 9723−9728.
(293) Aubry, C.; Holmes, J. L.; Terlouw, J. K. Effect of Methyl Substitution on the Thermochemistry of Ketene. *J. Phys. Chem. A* **1997**, *101*, 5958−5961.
(294) Davister, M.; Locht, M. The Dissociative Electron Ionization of $C_2H_2$, $C_2D_2$ and $C_2HD$. Investigation of the $[C_2H(D)]^+$ and $[H(D)]^+$ Dissociation Channels and the (D)H−$C_2$H(D) Binding Energy. *Chem. Phys.* **1994**, *189*, 805−824.
(295) Davister, M.; Locht, R. The Dissociative Ionization of $C_2H_2$ and $C_2D_2$. The $[CH(CD)]^+$ Dissociation Channel. The H(D)C≡C(D)H Binding Energy. *Chem. Phys.* **1995**, *191*, 333−346.
(296) Locht, R.; Servais, C. How Complex Can Be the Unimolecular Decomposition of a Simple Molecule? The Case of Acetylene. An Electron Impact and PIPECO Investigation. *Z. Phys. Chem. (Munich)* **1996**, *195*, 153−179.
(297) Laskin, J.; Hadas, B.; Märk, T. D.; Lifshitz, C. New Evidence in Favor of a High (10 eV) $C_2$ Binding Energy in $C_{60}$. *Int. J. Mass Spectrom.* **1998**, *177*, L9-L13.
(298) Lifshitz, C. $C_2$ Binding Energy in $C_{60}$. *Int. J. Mass Spectrom.* **2000**, *198*, 1−14.
(299) Berkowitz, J. Sum Rules and the Photoabsorption Cross Sections of $C_{60}$. *J. Chem. Phys.* **1999**, *111*, 1446−1453.
(300) Afzaaol, S.; Freiser, B. S. Gas-Phase Photodissociation Study of $Ag(Benzene)^+$ and $Ag(Toluene)^+$. *Chem. Phys. Lett.* **1994**, *218*, 254−260.
(301) Hayes, T.; Bellert, D.; Buthelezi, T.; Brucat, P. J. The Photodissociation of $V^+(CH_4)$. *Chem. Phys. Lett.* **1997**, *164*, 220−224.
(302) Russon, L. M.; Heidecke, S. A.; Birke, M. K.; Conceicao, J.; Morse, M. D.; Armentrout, P. B. Photodissociation Measurements of Bond Dissociation Energies: $Ti_2^+$, $V_2^+$, $Co_2^+$, and $Co_3^+$. *J. Chem. Phys.* **1994**, *100*, 4747−4755.
(303) Husband, J.; Aguirre, F.; Ferguson, P.; Metz, R. B. Vibrationally Resolved Photofragment Spectroscopy of $FeO^+$. *J. Chem. Phys.* **1999**, *111*, 1433−1437.
(304) Husband, J.; Aguirre, F.; Thompson, C. J.; Laperle, C. M.; Metz, R. B. Photofragment Spectroscopy of $FeCH_2^+$, $CoCH_2^+$, and $NiCH_2^+$ Near the $M^+$-$CH_2$ Dissociation Threshold. *J. Phys. Chem. A* **2000**, *104*, 2020−2025.
(305) Aguirre, F.; Husband, J.; Thompson, C. J.; Metz, R. Gas-Phase Photodissociation of $AuCH_2^+$: The Dissociation Threshold of Jet-Cooled and Rotationally Thermalized Ions. *Chem. Phys. Lett.* **2000**, *318*, 466−470.
(306) Lian, L.; Su, C.-X.; Armentrout, P. B. Collision-Induced Dissociation of $Ti_n^+$ ($n$ = 2−22) with Xe: Bond Energies, Geometric Structures, and Dissociation Pathways. *J. Chem. Phys.* **1992**, *97*, 4084−4093.
(307) Su, C.-X.; Hales, D. A.; Armentrout, P. B. Collision-Induced Dissociation of $V_n^+$ ($n$ = 2−20) with Xe: Bond Energies, Dissociation Pathways, and Structures. *J. Chem. Phys.* **1993**, *99*, 6613−6623.
(308) Hales, D. A.; Armentrout, P. B. Effect of Internal Excitation of the Collision-Induced Dissociation and Reactivity of $Co_2^+$. *J. Cluster Sci.* **1990**, *1*, 127−142.
(309) Hales, D. A.; Su, C.-X.; Lian, L.; Armentrout, P. B. Collision-Induced Dissociation of $Co_n^+$ ($n$ = 2−18) with Xe: Bond Energies of Cationic and Neutral Cobalt Clusters, Dissociation Pathways, and Structures. *J. Chem. Phys.* **1994**, *100*, 1049−1057.
(310) Spain, E. M.; Morse, M. D. Bond Strengths of Transition Metal Dimers: TiV, $V_2$, TiCo, and VNi. *J. Phys. Chem.* **1992**, *96*, 2479−2486.
(311) Sherwood, C. R.; Hanold, K. A.; Garner, M. C.; Strong, K. M.; Continetti, R. E. Translational Spectroscopy Studies of the Photodissociation Dynamics of $O_4^-$. *J. Chem. Phys.* **1996**, *105*, 10803−10811.
(312) Osborn, D. L.; Leahy, D. J.; Cyr, D. R.; Neumark, D. M. Photodissociation Spectroscopy and Dynamics of the $N_2O_2^-$ Anion. *J. Chem. Phys.* **1996**, *104*, 5026−5039.
(313) Ding, L. N.; Kleiber, P. D.; Young, M. A.; Stwalley, W. C.; Lyyra, A. M. Photodissociation Spectroscopy of $Mg_2^+$. *Phys. Rev. A* **1993**, *48*, 2024−2030.
(314) Sowa Resat, M.; Zengin, V.; Garner, M. C.; Continetti, R. E. Dissociative Photodetachment Dynamics of Isomeric Forms of $N_3O_2^-$. *J. Phys. Chem. A* **1998**, *102*, 1719−1724.

(315) Continetti, R. E.; Cyr, D. R.; Metz, R. B.; Neumark, D. M. Fast Beam Studies of $N_3$ Photodissociation. *Chem. Phys. Lett.* **1991**, *182*, 406−411.
(316) Nicovich. J. M.; Dreutter, K. D.; van Dijk, C. A.; Wine, P. H. Temperature-Dependent Studies of the Reactions $Br(^2P_{3/2}) + H_2S \leftrightarrow SH + HBr$ and $Br(^2P_{3/2}) + CH_3SH \leftrightarrow CH_3S + HBr$. Heats of Formation of SH and $CH_3S$ Radicals. *J. Phys. Chem.* **1992**, *96*, 2518−2528.
(317) Continetti, R. E. Photoelectron-Photofragment Coincidence Studies of Dissociation Dynamics. *Int. Rev. Phys. Chem.* **1998**, *17*, 227−260.
(318) deTorchia, J. W.; Sullivan, K. O.; Sunderlin, L. S. Thermochemistry of $N_3O_2^-$. *J. Phys. Chem. A* **1999**, *103*, 11109−11114.
(319) Travers, M. J.; Cowles, D. C.; Ellison, G. B. Reinvestigation of the Electron Affinities of $O_2$ and NO. *Chem. Phys. Lett.* **1989**, *164*, 449−455.
(320) McMahon, T. B. Experimental Approaches to the Unimolecular Dissociation of Gaseous Cluster Ions. In *Advances in Gas-Phase Ion Chemistry*; Adams, N. B., Babcock, L. M., Eds.; JAI: Greenwich, CT, 1996; Vol. 2, pp 41−85.
(321) Huang, F.-S.; Dunbar, R. C. Time-Resolved Photodissociation of Toluene Ion. *Int. J. Mass Spectrom. Ion Processes* **1991**, *109*, 151−170.
(322) Ho, Y.-P.; Dunbar, R. C.; Lifshitz, C. C−H Bond Strength of Naphthalene Ion. A Reevaluation Using New Time-Resolved Photodissociation Results. *J. Am. Chem. Soc.* **1995**, *117*, 6504−6508.
(323) Ray, U.; Jarrold, M. F. Photodissociation Kinetics and Optical Spectroscopy of Metal Cluster Ions. In *Advances in Metal and Semiconductor Clusters*; Duncan, M. A., Ed.; JAI: Greenwich, CT, 1993; Vol. 1, pp 1−36.
(324) Hild, U.; Dietrich, G.; Krückeberg, S.; Lindinger, M.; Lückenkirchen, K.; Schweikhard, L.; Walther, C.; Ziegler, J. Time-Resolved Photofragmentation of Stored Silver Clusters $Ag_n^+$ ($n$ = 8−21). *Phys. Rev. A* **1998**, *57*, 2786−2793.
(325) Grebner, T. L.; Neusser. Dissociation Rates of Energy-Selected Benzene Cations: Comparison of Experimental Results from Ion Cyclotron Resonance and Cylindrical Ion Trap Time-of-Flight Mass Spectrometry. *Int. J. Mass Spectrom.* **1999**, *185/186/187*, 517−532.
(326) Kühlewind, H.; Kiermeier, A.; Neusser, H. J. Multiphoton Ionization in a Reflectron Time-of-Flight Mass Spectrometer: Individual Rates of Competing Dissociation Channels in Energy-Selected Benzene Cation. *J. Chem. Phys.* **1986**, *85*, 4427−4435.
(327) Klippenstein, S. J.; Faulk, J. D.; Dunbar, R. C. A Combined Theoretical and Experimental Study of the Dissociation of Benzene Cation. *J. Chem. Phys.* **1993**, *98*, 243−256.
(328) Ho, Y.-P.; Dunbar, R. C. Radiative Cooling Rate of 9-Cyanophenanthrene Ions by Time-Resolved Photodissociation Thermometry. *Int. J. Mass Spectrom. Ion Processes* **1996**, *154*, 133−144.
(329) Armentrout, P. B.; Hales, D. A.; Lian, L. Collision-Induced Dissociation of Transition-Metal Clusters. In *Advances in Metal and Semiconductor Clusters*; Duncan, M. A., Ed.; JAI: Greenwich, CT, 1994; Vol. 2, pp 1−39.
(330) Ervin, K. M.; Armentrout, P. B. Translational Energy Dependence of $Ar^+ + XY \rightarrow ArX^+ + Y$ (XY = $H_2$, $D_2$, HD) from Thermal to 30 eV c.m.. *J. Chem. Phys.* **1985**, *83*, 166−189.
(331) Hanley, L.; Ruatta, S. A.; Anderson, S. L. Collision-Induced Dissociation of Aluminum Cluster Ions: Fragmentation Patterns, Bond Energies, and Structures for $Al_2^+ - Al_7^+$. *J. Chem. Phys.* **1987**, *87*, 260−268.
(332) Basir, Y. J.; Christian, J. F.; Wan, Z.; Anderson, S. L. A Triple-Sector, Guided-Ion-Beam Mass Spectrometer for Cluster Ion and Fullerene Scattering. *Int. J. Mass Spectrom. Ion Processes* **1997**, *171*, 159−172.
(333) Williams, S.; Chiu, Y.-H.; Levandier, D. J.; Dressler, R. A. Deuterium Isotope Effects in Collision-Induced Dissociation and Photodissociation of the $(N_2O, H_2O)^+$ Cluster Ion. *J. Chem. Phys.* **1998**, *108*, 9383−9389.
(334) DeTuri, V. F.; Hintz, P. A.; Ervin, K. M. Translational Activation of the $S_N2$ Reactions $Cl^- + CH_3Cl$ ($CD_3Cl$) $\rightarrow$ $ClCH_3$ ($ClCD_3$) + $Cl^-$: Guided Ion Beam Study. *J. Phys. Chem. A* **1997**, *101*, 5969−5986.
(335) Do, K.; Klein, T. P.; Pommerening, C. A.; Sunderlin, L. S. A New Flowing Afterglow − Guided Ion Beam Tandem Mass Spectrometer. Applications to the Thermochemistry of Polyiodide Ions. *J. Am. Soc. Mass Spectrom.* **1997**, *8*, 688−696.
(336) Sublemontier, O.; Poisson, L.; Pradel, P.; Mestdagh, J. M.; Visticot, J. P. Tandem Time-of-Flight Experiment for Low Energy Collision Studies. *J. Am. Soc. Mass Spectrom.* **2000**, *11*, 160−166.
(337) Gerlich, D. Inhomogeneous RF Fields: A Versatile Tool for the Study of Processes with Slow Ions. *Adv. Chem. Phys.* **1992**, *82*, 1−176.
(338) Tosi, P. High-Resolution Measurements of Integral Cross Sections in Ion−Molecule Reactions from Low-Energy Crossed-Beam Experiments. *Chem. Rev.* **1992**, *92*, 1667−1684.
(339) Graul, S. T.; Squires, R. R. Gas-Phase Acidities Derived from Threshold Energies for Activated Reactions. *J. Am. Chem. Soc.* **1990**, *112*, 2517−2529.
(340) Klassen, J. S.; Kebarle, P. Collision-Induced Dissociation Threshold Energies of Protonated Glycine, Glycinamide, and Some Related Small Peptides and Peptide Amino Amides. *J. Am. Chem. Soc.* **1997**, *119*, 6552−6563.
(341) Magnera, T. F.; David, D. E.; Stulik, D.; Orth, R. G.; Jonkman, H. T.; Michl, J. Production of Hydrated Metal Ions by Fast Ion or Atom Beam Sputtering. Collision-Induced Dissociation and Successive Hydration Energies of Gaseous $Cu^+$ with 1−4 Water Molecules. *J. Am. Chem. Soc.* **1989**, *111*, 5036−5043.
(342) Forbes, R. A.; Lech, L.; Freiser, B. S. Study of Endothermic Reactions Involving Transition Metal Ions: The FTMS Analogy of the Ion Beam Experiment. *Int. J. Mass Spectrom. Ion Processes* **1987**, *77*, 107−121.
(343) Hop, C. E. C. A.; McMahon, T. B.; Willet, G. D. Determinations of Bond Dissociation Energies via Energy-Resolved Collision Induced Dissociation in a Fourier Transfrom Ion Cyclotron Resonance Spectrometer. *Int. J. Mass Spectrom. Ion Processes* **1990**, *101*, 191−208.
(344) Beyer, M.; Bondybey, V. E. Energy Resolved Measurement of Endothermic Reaction and Dissociation Thresholds: Fourier Transform Ion Cyclotron Resonance Mass Spectrometry Meets Guided Ion Beam. *Rapid Commun. Mass Spectrom.* **1997**, *11*, 1588−1591.
(345) Markin, E. M.; Sugawara, K. Energy-Resolved Collision-Induced Dissociation of $Fe_2(CO)_y^+$ ($y$ = 1−9). *J. Phys. Chem. A* **2000**, *104*, 1416−1422.
(346) Craig, S. L.; Brauman, J. I. Phase-Shifting Acceleration of Ions in an Ion Cyclotron Resonance Spectrometer: Kinetic Energy Distribution and Reaction Dynamics. *J. Phys. Chem. A* **1997**, *101*, 4745−4752.
(347) Sunderlin, L. S.; Wang, D.; Squires, R. R. Bond Strengths in First-Row-Metal Carbonyl Anions. *J. Am. Chem. Soc.* **1993**, *115*, 12060−12070.
(348) Aristov, N.; Armentrout, P. B. Collision-Induced Dissociation of Vanadium Monoxide Ion. *J. Phys. Chem.* **1986**, *90*, 5135−5140.
(349) Sievers, M. R.; Chen, Y.-M.; Armentrout, P. B. Metal Oxide and Carbide Thermochemistry of $Y^+$, $Zr^+$, $Nb^+$, and $Mo^+$. *J. Chem. Phys.* **1996**, *105*, 6322−6233.
(350) Spasov, V. A.; Lee, T.-H.; Maberry, J. P.; Ervin, K. M. Measurement of the Dissociation Energies of Anionic Silver Clusters ($Ag_n^-$, $n$ = 2−11) by Collision-Induced Dissociation. *J. Chem. Phys.* **1999**, *110*, 5208−5217.
(351) Schultz, R. H.; Armentrout, P. B. Reactions of $N_4^+$ with Rare Gases from Thermal to 10 eV Center-of-Mass Energy: Collision-Induced Dissociation, Charge Transfer and Ligand Exchange. *Int. J. Mass Spectrom. Ion Processes* **1991**, *107*, 29−48.
(352) Spasov, V. A.; Lee, T.-H.; Ervin, K. M. Threshold Collision-Induced Dissociation of Anionic Copper Clusters and Copper Cluster Monocarbonyls. *J. Chem. Phys.* **2000**, *112*, 1713−1720.
(353) Spasov, V. A.; Ervin, K. M. Binding Energies of Palladium Carbonyl Cluster Anions: Collision-Induced Dissociation of $Pd_3(CO)_n^-$ ($n$ = 0−6). *J. Chem. Phys.* **1998**, *109*, 5344−5350.
(354) Rodgers, M. T.; Armentrout, P. B. Absolute Binding Energies of Sodium Ions to Short Chain Alcohols, $C_nH_{2n+2}O$, $n$ = 1−4, Determined by Threshold Collision-Induced Dissociation Experiments and Ab Initio Theory. *J. Phys. Chem. A* **1999**, *103*, 4955−4963.
(355) Nizzi, K. E.; Pommerening, C. A.; Sunderlin, L. S. Gas-Phase Thermochemistry of Polyhalide Anions. *J. Phys. Chem. A* **1998**, *102*, 7674−7679.
(356) Wenthold, P. G.; Squires, R. R. Biradical Thermochemistry from Collision-Induced Dissociation Threshold Energy Measurements. Absolute Heats of Formation of ortho-, meta-, and para-Benzyne. *J. Am. Chem. Soc.* **1994**, *116*, 6401−6412.
(357) Ray, D.; Feller, D.; More, M. B.; Glendening, E. D.; Armentrout, P. B. Cation-Ether Complexes in the Gas Phase: Bond Dissociation Energies and Equilibrium Structures of $Li^+$(1,2-Dimethoxyethane)$_x$, $x$ = 1 and 2, and $Li^+$(12-Crown-4). *J. Phys. Chem.* **1996**, *100*, 16116−16125.
(358) More, M. B.; Ray, D.; Armentrout, P. B. Cation-Ether Complexes in the Gas Phase: Bond Dissociation Energies of $Na^+$ (Dimethyl Ether)$_x$, $x$ = 1−4; $Na^+$(1,2-Dimethoxyethane)$_x$, $x$ = 1−2; and $Na^+$(12-Crown-4). *J. Phys. Chem. A* **1997**, *101*, 831−839.
(359) More, M. B.; Ray, D.; Armentrout, P. B. Cation-Ether Complexes in the Gas Phase: Bond Dissociation Energies of $M^+$(Dimethyl Ether)$_x$, $x$ = 1=3, $M^+$(1,2-Dimethoxyethane)$_x$, $x$ = 1 and 2, and $M^+$(12-Crown-4) Where M = Rb and Cs. *J. Phys. Chem. A* **1997**, *101*, 7007−7017.
(360) More, M. B.; Ray, D.; Armentrout, P. B. Cation-Ether Complexes in the Gas Phase: Bond Dissociation Energies of $K^+$(Dimethyl Ether)$_x$, $x$ = 1−4; $K^+$(1,2-Dimethoxyethane)$_x$, $x$ = 1 and 2; and $K^+$(12-Crown-4). *J. Phys. Chem. A* **1997**, *101*, 4254−4262.
(361) Armentrout, P. B. Cation-Ether Complexes in the Gas Phase: Thermodynamic Insight Into Molecular Recognition. *Int. J. Mass Spectrom.* **1999**, *193*, 227−240.

(362) Shi, Y.; Ervin, K. M. Gas-Phase Acidity and C−H Bond Energy of Diacetylene. *Chem. Phys. Lett.* **2000**, *318*, 149−154.
(363) Pommerening, C. A.; Bachrach, S. M.; Sunderlin, L. S. Proton Affinity of $SO_3$. *J. Am. Soc. Mass Spectrom.* **1999**, *10*, 856−861.
(364) Pommerening, C. A.; Bachrach, S. M.; Sunderlin, L. S. Addition of Protonated Water to $SO_3$. *J. Phys. Chem. A* **1999**, *103*, 1214−1220.
(365) Taylor, T. R.; Xu, C.; Neumark, D. M. Photoelectron Spectra of the $C_{2n}H^-$ ($n = 1-4$) and $C_{2n}D^-$ ($n = 1-3$) Anions. *J. Chem. Phys.* **1998**, *108*, 10018−10026.
(366) McLuckey, S. A.; Goeringer, D. E. Slow Heating Methods in Tandem Mass Spectrometry. *J. Mass Spectrom.* **1997**, *32*, 461−474.
(367) Thorne, L. R.; Beauchamp, J. L. Infrared Photochemistry of Gas-Phase Ions. In *Gas-Phase Ion Chemistry*; Bowers, M. T., Ed.; Academic: Orlando, 1984; Vol. 3, pp 41−97.
(368) Surya, P. I.; Roth, L. M.; Ranatunga, D. R. A.; Freiser, B. S. Infrared Multiphoton Dissociation of Transition Metal Containing Ions: $MC_nH_{2n}^+$ (M = Fe, Co, Ni; $n = 2-5$). *J. Am. Chem. Soc.* **1996**, *118*, 1118−1125.
(369) Dunbar, R. C.; McMahon, T. B. Activation of Unimolecular Reactions by Ambient Blackbody Radiation. *Science* **1998**, *279*, 194−197.
(370) Sena, M.; Riveros, J. Thermal Dissociation of Acetophenone Molecular Ions Activated by Infrared Radiation. *J. Phys. Chem. A* **1997**, *101*, 4384−4391.
(371) Riveros, J.; Sena, M.; Guedes, G.; Xavier, L. A.; Slepetys, R. F. Recent Advances in the Energetics and Mechanisms of Gas-Phase Ionic Reactions, *Pure Appl. Chem.* **1998**, *70*, 1969−1976.
(372) Price, W. D.; Schnier, P. D.; Jockusch, R. A.; Strittmatter, E. F.; Williams, E. R. Unimolecular Reaction Kinetics in the High-Pressure Limit Without Collisions. *J. Am. Chem. Soc.* **1996**, *118*, 10640−10644.
(373) Strittmatter, E. F.; Schnier, P. D.; Kassen, J. S.; Williams, E. R. Dissociation Energies of Deoxyribose Nucleotide Dimer Anions Measured Using Blackbody Infrared Radiative Dissociation. *J. Am. Soc. Mass Spectrom.* **1999**, *10*, 1095−1104.
(374) Krückberger, S.; Dietrich, L.; Lützenkirchen, K.; Schweikhard, L.; Walther, C.; Ziegler, J. Multiple-Collision Induced Dissociation of Trapped Silver Clusters $Ag_n^+$ ($n = 2-25$). *J. Chem. Phys.* **1999**, *110*, 7216−7227.
(375) Price, W. D.; Williams, E. R. Activation of Peptide Ions by Blackbody Radiation: Factors That Lead to Dissociation Kinetics in the Rapid Energy Exchange Limit. *J. Phys. Chem. A* **1997**, *101*, 8844−8852.
(376) Uechi, G. T.; Dunbar, R. C. Thermometric Study of $CO_2$ Laser Heating and Radiative Cooling of *n*-Butylbenzene Ions. *J. Chem. Phys.* **1993**, *98*, 7888−7897.
(377) Laskin, J.; Byrd, M., Futrell, J. Internal Energy Distributions Resulting from Sustained Off-Resonance Excitation in FTMS. I. Fragmentation of the Bromobenzene Radical Cation. *Int. J. Mass Spectrom.* **2000**, *195/196*, 285−302.
(378) Fujiwara, M.; Yasuhide, N. Simulation for Internal Energy Deposition in Sustained Off-Resonance Irradiation Collisional Activation Using a Monte Carlo Method. *Rapid Commun. Mass Spectrom.* **1999**, *13*, 1633−1638.
(379) Cancilla, M. T.; Wong, A. W.; Voss, L. R.; Lebrilla, C. B. Fragmentation Reactions in the Mass Spectrometry Analysis of Neutral Oligasaccharides, *Anal. Chem.* **1999**, *71*, 3206−3218.
(380) Katritzky, A. R.; Shipkova, P. A.; Qi, M.; Nichols, D. A.; Burton, R. D.; Watson, C. H.; Eyler, J. R.; Tamm, T.; Karelson, M.; Zerner, M. C. Study of Radical Merostabilization by Electrospray FTICR/MS. *J. Am. Chem. Soc.* **1996**, *118*, 11905−11911.
(381) Gauthier, J. W.; Trautman, T. R.; Jacobson, D. B. Sustained Off-Resonance Irradiation for Collision Activated Dissociation Involving Fourier Transform Mass Spectrometry. Collision-Activated Dissociation Technique That Emulates Infrared Multiphoton Dissociation. *Anal. Chim. Acta* **1991**, *246*, 211−225.
(382) McLuckey, S. A.; Cameron, D.; Cooks, R. G. Proton Affinities from Dissociations of Proton-Bound Dimers. *J. Am. Chem. Soc.* **1981**, *103*, 1313−1317.
(383) Cooks, R. G.; Patrick, J. S.; Kotiaho, T.; McLuckey, S. A. Thermochemical Determinations by the Kinetic Method. *Mass Spectrom. Rev.* **1994**, *13*, 287−339.
(384) Cooks, R. G.; Wong, P. S. H. Kinetic Method of Making Thermochemical Determinations: Advances and Applications. *Acc. Chem. Res.* **1998**, *31*, 379−386.
(385) Cooks, R. G.; Koskinen, J. T.; Thomas, P. D. The Kinetic Method of Making Thermochemical Determinations. *J. Mass Spectrom.* **1999**, *34*, 85−92.
(386) Drahos, L.; Vékey, K. How Closely Related Are the Effective and the Real Temperature? *J. Mass Spectrom.* **1999**, *34*, 79−84.
(387) Chen, G.; Cooks, R. G.; Bunk, D. M.; Welch, M. J.; Christie, J. R. Partitioning of Kinetic Energy to Internal Energy in the Low Energy Collision-Induced Dissociations of Proton-Bound Dimers of Polypeptides. *Int. J. Mass Spectrom.* **1999**, *185/186/187*, 75−90.
(388) Seburg, R. A.; Squires, R. R. The Electron Affinity of Cyclopropyl Radical Measured by the Kinetic Method. *Int. J. Mass Spectrom. Ion Processes* **1997**, *167/168*, 541−557.
(389) Holmes, J. L.; Aubry, C.; Mayer, P. M. Proton Affinities of Primary Alkanols: An Appraisal of the Kinetic Method. *J. Phys. Chem. A* **1999**, *103*, 705−709. Erratum, *ibid.*, **1999**, *103*, 6492.
(390) Strittmatter, E. F.; Wong, R. L.; Williams, E. R. Gas-Phase Basicity of $(CH_3)_3N^+-C_6H_4-COO^-$ Zwitterions: A New Class of Organic Superbases. *J. Am. Chem. Soc.* **2000**, *122*, 1247−1248.
(391) Craig, S. L.; Zhong, M.; Choo, B.; Brauman, J. I. Branching Ratios in Activated Systems. *J. Phys. Chem. A* **1997**, *101*, 19−24.
(392) Armentrout, P. B. Is the Kinetic Method a Thermodynamic Method? *J. Mass Spectrom.* **1999**, *34*, 74−78.
(393) Cao, J.; Holmes, J. L. Determining the Proton Affinities of Nitriles by the Kinetic Method. *Eur. Mass Spectrom.* **1999**, *5*, 19−22.
(394) Cao, J.; Holmes, J. L. The Proton Affinities of Amin-Alkanes. A Test Case for the Kinetic Method. *Int. J. Mass Spectrom.* **2000**, *195−196*, 525−532.
(395) Thomas, P. D.; Cooks, R. G.; Vékey, K.; Drahos, L. Comments on 'Proton Affinities of Primary Alkanols: An Appraisal of the Kinetic Method'. *J. Phys. Chem. A* **2000**, *104*, 1359−1361.
(396) Higgins, P. R.; Bartmess, J. E. The Gas-Phase Acidities of Long Chain Alcohols. *Int. J. Mass Spectrom. Ion Processes* **1998**, *175*, 71−79.
(397) Boand, G.; Houriet, R.; Gäumann, T. Gas-Phase Acidities of Aliphatic Alcohols. *J. Am. Chem. Soc.* **1983**, *105*, 2203−2206.
(398) Haas, M. J.; Harrison, A. G. The Fragmentation of Proton-Bound Cluster Ions and the Gas-Phase Acidities of Alcohols. *Int. J. Mass Spectrom. Ion Processes* **1993**, *124*, 115−124.
(399) Cheng, X.; Wu, Z.; Fenselau, C. Collision Energy Dependence of Proton-Bound Dimer Dissociation: Entropy Effects, Proton Affinities, and Intramolecular Hydrogen-Bonding in Protonated Peptides. *J. Am. Chem. Soc.* **1993**, *115*, 4844−4848.
(400) Wu, Z.; Fenselau, C. Gas-Phase Basicities and Proton Affinities of Lysine and Histidine Measured from the Dissociation of Proton-Bound Dimers. *Rapid Commun. Mass Spectrom.* **1994**, *8*, 777−780.
(401) Cerda, B. A.; Wesdemiotis, C. $Li^+$, $Na^+$, and $K^+$ Binding to the DNA and RNA Nucleobases. Bond Energies and Attachment Sites from the Dissociation of Metal Ion-Bound Heterodimers. *J. Am. Chem. Soc.* **1996**, *118*, 11884−11892.
(402) Cerda, B. A.; Hoyau, S.; Ohanessian, G.; Wesdemiotis, C. $Na^+$ Binding to Cyclic and Linear Dipeptides. Bond Energies, Entropies of $N^+$ Complexation, and Attachment Sites from the Dissociation of $Na^+$−Bound Heterodimers and Ab Initio Calculations. *J. Am. Chem. Soc.* **1998**, *120*, 2437−2448.
(403) Cerda, B. A.; Wesdemiotis, C. Gas-Phase Copper(I) Ion Affinities of Valine, Lysine, and Arginine Based on the Dissociation of $Cu^+$−Bound Heterodimers at Varying Internal Energies. *Int. J. Mass Spectrom.* **1999**, *185−187*.
(404) Nold, M. J.; Cerda, B. A.; Wesdemiotis, C. Proton Affinities of the N- and C−Terminal Segments Arising Upon the Dissociation of the Amide Bond in Protonated Peptides. *J. Am. Soc. Mass Spectrom.* **1999**, *10*, 1−8.
(405) Denault, J. W.; Chen, G.; Cooks, R. G. Electron Affinity of 1,3,5,7-Cyclooctatettraene Determined by the Kinetic Method. *J. Am. Soc. Mass Spectrom.* **1998**, *9*, 1141−1145.
(406) Armentrout, P. B. Entropy Measurements and the Kinetic Method: A Statistically Meaningful Approach. *J. Am. Soc. Mass Spectrom.* **2000**, *11*, 371−379.
(407) Wenthold, P. G. Determination of the Proton Affinities of Bromo- and Iodoacetonitrile Using the Kinetic Method with Full Entropy Analysis. *J. Am. Soc. Mass Spectrom.* **2000**, *11*, 601−605.
(408) Gidden, J.; van Koppen, P. A. M.; Bowers, M. T. Dehydrogenation of Ethene by $Ti^+$ and $V^+$: Excited-State Effects on the Mechanism for C−H Bond Activation from Kinetic Energy Release Distributions. *J. Am. Chem. Soc.* **1997**, *119*, 3935−3941.
(409) van Koppen, P. A. M.; Bowers, M. T.; Haynes, C. L.; Armentrout, P. B. Reactions of Ground-State $Ti^+$ and $V^+$ with Propane: Factors That Govern C−H and C−C Bond Cleavage Product Branching Ratios. *J. Am. Chem. Soc.* **1998**, *120*, 5704−5712.
(410) Urbain, P.; Leyh, B.; Remacle, F.; Lorquet, A. J.; Flammang, R.; Lorquet, J. C. Unimolecular Reaction Dynamics from Kinetic Energy Release Distributions. III. A Comparative Study of the Halogenobenzene Cations. *J. Chem. Phys.* **1999**, *110*, 2911−2921.
(411) Sievers, M. R.; Jarvis, L. M.; Armentrout, P. B. Tranistion-Metal Ethene Bonds: Thermochemistry of $M^+(C_2H_4)_n$ (M = Ti−Cu, $n = 1$ and 2) Complexes. *J. Am. Chem. Soc.* **1998**, *120*, 1891−1899.
(412) Meot-Ner (Mautner), M.; Nelson, S. F.; Willi, M. R.; Firgo, T. B. Special Effects of an Unusually Large Neutral to Radical Cation Geometry Change. Adiabatic Ionization Energies and Proton Affinities of Alkylhydrazines. *J. Am. Chem. Soc.* **1984**, *106*, 7384−7389.
(413) Hoyau, S.; Norrman, K.; McMahon, T. B.; Ohanessian, G. A Quantitative Basis for a Scale of $Na^+$ Affinities of Organic and

Small Biological Molecules in the Gas Phase. *J. Am. Chem. Soc.* **1999**, *121*, 8864−8875.
(414) Armentrout, P. B.; Rodgers, M. T. An Absolute Sodium Cation Affinity Scale: Threshold Collision-Induced Dissociation Experiments and Ab Initio Theory. *J. Phys. Chem. A* **2000**, *104*, 2238−2247.
(415) Kebarle, P. Equilibrium Studies of the Solvated Proton by High-Pressure Mass Spectrometry. Thermodynamic Determinations and Implications for the Electrospray Ionization Process. *J. Mass Spectrom.* **1997**, *32*, 922−929.
(416) Deng, H.; Kebarle, P. Bond Energies of Copper Ion-ligand Complex $CuL_2^+$ Determined in the Gas Phase by Ion-ligand Exchange Equilibria. *J. Am. Chem. Soc.* **1998**, *120*, 2925−2931.
(417) Taft, R. W.; Anvia, F.; Gal, J. F.; Walsh, S.; Capon, M.; Holmes, M. C.; Hosn, K.; Oloumi, G.; Vasanwala, R.; Yazdani, S. Free Energies of Cation−Molecule Complex Formation and of Cation−Solvent Transfers. *Pure Appl. Chem.* **1990**, *62*, 17−23.
(418) Burk, P.; Koppel, I. A.; Koppel, I.; Kurg, R.; Gal, J.-F.; Maria, P.-C.; Herreros, M.; Notario, R.; Abbound, J.-L. M.; Anvia, F.; Taft, R. W. Revised and Expanded Scale of Gas-Phase Lithium Cation Basicities. An Experimental and Theoretical Study. *J. Phys. Chem. A* **2000**, *104*, 2824−2833.
(419) Peschke, M.; Blades, A. T.; Kebarle, P. Hydration Energies and Entropies for $Mg^{2+}$, $Ca^{2+}$, $Sr^{2+}$, and $Ba^{2+}$, from Gas-Phase Ion−Water Molecule Equilibria Determinations. *J. Phys. Chem. A* **1998**, *102*, 9978−9985.
(420) Bogdanov, B.; Peschke, M.; Tonner, D. S.; Szulejko, J. E.; McMahon, T. B. Stepwise Solvation of Halides by Alcohol Molecules in the Gas Phase. *Int. J. Mass Spectrom.* **1999**, *185/186/187*, 707−725.
(421) Meot-Ner, M.; Sieck, L. W. Equilibrium Studies by Pulsed High-Pressure Mass Spectrometry: A Calibration, and Some Pitfalls and Solutions. *Int. J. Mass Spectrom. Ion Processes* **1991**, *109*, 187−208.
(422) McMahon, T. B.; Kebarle, P. Bridging the Gap. A Continuous Scale of Gas-Phase Basicities from Methane to Water from Pulsed Electron Beam High-Pressure Mass Spectrometry Equilibria. *J. Am. Chem. Soc.* **1985**, *107*, 2612−2617.
(423) McMahon, T. B. High-Pressure Mass Spectrometry. In *Energetics of Stable Molecules and Reactive Intermediates*; Minas da Piedade, M. E., Ed.; Kluwer Academic: Dordrecht, 1999; pp 259−380.
(424) Kemper, P. R.; Hsu, M.; Bowers, M. T. Transition-Metal Ion−Rare Gas Clusters: Bond Strengths and Molecular Parameters for $Co^+(He/Ne)_n$, $Ni^+(He/Ne)_n$, and $Cr^+(He/Ne/Ar)$. *J. Phys. Chem.* **1991**, *95*, 10600−10609.
(425) Kemper, P. R.; Weis, P.; Bowers, M. T. $Cr^+(H_2)_n$ Clusters: Asymmetric Bonding from a Symmetric Ion. *Int. J. Mass Spectrom. Ion Processes* **1997**, *160*, 17−37.
(426) Bushnell, J. E.; Maître, P.; Kemper, P. R.; Bowers, M. T. Binding Energies of $Ti^+(H_2)_{1-6}$ Clusters: Theory and Experiment. *J. Chem. Phys.* **1997**, *106*, 10153-1067.
(427) Wolf, J. F.; Staley, R. H.; Koppel, I.; Taagepera, M.; McIver, R. T., Jr.; Beauchamp, J. L.; Taft, R. W. Gas-Phase Basicities and Relative Proton Affinities of Compounds Between Water and Ammonia from Pulsed ICR Thermal Equilibria. *J. Am. Chem. Soc.* **1977**, *99*, 5417−5429.
(428) Bartmess, J. E.; Scott, J. A.; McIver, R. T., Jr. Scale of Acidities in the Gas Phase from Methanol to Phenol. *J. Am. Chem. Soc.* **1979**, *101*, 6046−6056.
(429) Aue, D. H.; Bowers, M. T. Stabilities of Positive Ions from Equilibrium Gas-Phase Basicity Measurements. In *Gas-Phase Ion Chemistry*; Bowers, M. T., Ed.; Academic: New York, 1979; pp 1−51.
(430) Larson, J. W.; McMahon, T. B. Fluoride and Chloride Affinities of Main Group Oxides, Fluorides, Oxofluorides, and Alkyls. Quantitative Scales of Lewis Acidities from Ion Cyclotron Resonance Halide-Exchange Equilibria. *J. Am. Chem. Soc.* **1985**, *107*, 766−773.
(431) Richardson, D. E. Applications of Gas-Phase Electron-Transfer Equilibria in Organometallic Redox Thermochemistry. In *Organometallic Ion Chemistry*; Freiser, B. S., Ed.; Kluwer Academic: Dordrecht, 1996; pp 259−282.
(432) Chabinyc, M. L.; Brauman, J. I. Hydrogen Bond Strength and Acidity. Structural and Energetic Correlations for Acetylides and Alcohols. *J. Phys. Chem. A* **1999**, *46*, 9163−9166.
(433) Jarek, R. L.; Miles, T. D.; Trester, M. L.; Denson, S. C.; Shin, S. K. Solvation of $Li^+$ by Acetone, THF, Diethyl Ether in the Gas Phase and the Ion−Molecule Association Mechanism. *J. Phys. Chem. A* **2000**, *2000*, 2230−2237.
(434) Sunner, J.; Kebarle, P. Unimolecular Dissociation of Ions. Effect on Mass-Spectrometric Measurements of Ion−Molecule Association Equilibria. *J. Phys. Chem.* **1981**, *85*, 327−335.
(435) Dearden, D. V.; Dejsupa, C.; Liang, Y.; Bradshaw, J. S.; Izatt, R. M. Intrinsic Contributions to Chiral Recognition: Discrimination Between Enantiomeric Amines by Dimethyldiketopyridino-18-Crown-6 in the Gas Phase. *J. Am. Chem. Soc.* **1997**, *119*, 353−359.
(436) Schauer, M. M.; Jefferts, S. R.; Dunn, G. H. Nonresonant Charge Transfer in the Threshold Region for $^3He^+ + {}^4He \rightleftharpoons {}^3He + {}^4He^+$. *Phys. Rev. A* **1990**, *42*, 5332−5337.
(437) Krug, R. R.; Hunter, W. G.; Grieger, R. A. Enthalpy−Entropy Compensation. 1. Some Fundamental Statistical Problems Associated with Analysis of van't Hoff and Arrhenius Data. *J. Phys. Chem.* **1976**, *80*, 0, 2335−2341.
(438) Smith, B. J.; Radom, L. Assigning Absolute Values to Proton Affinities: A Differentiation Between Competing Scales. *J. Am. Chem. Soc.* **1993**, *115*, 4885−4888.
(439) East, A. L. L.; Smith, B. J.; Radom, L. Entropies and Free Energies of Protonation and Proton-Transfer Reactions. *J. Am. Chem. Soc.* **1997**, *119*, 9014−9020.
(440) Rodgers, M. T.; Armentrout, P. B. Absolute Alkali Metal Ion Binding Affinities of Several Azoles Determined by Threshold Collision-Induced Dissociation. *Int. J. Mass Spectrom.* **1999**, *185/186/187*, 359−380.
(441) Decouzon, M.; Formento, A.; Gal, J.-F.; Herreros, M.; Li, L.; Maria, P.-C.; Koppel, I.; Kurg, R. Lithium-Cation and Proton Affinities of Sulfoxides and Sulfones: A Fourier Transform Ion Cyclotron Resonance Study. *J. Am. Soc. Mass Spectrom.* **1997**, *8*, 262−269.
(442) Buncel, E.; Chen, A.; Decouzon, M.; Fancy, S. A.; Gal, J.-F. Fourier Transform Ion Cyclotron Resonance Determination of Lithium Cation Basicities by the Kinetic Method: Upward Extension of the Scale to Phosphoryl Compounds. *J. Mass Spectrom.* **1998**, *33*, 757−765.
(443) Rodgers, M. T.; Armentrout, P. B. Collision-Induced Dissociation Measurements on $Li^+(M_2O)_n$, $n = 1-6$: The First Direct Measurement of the $Li^+-OH_2$ Bond Energy. *J. Phys. Chem. A* **1997**, *101*, 1238−1249.
(444) Rodgers, M. T.; Armentrout, P. B. Absolute Binding Energies of Lithium Ions to Short Chain Alcohols, $C_nH_{2n+2}O$, $n = 1-4$, Determined by Threshold Collision-Induced Dissociation. *J. Phys. Chem. A* **1997**, *101*, 2614−2625.
(445) DeTuri, V. F.; Su, M. A.; Ervin, K. M. Dynamics of Endoergic Bimolecular Proton-Transfer Reactions: $F^- + ROH \rightarrow HF + RO^-$ (R = H, $CH_3$, $CH_3CH_2$, $(CH_3)_2CH$, and $(CH_3)_3C$). *J. Phys. Chem. A* **1999**, *103*, 1468−1479.
(446) Tosi, P.; Dmitriev, O.; Bassi, D.; Wick, O.; Gerlich, D. Experimental Observation of the Energy Threshold in the Ion−Molecule Reaction $N^+ + D_2 \rightarrow ND^+ + D$. *J. Chem. Phys.* **1994**, *100*, 4300−4307.
(447) Lu, W.; Tosi, P.; Filippi, M.; Bassi, D. Reactions of $C^+(^2P_u)$ with $CO(^1\Sigma^+)$ from Thermal Energies to 30 eV. *J. Chem. Phys.* **2000**, *112*, 1330−1334.
(448) Armentrout, P. B. Periodic Trends in the Reactions of Atomic Ions with Molecular Hydrogen. *Int. Rev. Phys. Chem.* **1990**, *9*, 115−148.
(449) Chyall, L. J.; Squires, R. R. The Proton Affinity and Absolute Heat of Formation of Trifluoromethanol. *J. Phys. Chem.* **1996**, *100*, 16435−16440.
(450) Basir, Y. J.; Anderson, S. L. Transition-Metal $C_{60}$ Bonding by Guided Ion Beam Scattering. *Int. J. Mass Spectrom.* **1999**, *185/186/187*, 603−615.
(451) Clemmer, D. A.; Armentrout, P. B. Direct Determination of the Adiabatic Ionization Energy of $NO_2$ as Measured by Guided Ion Beam Mass Spectrometry. *J. Chem. Phys.* **1992**, *97*, 2451−2458.
(452) Parent, D. C.; Anderson, S. L. Chemistry of Metal and Semimetal Cluster Ions. *Chem. Rev.* **1992**, *92*, 1541−1565.
(453) Armentrout, P. B.; Clemmer, D. E. Guided Ion Beam Studies of the Energetics of Organometallic Species. In *Energetics of Organometallic Species*; Martinho Simões, J. A., Ed.; Kluwer Academic: Dordrecht, 1992; pp 321−356.
(454) Armentrout, P. B. Building Organometallic Complexes from the Bare Metal: Thermochemistry and Electronic Structure Along the Way. *Acc. Chem. Res.* **1995**, *28*, 430−436.
(455) Armentrout, P. B. Guided-Ion Beam Studies of Ionic Transition Metal Clusters and Complexes. In *Metal−Ligand Interactions—Structure and Reactivity*; Russo, N., Salahub, D. R., Eds.; Kluwer: Dordrecht, 1996; pp 23−48.
(456) Adams, N. G.; Smith, D. Study of the Nearly Thermoneutral Reactions of $N^+$ with $H_2$, HD, and $D_2$. *Chem. Phys. Lett.* **1985**, *117*, 67−70.
(457) Luine, J. A.; Dunn, G. H. Ion−Molecule Reaction Probabilities Near 10 K, *Astrophys. J.* **1985**, *299*, L67−L70.
(458) Marquette, J. B.; Rowe, B. R.; Duperyrat, G.; Roueff, E. CRESU Study of the Reaction $N^+ + H_2 \rightarrow NH^+ + H$ Between 8 and 70 K and Interstellar Chemistry Implications. *Astron. Astrophys.* **1985**, *147*, 115−120.
(459) Marquette, J. B.; Rebrion, C.; Rowe, B. R. Reactions of $N^+(^3P)$ Ions with normal, para, and Deuterated Hydrogen at Low Temperature. *J. Chem. Phys.* **1988**, *89*, 2041−2047.
(460) Gerlich, D. Reactive Scattering of $N^+ + H_2$ and Deuterated Analogues: Statistical Calculation of Cross Sections and Rate Coefficients. *J. Chem. Phys.* **1989**, *90*, 3574−3581.
(461) Gerlich, D. Experimental Investigations of Ion−Molecule Reactions Relevant to Interstellar Chemistry. *J. Chem. Soc., Faraday Trans.* **1993**, *89*, 2199−2208.

(462) Sunderlin, L. S.; Armentrout, P. B. Rotational Temperature Dependence of the Reactions of $N^+$ and $C^+$ with $H_2$, HD, and $D_2$. *J. Chem. Phys.* **1994**, *100*, 5639−5645.

(463) Anderson, W. R. Oscillator Strengths of $NH_2$ and the Heats of Formation of NH and $NH_2^+$. *J. Phys. Chem.* **1989**, *93*, 530−536.

(464) Tarroni, R.; Palmieri, P.; Mitrushenko, A.; Tosi, P.; Bassi, D. Dissociation Energies and Heats of Formation of NH and $NH^+$. *J. Chem. Phys.* **1997**, *106*, 10265−10272.

(465) de Beer, E.; Born, M.; de Lange, C. A.; Westwood, N. P. C. A Rotationally Resolved REMPI−PES Study of the NH Radical. *Chem. Phys. Lett.* **1991**, *186*, 40−46.

(466) Gibson, S. T.; Greene, J. P.; Berkowitz, J. Photoionization of the Amidogen Radical. *J. Chem. Phys.* **1985**, *83*, 4319−4328.

(467) Stephens, J. C.; Yamaguchi, Y.; Schaefer, H. F., III. The Adiabatic and Vertical Ionization Potentials of $NH_2$ to the Three Lowest-Lying States of $NH_2^+$. *J. Mol. Struct. (THEOCHEM)* **1999**, *461*−*462*, 41−53.

(468) Lin, C.-Y.; Dunbar, R. C.; Haynes, C. L.; Armentrout, P. B.; Tonner, D. S.; McMahon, T. B. Dissociation Thermochemistry of Tetra Methylsilane Ion. Comparative Determination by Thermal Dissociation and Threshold Collisional Dissociation. *J. Phys. Chem.* **1996**, *100*, 19659−19665.

(469) Dopfer, O.; Müller-Dethlefs, K. $S_1$ Excitation and Zero Kinetic Energy Spectra of Partly Deuterated 1:1 Phenol-Water Complexes. *J. Chem. Phys.* **1994**, *101*, 8508−8516.

(470) Ryzhov, V.; Yang, C.-N.; Klippenstein, S. J.; Dunbar, R. C. Binding Energies of Chromium Cations with Fluorobenzenes from Radiative Association Kinetics. *Int. J. Mass Spectrom.* **1999**, *185*−*187*, 913−923.

(471) Dunbar, R. C. Polyatomic Ion−Molecule Radiative Association: Theoretical Framework and Predictions: Observations of $NO^+ + C_6H_5CN$ as an Example. *Int. J. Mass Spectrom. Ion Processes* **1990**, *100*, 423−443.

(472) Ryzhov, V.; Dunbar, R. C. Size Dependence of Radiative Association Rates. *Int. J. Mass Spectrom. Ion Processes* **1997**, *167*/*168*, 627−635.

(473) Ryzhov, V.; Yang, Y.-C.; Klippenstein, S. J.; Dunbar, R. C. Temperature Dependence of Radiative Association Rates. *J. Phys. Chem. A* **1998**, *102*, 8865−8870.

(474) Bohme, D. K.; Mackay, G. I.; Schiff, H. I. Proton Affinities from Kinetics of Proton-Transfer Reactions. VII. Proton Affinities of $O_2$, $H_2$, Kr, O, $N_2$, Xe, $CO_2$, $CH_4$, $N_2O$, and CO. *J. Chem. Phys.* **1980**, *73*, 4976−4986.

(475) Grabowski, J. J. Anion−Molecule Experiments: Reactive Intermediates and Mechanistic Organic Chemistry. In *Advances in Gas-Phase Ion Chemistry*; Adams, N. G., Babcock, L. M., Eds.; JAI Press: Greenwich, CT, 1992; Vol. 1, pp 43−81.

(476) Hare, M.; Emrick, T.; Eaton, P. E.; Kass, S. R. Cubyl Anion Formation and an Experimental Determination of the Acidity of C−H Bond Dissociation Energy of Cubane. *J. Am. Chem. Soc.* **1997**, *119*, 237−238.

(477) Broadus, K. M.; Kass, S. R. Benzocyclobutenone Enolate: An Anion with an Antiaromatic Resonance Structure. *J. Chem. Soc., Perkin Trans. 2* **1999**, *1999*, 2389−2396.

(478) Seburg, R. A.; Hill, B. T.; Squires, R. R. Synthesis, Properties and Reactivity of the Phenylcarbene Anion in the Gas Phase. *J. Chem. Soc., Perkin Trans. 2* **1999**, *1999*, 2249−2256.

(479) Decker, B. K.; Adams, N. G.; Babcock, L. M. Gas-Phase Reactivity of $HS_2H^+$ and $S_2^+$: An Investigation of the Gas Basicity and Proton Affinity of $HS_2$. *Int. J. Mass Spectrom.* **1999**, *185*/*186*/*187*, 727−743.

(480) O'Hair, R. A.; DePuy, C. H.; Bierbaum, V. M. Gas-Phase Chemistry and Thermochemistry of the Hydroxysulfide Anion, $HOS^-$. *J. Phys. Chem.* **1993**, *97*, 7955−7961.

(481) Gronert, S. An Ab Initio Study of Proton Transfers from Gas-Phase Dications: Complications in Kinetic Methods for Determining Acidities. *J. Am. Chem. Soc.* **1996**, *118*, 3525−3526.

(482) Stevens Miller, A. E.; Miller, T. M. Gas-Phase Acidities of Transition-Metalcarbonyls and Trifluorophosphine Hydrides. In *Energetics of Organometallic Species*; Martinho Simões, J. A., Ed.; Kluwer Academic: Dordrecht, 1992; pp 252−267.

(483) Natterer, J.; Koch, W.; Schröder, D.; Goldberg, N.; Schwarz, H. Combined Experimental and Theoretical Study of the C−H Bond Strength and the Gas-Phase Acidity of Triacetylene, $C_6H_2$, and the Electron Affinity of the $C_6H$ Radical. *Chem. Phys. Lett.* **1994**, *229*, 429−434.

(484) Bouchoux, G.; Salpin, J. Y.; Leblanc, D. A Relationship Between the Kinetics and Thermochemistry of Proton-Transfer Reactions in the Gas Phase. *Int. J. Mass Spectrom. Ion Processes* **1996**, *153*, 37−48.

(485) Bouchoux, G.; Salpin, J.-Y. Thermokinetic Determination of Gas-Phase Basicities. Application to Ketene, Methylketene, and Formaldimine. *J. Phys. Chem.* **1996**, *100*, 16555−16560.

(486) Bouchoux, G.; Salpin, J.-Y. Re-Evaluated Gas-Phase Basicity and Proton Affinity Data from the Thermokinetic Method. *Rapid Commun. Mass Spectrom.* **1999**, *13*, 932−936.

(487) Agmon, N.; Levine, R. D. Energy, Entropy and the Reaciton Coordinate: Thermodynamic-Like Relations in Chemical Kinetics. *Chem. Phys. Lett.* **1977**, *52*, 197−201.

(488) Betowski, D.; Mackay, G.; Payzant, J.; Bohme, D. The Equilibrium $SH^- + HCN \rightleftarrows CN^- + H_2S$ and the Determination of $D_0$(H−CN). *Can. J. Chem.* **1975**, *53*, 2365−2370.

(489) DePuy, C. H.; Bierbaum, V. M.; Damrauer, R. Relative Gas-Phase Acidities of the Alkanes. *J. Am. Chem. Soc.* **1984**, *106*, 4051−4053.

(490) DePuy, C. H.; Gronert, S.; Barlow, S. E.; Bierbaum, V. M.; Damrauer, R. The Gas-Phase Acidities of the Alkanes. *J. Am. Chem. Soc.* **1989**, *111*, 1968−1973.

(491) Wenthold, P. G.; Squires, R. R. Determination of the Gas-Phase Acidities of Halogen-Substituted Aromatic Compounds Using the Silane-Cleavage Method. *J. Mass Spectrom.* **1995**, *30*, 17−24.

(492) Holman, R. W.; Sumpter, T. L.; Farrar, J.; Weigel, K.; Bartmess, J. E. Competitive Reactivity as a Probe for Reaction Coordinates in Gas-Phase Ion−Molecule Chemistry. *J. Phys. Org. Chem.* **1997**, *10*, 585−589.

(493) Viggiano, A. A.; Morris, R. A. Rotational and Vibrational Energy Effects on Ion−Molecule Reactivity as Studied by the VT-SIFDT Technique. *J. Phys. Chem.* **1996**, *100*, 19227−19240.

(494) Hierl, P. M.; Morris, R. A.; Viggiano, A. A. Rate Coefficients for the Endothermic Reactions $C^+(^2P) + H_2$ ($D_2$) → $CH^+$ ($CD^+$) + H(D) as Functions of Temperature from 400 to 1300 K. *J. Chem. Phys.* **1997**, *106*, 10145−10152.

(495) Viggiano, A. A.; Arnold, S. T.; Morris, R. A. Reactions of Mass-Selected Cluster Ions in a Thermal Bath Gas. *Int. Rev. Phys. Chem.* **1998**, *17*, 147−184.

(496) Maier, W. D. Atom Transfer in Endothermic Ion−Molecule Reactions. *J. Chem. Phys.* **1967**, *46*, 4991−4992.

(497) Lindemann, E.; Frees, L. C.; Rozette, R. W.; Koski, W. S. Threshold and Cross Section of the Reaction of $C^+$ with Molecular Hydrogen. *J. Chem. Phys.* **1972**, *56*, 1003−1004.

(498) Adams, N. G.; Smith, D.; Millar, T. J. Importance of Kinetically Excited Ions in the Synthesis of Interstellar Molecules. *Mon. Not. R. Astron. Soc.* **1984**, *211*, 857−865.

(499) Ervin, K. M.; Armentrout, P. B. Threshold Behavior of Endothermic Reactions: $C^+(^2P) + H_2 \rightarrow CH^+ + H$. *J. Chem. Phys.* **1984**, *80*, 2978−2980.

(500) Twiddy, N. D.; Mohebati, A.; Tichý, M. Measurements of the Reaction Rate Coefficients of the Endoergic Reactions $C^+(^2P) + H_2(D_2) \rightarrow CH^+(CD^+) + H(D)$ from Threshold to Centre-of-Mass Energy 0.8 eV. *Int. J. Mass Spectrom. Ion Processes* **1986**, *74*, 251−263.

(501) Ervin, K. M.; Armentrout, P. B. $C^+(^2P) + H_2$ ($D_2$, HD) → $CH^+$ ($CD^+$) + H(D). I. Reaction Cross Sections and Kinetic Isotope Effects from Threshold to 15 eV c.m. *J. Chem. Phys.* **1986**, *84*, 6738−6749.

(502) Ervin, K. M.; Armentrout, P. B. $C^+(2P) + H_2$ ($D_2$, HD) → $CH^+$ ($CD^+$) + H(D). II. Statistical Phase Space Theory. *J. Chem. Phys.* **1986**, *84*, 6750−6760.

(503) Gerlich, D.; Disch, R.; Scherbarth, S. $C^+ + H_2(j) \rightarrow CH^+ + H$: The Effect of Reagent Rotation on the Integral Cross Section in the Threshold Region. *J. Chem. Phys.* **1987**, *87*, 350−359.

(504) Helm, H.; Cosby, P. C.; Graff, M. M.; Moseley, J. T. Photofragment Spectroscopy of $CH^+$: Laser Excitation of Shape Resonances in the A $^1\Pi$ State. *Phys. Rev. A* **1982**, *25*, 304−321.

(505) Hechtfischer, U.; Amitay, Z.; Forck, P.; Lange, M.; Linkemann, J.; Schmitt, M.; Schramm, U.; Schwalm, D.; Wester, R.; Zajfman, D.; Wolf, A. Near-Threshold Photodissociation of Cold $CH^+$ in a Storage Ring. *Phys. Rev. Lett.* **1998**, *80*, 2809−2812.

(506) Ayala, J. A.; Wentworth, W. E.; Chen, E. C. M. Electron Attachment to Halogens. *J. Phys. Chem.* **1981**, *85*, 768−777.

(507) Chen, E. C. M. Determination of Molecular Electron Affinities Using the Electron Capture Detector in the Pulse Sampling Mode at Steady State. *J. Phys. Chem.* **1983**, *87*, 45−49.

(508) Chen, E. C. M.; Wentworth, W. E. Experimental Determination of Electron Affinities of Organic Molecules. *Mol. Cryst. Liq. Cryst.* **1989**, *171*, 271−285.

(509) Chen, E. C. M.; Chen, E. S.; Milligan, M. S.; Wentworth, W. E.; Wiley: J. R. Experimental Determination of the Electron Affinities of Nitrobenzene, Nitrotoluene, Pentafluoronitrobenzene, and Isotopic Nitrobenzenes and Azulenes. *J. Phys. Chem.* **1992**, *96*, 2385−2390.

(510) Ruoff, R. S.; Kadish, K. M.; Boulas, P.; Chen, E. C. M. The Relationship Between the Electron Affinities and Half-Wave Reduction Potentials of Fullerenes, Aromatic Hydrocarbons, and Metal Complexes. *J. Phys. Chem.* **1995**, *99*, 8843−8850.

(511) Chen, E. C. M.; Welk, N.; Chen, E. S.; Wentworth, W. E. Electron Affinity, Gas-Phase Acidity, Bond Dissociation Energy, and Negative Ion States of Nitromethane. *J. Phys. Chem. A* **1999**, *103*, 9072−9079.

(512) Chen, E. C. M.; Carr, S.; Wentworth, W. E.; Chen, E. S. D. Modified Kinetic Model of the Electron-Capture Detector. Molecular Electron Affinities and Electron Collection Modes. *J. Chromatogr. A* **1998**, *827*, 91−104.

(513) Chen, E. C. M.; Wiley: J. R.; Batten, C. F.; Wentworth, W. E. Determination of the Electron Affinities of Molecules Using Negative Ion Mass Spectrometry. *J. Phys. Chem.* **1994**, *98*, 88−94.

(514) Becker, R. S.; Chen, E. Extension of Electron Affinities and Ionization Potentials of Aromatic Hydrocarbons. *J. Chem. Phys.* **1966**, *45*, 2403−2410.
(515) Wojnarovits, L.; Flodiak, G. Electron Capture Detection of Aromatic Hydrocarbons. *J. Chromatogr.* **1981**, *206*, 511−519.
(516) Celotta, R. J.; Bennett, R. A.; Hall, J. L.; Siegel, M. W.; Levine, J. Molecular Photodetachment Spectrometry. II. The Electron Affinity of $O_2$ and the Structure of $O_2^-$. *Phys. Rev. A* **1972**, *6*, 631−642.
(517) Herbst, E.; Patterson, T. A.; Lineberger, W. C. Laser Photodetachment of $NO_2^-$. *J. Chem. Phys.* **1974**, *61*, 1300−1304.
(518) Siegel, M. W.; Celotta, R. J.; Hall, J. L.; Levine, J.; Bennett, R. A. Molecular Photodetachment Spectroscopy. I. The Electron Affinity of Nitric Oxide and the Molecular Constants of $NO^-$. *Phys. Rev. A* **1972**, *6*, 607−631.
(519) Smith, D.; Spanel, P. Studies of Electron Attachment at Thermal Energies Using the Flowing Afterglow-Langmuir Probe Technique. In *Adv. At. Mol. Opt. Phys.*; Bederson, B., Dalgarno, A., Eds.; Acadmeic: Boston, 1994; Vol. 32, pp 307−343.
(520) Smith, D.; Spanel, P.; Märk, T. D. Electron Attachment to $C_{60}$ at Low Energies. *Chem. Phys. Lett.* **1993**, *213*, 202−206.
(521) Parkes, D. A.; Sugden, T. M. Electron Attachment and Detachment in Nitric Oxide. *J. Chem. Soc., Faraday Trans. 2* **1972**, *68*, 600−614.
(522) Miller, T. M.; Morris, R. A.; Stevens Miller, A. E.; Viggiano, A. A.; Paulson, J. F. Observation of Thermal Electron Detachment from Cyclo-$C_4H_8^-$ in FALP Experiments. *Int. J. Mass Spectrom. Ion Processes* **1994**, *135*, 195−205.
(523) Ruscic, B.; Feller, D.; Dixon, D. A.; Peterson, K. A.; Harding, L. B.; Asher, R. L.; Wagner, A. F. Evidence for a Lower Enthalpy of Formation of Hydroxyl Radical and a Lower Gas-Phase Bond Dissociation Energy of Water. *J. Phys. Chem. A* **2001**, *105*, 1−4.
(524) Bowers, M. T., Ed. *Int. J. Mass Spectrom.* **2000**, *200*.

CR990081L